PREPARATION OF THORIUM NITRIDES AND THEIR OXIDATION BEHAVIOR

トリウム窒化物の作成および その酸化挙動に関する研究

Masayoshi UNO

1988

DOCTOR THESIS

PREPARATION OF THORIUM NITRIDES AND THEIR OXIDATION BEHAVIOR

Masayoshi UNO

1988

CONTENTS

1 INTRODUCTION

1-1 GENERAL INTRODUCTION

Because the resources of uranium are limited, it is necessary to develop reactors which can convert almost all of the ^{238}U to ^{239}Pu. Also the vast resources of thorium can be used by converting fertile ^{232}Th into fissile ^{233}U. Although the current policy on nuclear development is emphasizing U-Pu fuel cycle development, it is proposed to establish the Th-U fuel cycle from the viewpoint of proliferation resistance.

The major nuclear reactions involved in breeding in ^{232}Th is shown in Fig. 1-1. The shaded area is that of greatest interest. The nucleus of the thorium atom(^{232}Th) can undergo reaction with a neutron to form ^{233}Th which is relatively short-lived. Subsequent radioactive disintegrations of this isotope produce, through ^{233}Pa, a relatively long-lived ^{233}U which can be caused to fission and serve as an atomic fuel in a manner similar to ^{235}U and ^{239}Pu. As the η value of ^{233}U, the ratio of neutrons produced per neutron absorbed in ^{233}U, is more than 2 over the full range of neutron energy, there are possibilities to realize a breeding reactor or a high conversion reactor utilizing ^{232}Th-^{233}U fuel cycle in a wide range of the neutron energy.

A large number of chemical states of thorium fuel are considered depending on the type of reactors and the system of the fuel cycles. Limiting to ceramic fuels, thorium dioxide, thorium carbides and thorium mononitride are candidates for the fuel elements of thorium reactors. In order to realize a thorium reactor, it is important to know their physical, chemical, thermal and mechanical properties and chemical reactivity with cladding material and coolant material as well as irradiation behavior.

Thorium dioxide, ThO_2 is the only solid compound in the Th-O system and has the melting point of 3390°C. While UO_2 has a range of non-stoichiometric composition, ThO_2 is a stoichiometric compound at temperatures below 1754°C. Moreover, ThO_2

is chemically stable and has a low vapor pressure and relatively high thermal conductivities. ThO_2 and its solid solution with UO_2 or PuO_2 are considered to be some of the most suitable fuels for FBR as well as heavy water and light water breeder reactors. Next to ThO_2, the most promising thorium ceramic fuels are thorium carbides. Thorium monocarbide, ThC, in particular, has a relatively high melting point, a high thorium density, a suitable isotropic structure of NaCl type up to high temperatures and a high thermal conductivity although ThC is chemically very reactive. Though knowledge on some properties of the thorium carbides are available, the information on the properties is not sufficient compared with that on the oxide. The advantage of thorium mononitride as a nuclear fuel is its high thermal conductivity and lower reactivity to air compared with thorium carbides. The fact that ThN is easily soluble in HNO_3 makes it attractive from the viewpoint of down stream chemistry in thorium fuel cycle. However, since the absorption cross section for the thermal neutron of ^{14}N is relatively large, the nitride is not suitable for the fuel of thermal reactors. The information on the preparation and properties of thorium nitride is very scarce even though compared with thorium carbides. Moreover, almost all the data have been measured with poorly characterized samples.

One of the main purposes of the present work is to study basic problems in preparing pure ThN. Particularly, on account of the instability of thorium nitrides with respect to ThO_2, efforts had to be expended on the study on the oxidation behavior of Th_3N_4.

1-2 PRESENT STATUS OF THE KNOWLEDGE ON THORIUM OXIDE AND THORIUM NITRIDES

The present status of the knowledge on thorium oxide and thorium nitrides will be briefly reviewed in the following.

Thorium oxide

The phase diagram of Th-O system reported by Benz[1] is shown in Fig. 1-2. ThO_2 is the only stable oxide in the condensed state and has the melting point of 3390°C which is the highest melting point of all the known binary oxides. As seen from the phase diagram, thorium dissolves in ThO_2 to some extent at elevated temperatures. However, Ackermann et al.[2] reported the congruent sublimation composition of $ThO_{1.998}$ at 2727°C indicating that ThO_2 phase is stable with an oxygen defficiency. Moreover, Foex[3] reported that below 1400°C ThO_2 suffers no weight change when the atmosphere is changed from an oxidizing (O_2) to reducing(H_2 or CO) one. The ThO_2 has fluorite type structure whose lattice parameter is 5.597 ± 0.001Å. This structure does not undergo any polymorphic transformation up to its melting point.

Ackermann et al.[2] investigated the thermodynamic behavior of ThO_2 above 2800°K. The effective vapor pressure of $ThO_2(g)$, P, based on the assumption that the vapor is comprised entirely of dioxide molecules, was given by

$$\log P(atm) = 8.26 - 3.55 \times 10^4 / T$$

Thus, the vapor pressure of ThO_2 is a very low value such as the order of 3×10^{-8} atm at 2000°C. However, for the non-stoichiometric ThO_{2-x}, the vapor species of ThO increses and the total vapor pressure increses[4].

The thermal conductivities of ThO_2 and ThO_2-UO_2 were reported by Murabayashi et al.[5] and Takahashi et al.[6]. The thermal conductivity of ThO_2 is much higher than that of UO_2. However, a little addition of UO_2 in ThO_2 yields the lower thermal conductivity.

Thermodynamic data for ThO_2 are shown in Table 1-1[7].

ThO_2 is more stable against high temperature steam than UO_2[8]. It is also unreactive to common metals under their condition of use. Niobium, tantalum and tungsten are compatible with ThO_2 for more than 1000 hours at 1540°C[9]. ThO_2 forms

extensive solid solutions with CaO, Y_2O_3, the rare earth oxides and UO_x. Very limited solutions are formed with other oxides. The divalent and trivalent cations substitute for Th^{4+} in the fluorite structure with the formation of anion vacancies being the mechanism of maintaining electro-neutrality[10].

As for the mechnaical properties, the creep data at 1400-1800°C were reported by Poteat and Yust[11]. Watchman and Lam[12] investaigated the dependence of Young's modulus on temperature.

Self diffusion coefficints of thorium ion and oxygen ion in ThO_2 were summarized by Ando and Oishi[13].

Thoria powder is normally prepared by calcination of thorium oxalate precipitates which are obtained by adding oxalic acid to thorium nitrate solution[14]. It is difficult to fabricate high-density thoria pellets from the powder obtained in the above mentioned method[14,15,16].

Thorium nitrides

The phase diagram of Th-N system reported by Benz et al.[17] is shown in Fig. 1-3. There exist two thorium nitrides, Th_3N_4 and ThN in the system. ThN has a NaCl type structure and its lattice parameter is 5.159Å[17]. The crystal structure of Th_3N_4 was reported by Benz and Zachariasen[18] to be rhombohedral (a=9.398Å and α=23.78°). The previously reported Th_2N_3 has been identified as Th_2N_2O with the tetragonal lattice parameters a=3.883 and c=6.187Å[18].

The heat capacity of ThN at temperatures from 7 to 300K was measured by Danan et al.[19] and S°_{298} was calculated as 13.4±0.2 cal/k mol. The heat capacity of Th_3N_4 and ThN at 450-850K was measured by Ono et al.[20]. The vapor pressure of ThN in the temperature range of 2410-2790°C was reported by Aronson and Auskern[21] as follows;

$$\log P(atm) = 8.086 - 33244/T + 0.958\times10^{-17}T^5$$

The Th_3N_4 decomposes to ThN and N_2 at high temperatures before

melting and the nitrogen pressures equilibriated with Th_3N_4 have been measured by Aronson and Auskern[21] and by Kusakabe and Imoto[22]. The thermodynamic properties are summarized by M.H.Rand et al.[7].

The thermal conductivity of ThN is shown in Fig. 1-4[9] together with thermal conductivities of (Th,U)C, $(Th,U)C_2$, (Th,U)N and ThO_2. Such high thermal conductivity of ThN makes the people be interested in the use of the ThN as the nuclear fuel.

Although ThN is chemically stable compared with thorium carbides, it is much more reactive than ThO_2. The oxidation behavior of ThN and Th_3N_4 was studied by Ozaki et al.[23] and the hydrolysis of ThN powder was investigated by Sugihara and Imoto[24].

The information on the preparation and properties of thorium nitrides is very scarce. Therefore, it is necessary to establish the suitable method of the preparation and to measure the various properties of the well-characterized specimens for developing thorium nitride fuel.

1-3 OUTLINE OF THE PRESENT WORK

In Chapter 2, pulverization method of metallic thorium through hydriding process is described. This process consists of two steps; the formation of ThH_2 as the first step and the formation of Th_4H_{15} as the second step. The pulverization process is explored with the help of the visual observation of the appearance of the sample during the process. The p-c-T relationships for Th-H system are also determined at 200, 300, 350 and 800°C. From these results, a tentative equilibrium phase diagram for Th-H system is proposed.

In Chapter 3, the results obtained from the study on the preparation of thorium nitrides are presented. A large amount of experimental work is expended to prepare Th_3N_4 and some of the representative results are discussed in terms of conditions of nitriding process. Moreover, the crystal structure of Th_3N_4

is re-examined. For the preparation of ThN, thermal decomposition of Th_3N_4 is performed under various conditions and the products are examined as a function of temperature and time. The thermodynamic stability of the solids in the Th-N-O system is evaluated as a function of $P(O_2)$ and $P(N_2)$ and compared with the experimental results.

In Chapter 4, oxidation behavior of Th_3N_4 is studied. Th_3N_4 is oxidized in air at 0, 50 and 100°C. It is found that the products are of poorly-crystalline nature. The structual units of which the oxidation products are composed are discussed on the basis of the results obtained from X-ray diffraction, IR absorption spectroscopy and scanning electron microscopy.

In Chapter 5, the degree of crystallinity of ThO_2 is discussed in terms of the detected peak number, the Kα doublet resolution of the peaks and the integral breadth values of the peaks in the X-ray diffraction pattern. Moreover, the crystallite size and nonuniform strain are estimated by the line broadening technique. The local order of atoms is also estimated by radial distribution analysis.

Summarizing comments are given in Chapter 6.

REFERENCE

[1] R.Benz, J.Nucl.Mat., 29(1969)43.
[2] R.J.Ackermann, E.G.Rauh, R.J.Thorn and M.C.Cannon, J.Phys.Chem., 67(1963)762.
[3] M.Foex, C.R.Acad.Sci.,Paris, 215(1942)534.
[4] R.J.Ackermann and M.Tetenbaum, High Temp.Sci., 13(1980)91.
[5] M.Murabayashi, S.Namba, Y.Takahashi and T.Mukaibo, J.Nucl.Sci.Technol., 6(1969)128.
[6] Y.Takahashi and M.Murabayashi, J.Nucl.Sci.Technol., 12(1975)133.
[7] M.H.Rand, O.von Golobeck, R.Ferro, K.Girgis and A.L.Dragoo, in O.Kubascheski(ed.), "Thorium: Physico-Chemical Properties of its Compounds and Alloys", I.A.E.A., Vienna, 1975.
[8] J.M.Marakowitz and J.C.Clayton, WAPD-TM-909(1970).

[9] S.Peterson and C.E.Curtis, "Thorium Ceramic Data Manual", Vol.1 I-III, ORNL-4503(1970).
[10] R.C.Anderson, in A.M.Alper (ed.), "Refractory Materials", Vol.5 Academic Press, New York and London, 1970.
[11] L.E.Potet and C.S.Yust, J.Am.Ceram.Soc., 49(1966)410.
[12] J.B.Watchman and D.G.Lam, J,Am.Ceram.Soc., 42(1959)254.
[13] K.Ando and Y.Oishi, J.Nucl.Sci.Technol., 20(1983)973.
[14] J.M.Pope and K.C.Radford, J.Nucl.Mat., 52(1974)241.
[15] Y.Harada, Y.Baskin and J.H.Hadwerk, J.Am.Ceram.Soc., 45(1962)253.
[16] B.J.F.Palmer, J.A.Scoberg and A.Y.H.Gin, Am.Ceram.Soc.Bull., 62(1982)627.
[17] R.Benz, C.G.Hoffman and G.N.Rupert. J.Am.Chem.Soc., 89(1967)191.
[18] R.Benz and W.H.Zachariasen, Acta Cryst., 21(1969)838.
[19] J.Danan, C,H.de Novion and H.Dallaporta, Solid State Commun., 10(1972)775.
[20] F.Ono, M.Kanno and T.Mukaibo, J.Nucl.Sci.Technol., 10(1973)391.
[21] S.Aronson and A.B.Auskern, J.Phys.Chem., 70(1966)3937.
[22] T.Kusakabe and S.Imoto, J.Jap.Inst.Met., 35(1971)1115
[23] S.Ozaki. M.Kanno and T.Mukaibo, J.Nucl.Sci.Technol., 8(1971)41.
[24] S.Sugihara and S.Imoto, J.Nucl.Sci.Technol., 8(1971)630.

Table 1-1 Thermodynamic data of ThO_2

T / K	C_p / $calK^{-1}mol^{-1}$	fef / $calK^{-1}mol^{-1}$	$-\Delta G_f^\circ$ / kcal mol^{-1}
298.15	14.76	15.59	279.4
400	16.08	16.19	274.8
600	17.29	18.70	265.7
800	18.00	21.41	256.9
1000	18.57	23.95	248.1
1200	19.09	26.26	239.4
1400	19.57	28.37	230.9
1600	20.05	30.30	222.3
1800	20.51	32.09	213.8
2000	20.97	33.74	205.3
$\Delta H_f^\circ(298)$		-293.2 kcal/mol	
$\Delta S_f^\circ(298)$		-46.0 cal/mol K	

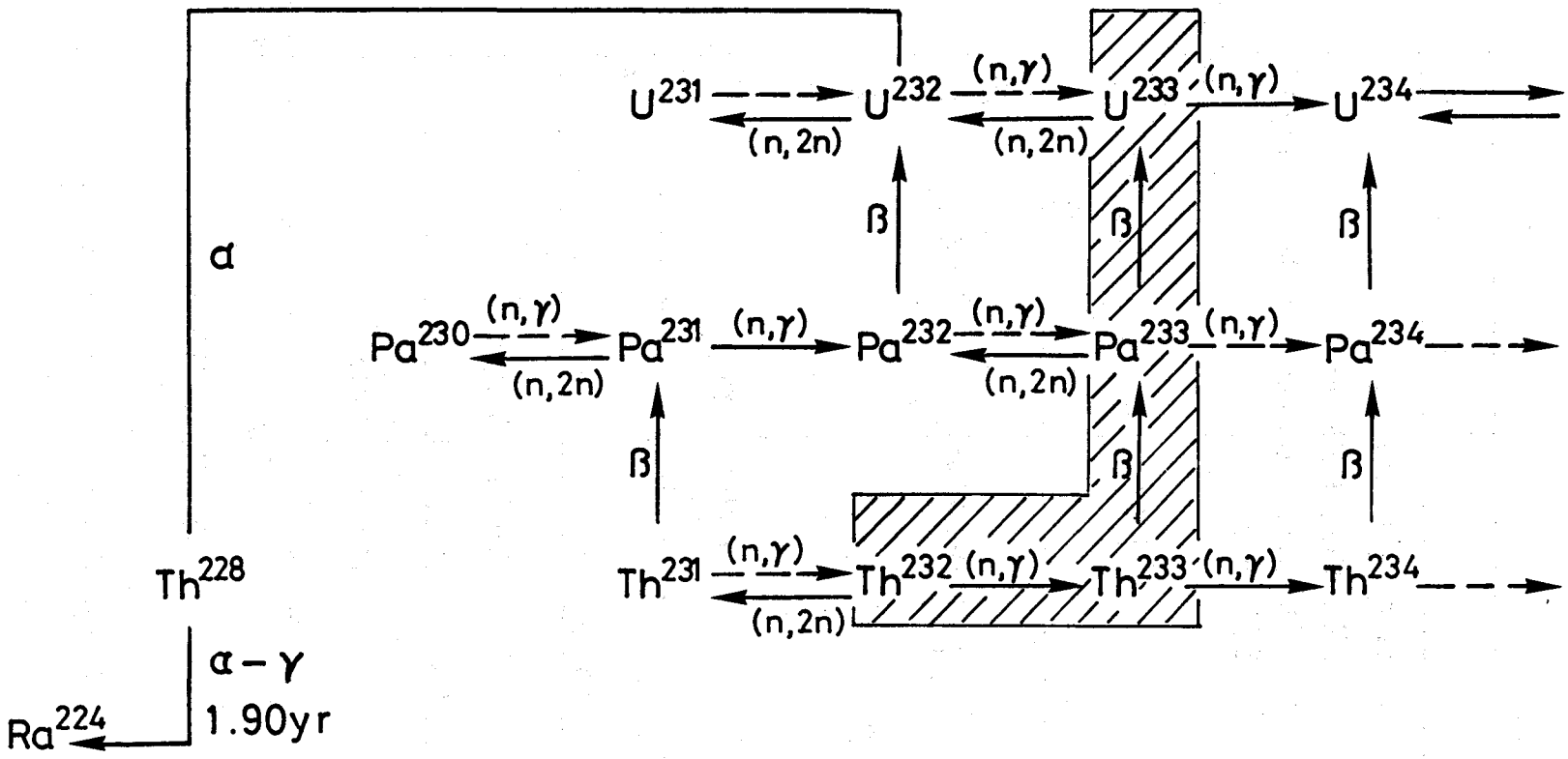

Fig. 1-1 Heavy-isotope buildup in thorium.

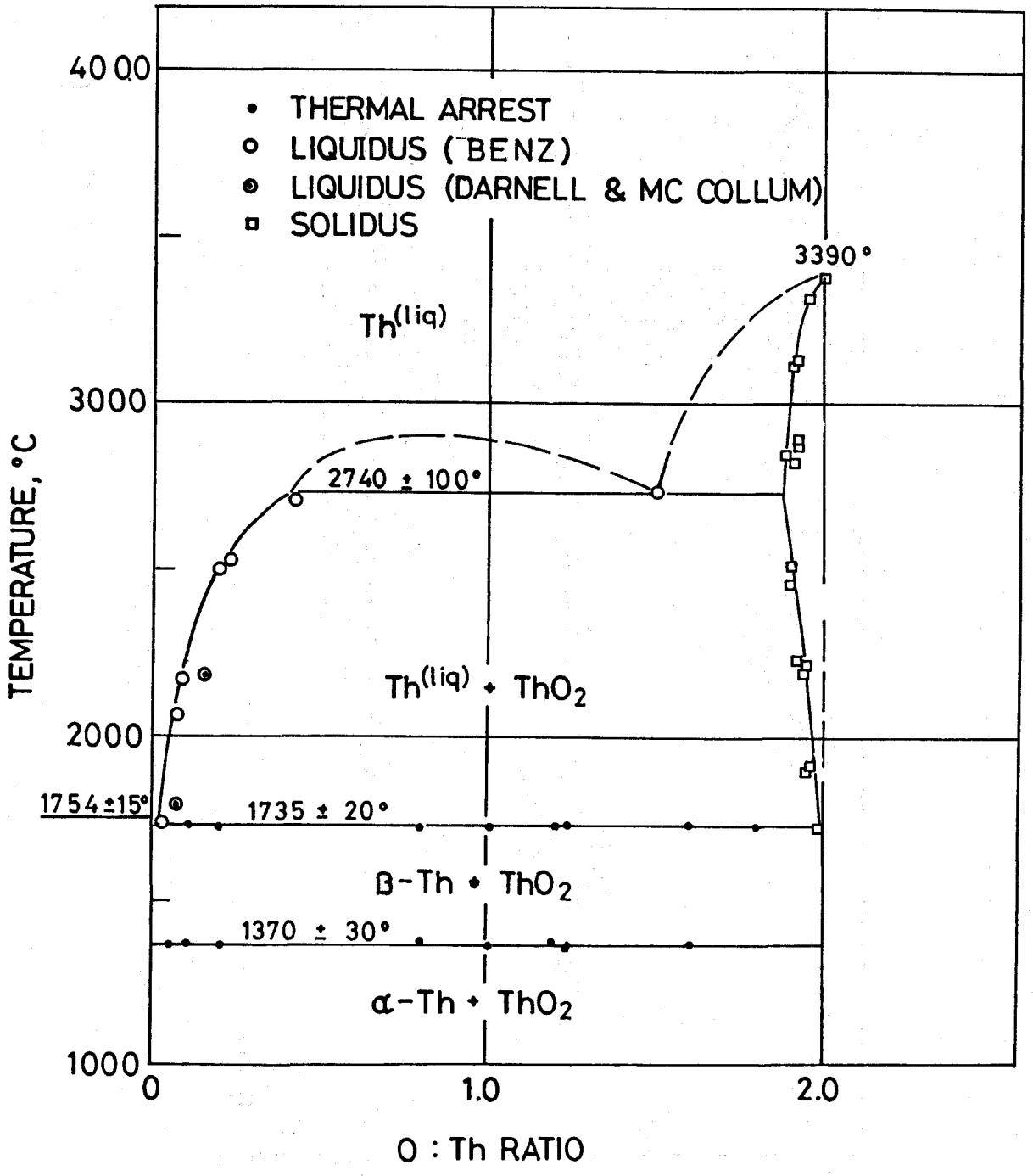

Fig. 1-2 Phase diagram of Th-O system

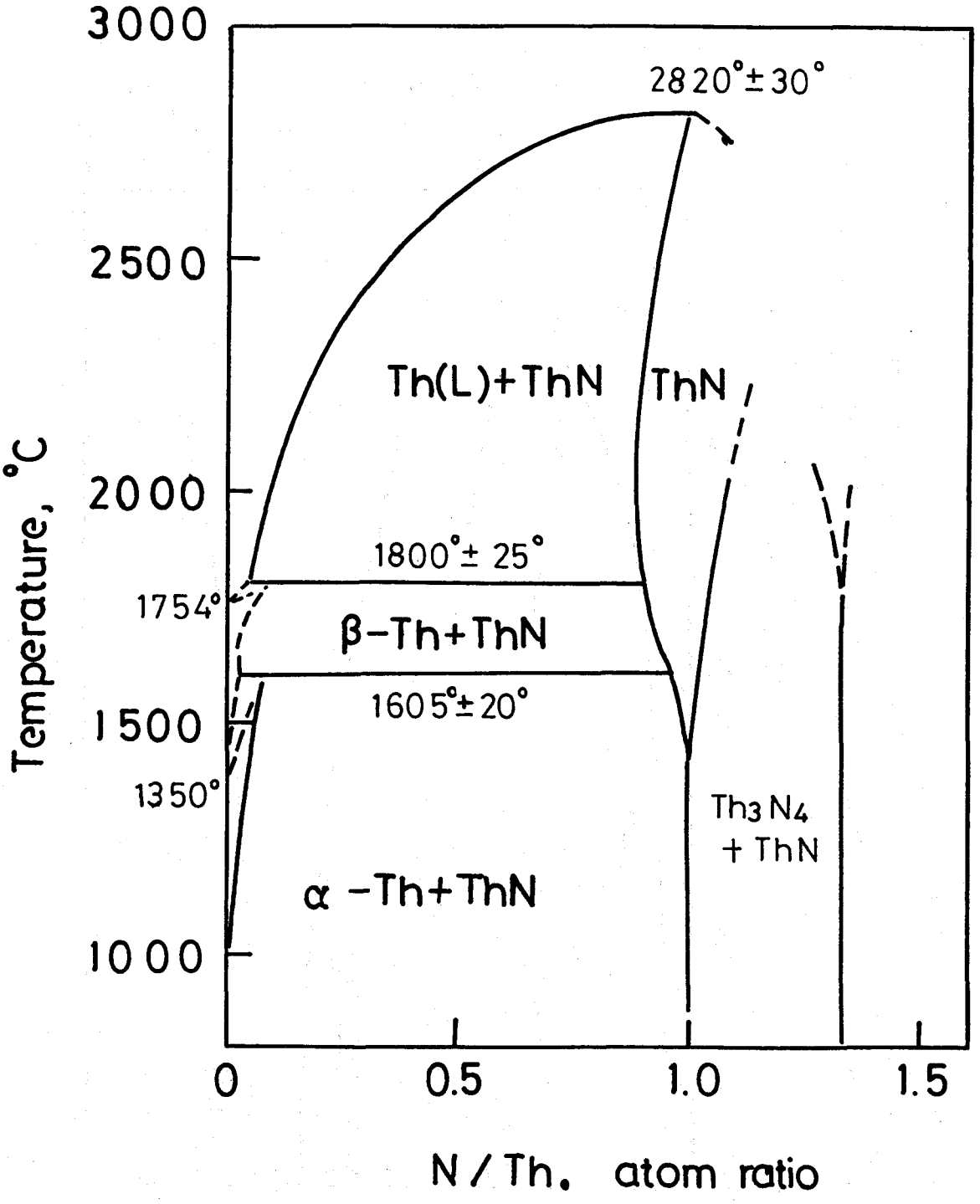

Fig. 1-3 Phase diagram of Th-N system

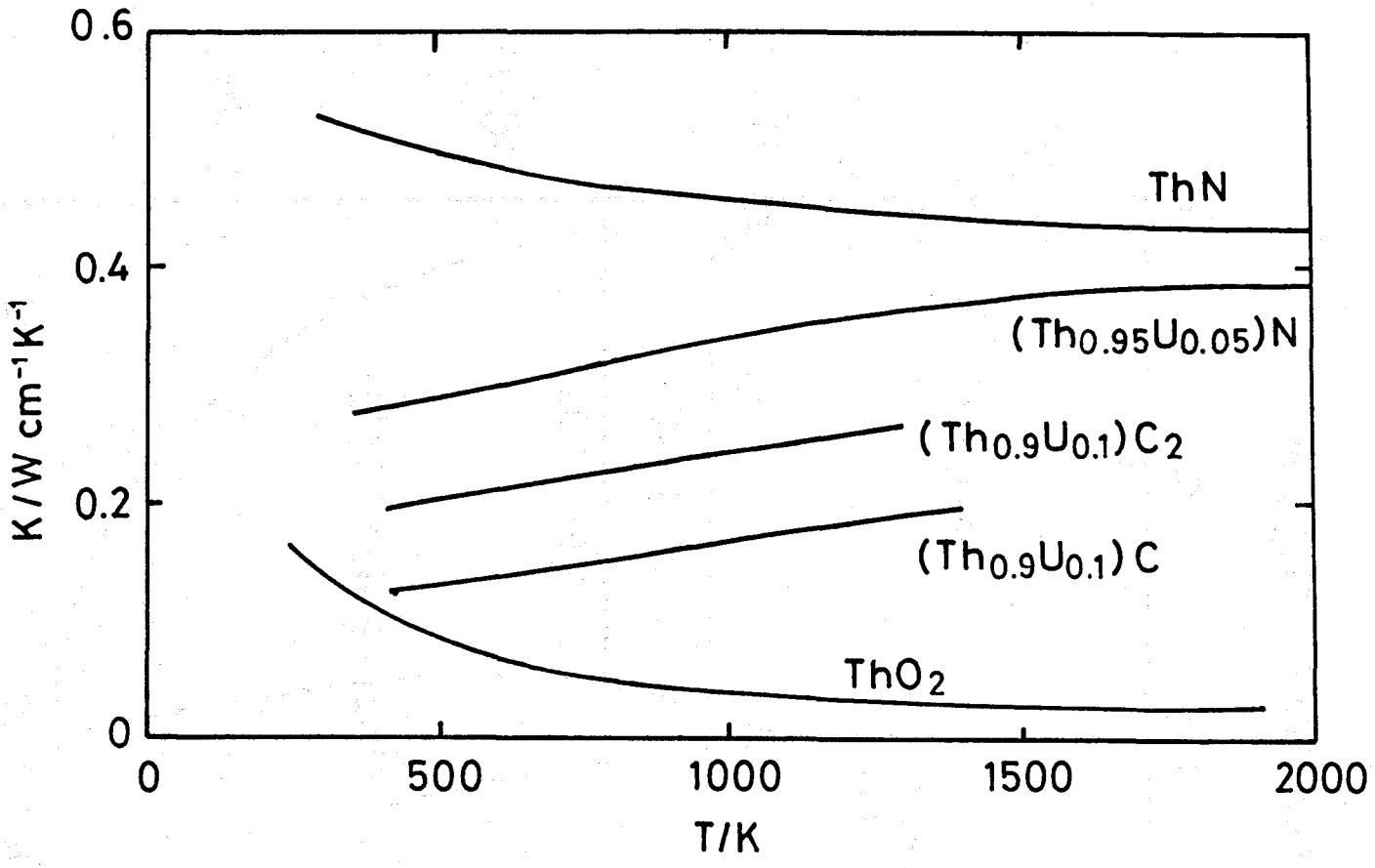

Fig. 1-4 Thermal conductivities of (Th,U)C, (Th,U)C_2 , ThN, (Th,U)N and ThO_2

2 PULVERIZATION OF THORIUM THROUGH HYDRIDING PROCESS

2-1 INTRODUCTION

The initial step of the preparation of ThN is the pulverization of metallic thorium since a thorium chip is used as the starting material in the present study .

It is common practice that metallic thorium is pulverized through hydriding process prior to nitriding thorium by the reaction of Th with N_2 or NH_3[1,2]. This process consisits of two steps: the formation of ThH_2 as the first step and the formation of Th_4H_{15} as the second step. However, no paper has reported explicitly as to at what stage of hydriding process pulverization occurs.

Rundle et al.[3] have first determined the crystal structure of ThH_2 to be a face-centered-tetragonal(fct) structure. According to the earlier work of Zachariasen[4], Th_4H_{15} crystallzies in bcc structure. The values of the lattice constants, a=5.734 and c=4.965Å for $ThH_{1.996}$ and a=9.116Å for Th_4H_{15} phase with H/Th=3.964 have been reported by Flotow and Osborne[5]. However, there is only a very limited knowlege of the variations of the lattice constants of the thorium hydrides with their H/Th ratio.

Although the pressure-composition-temperature(p-c-T) relationships for the two-phase region of Th and ThH_2 and for the mono-phase region of ThH_2 have been measured by a few authors[6,7], the equilibrium phase diagram for the Th-H system as a whole is far from being well-established, especially for the two-phase region consisting of ThH_2 and Th_4H_{15} and for the mono-phase region of Th_4H_{15}.

Thermodynamic quantities of ThH_2 and Th_4H_{15} with several restricted values of H/Th have been reported, but thier dependence on H/Th ratio still remains undetermined. It may be impossible at present to construct the phase diagram for the Th-H system from the reported values of thermodynamic quantities for ThH_2 and Th_4H_{15}.

In the present work, the pulverization process through

hydridng thorium has been explored with the help of the visual observation of the appearance of the sample during the process. The p-c-T relationships for Th-H system have been determined at 200, 300, 350 and 800°C. From these results, a tentative equilibrium phase diagram for Th-H system is proposed.

2-2 EXPERIMENTAL

The experimental apparatus shown in Fig. 2-1 consists of a vacuum system, a gas supply system, a pressure measurement system and a horizontal resistance furnace. A quartz reaciton tube, 450 mm in length and 20 mm in diameter, is placed in the cylindrical resistance furnace. The furnace comprises the upper and lower halves. They are connected with each other by a hinge in such a way that the upper half can be opened for visual observations of the specimen at intervals. Temperature measurement is performed by an A.C. thermocouple placed into a quartz tube of which the sealed end is located as close as possible to the specimen. Temperature is controlled by an on-off type thermoregulator activated by an A.C. thermocouple which is attached to the outer surface of the reaction tube. The vacuum system consists of rotary pumps and an oil-diffusion pumps with which the system can be evacuated up to 1×10^{-4} Pa. The gas supply system has an Hg bubbler, gas reservoirs and an Hg manometer.

Impurities in thorium ingot supplied from Mitsubishi Atomic Power Industry, Co. Ltd., are given in Table 2-1. Commercial hydrogen gas with a purity of 99.995% is used.

About 1 g of thorium specimen(2mm x 2mm x 20mm) is cut from thorium ingot with a crystal cutter. Specimen is polished with emery paper in xylene until it exhibits metallic luster. A quartz boat with an thorium specimen is placed in the center of the reaction tube. The system is evacuated to 1×10^{-4} Pa at room temperature, then hydrogen is admitted to the reaciton system through the gas supply system. After these operations, a desired experimental run is carried out.

2-3 RESULTS AND DISCUSSION

Hydriding process

The hydriding process in the literature[1,2] consists of the two hydriding steps and may be summarized as follows:

$$Th + H_2 = ThH_2 \qquad (600\text{-}700°C) \text{ the first step}$$
$$4ThH_2 + 3.5H_2 = Th_4H_{15} \qquad (200\text{-}350°C) \text{ the second step}$$

In the present work, a two-step hydriding process is also adopted. However, the second step is performed at 70°C. The selection of this temperature is guided by the work of Flotow and Osborne[5]. In preparing the Th_4H_{15} samples for thier calorimetric measurements, they made reaction of ThH_2 with H_2 at 60°C, and reported that the reaction proceeded very rapidly at this temperature.

A typical result of the hydrogen absorption behavior of thorium is given in Fig. 2-2. After placing the quartz boat with the thorium specimen(Photo. 1) in the center of the reaction tube and evacuating the system to 1×10^{-4} Pa, hydrogen gas was supplied gradually to the system from a commercial H_2 cylinder until the pressure reached 290 torr. Temperature was then raised to 650°C in about an hour. Hydrogen pressure approached a constant value in about half and an hour, showing the formation of ThH_2 phase. This state was maintained for about 22 hours to ensure the homogeneous hydride sample. Photo. 2 shows the appearance of the specimen at the point B in Fig. 2-2. As can be seen in Photo. 2, its color became grey and cracks occured on the edges of the specimen. Although temperature reached 70°C at the point C in Fig. 2-2, the pressure of hydrogen gas still remained unchanged. The color of the specimen was black and large crack appeared in the central part of the specimen(see Photo. 3) though the original shape of the specimen was retained. Thus, it is found that pulverization did not proceed appreciably at point C. Photo. 4 shows the appearance of the specimen at

the point D in Fig. 2-2. At this stage, the degree of pulverization proceeded to a considerable extent. This may correspond to the formation of Th_4H_{15} phase, since the hydrogen pressure reduced to about 180 torr at the point D. There still remained however, coarse granules , showing that a certain amount of unreacted ThH_2 existed. At the point E in Fig. 2-2, both temperature and hydrogen pressure reached constant values, respectively. This means the completion of the conversion of ThH_2 into Th_4H_{15} phase. As Photo. 5 shows, the specimen at the point E may be considered to be pulverized fine enough to be used as the starting materials for production of thorium nitrides.

From the above examples and the other similar experiments, it is found that the second step of the hydriding process, that is, the formation of Th_4H_{15}, is responsible for pulverization.

During the course of the present study, the second step of hydriding process at 200-300°C was also examined several times for comparison with hydriding at 70°C. The result shows that the hydriding at 70°C as the second step is much more effective for pulverization than at temperatures between 200 and 350°C.

P-c-T relationship

Pressure-composition-temperature relationships for Th-H system have been determined at temperatures, 200, 300, 350 and 800°C. Powdered Th_4H_{15} has been adopted as the starting materials for a series of p-c-T measurements at each temperature, since the use of powdered samples may make it easier to establish the equiribrium and to obtain the homogeneous specimen. The results of the measurements are shown in Fig. 2-3, where the p-c-T relationships at 800°C by Peterson and Rexer[6] and by Mallett and Campbell[7] are also given. The present result at 800°C may be in good agreement with those of the above mentioned authors within the experimental error. As far as the present author is concerned, no information on the isotherms at temper-

atures below 400°C is available in the literature. The measured p-c-T relationship at 200°C in the present work covers only the mono-phase region of Th_4H_{15}, while the data at 300°C involves the two-phase region of ThH_2 and Th_4H_{15} and the mono-phase region of Th_4H_{15}. The isotherm at 350°C shows a steep slope and it lies in the mono-phase region of ThH_2. According to the results of Peterson and Rexer[6], who have dertermined the isotherms in the ThH_2-region at temperatures from 500 to 800°C at intervals of 50°C, all of the isotherms have steep slopes and the neighboring isotherms are very close to one another. It should be noted that the isotherms at 300 and 350°C are distantly apart from each other, as can be seen in Fig. 2-3.

These results may suggest that the equilibrium hydrogen pressure in the two-phase region of ThH_2 and Th_4H_{15}, which should be drawn horizontally, varies very sensitively with temperature. In other words, the isotherm in this two-phase region descends very noticeably as temperature lowers.

In order to represent the state of the Th-H system, three variables, hydrogen pressure, composition and temperature, are required. The phase diagram of the Th-H system appearing in the literature up to the present are qualitative and exclusively the temperature-composition diagrams, where hydrogen pressure as one of the variables is not included explicitly. Figure 2-4 shows a tentative pressure-composition diagram for the Th-H system constructed from the results of the p-c-T measurements in the present work.

2-4 CONCLUSION

The conclusions drawn from the present study are:

1) In the hydriding process of thorium, which consists of the formation of ThH_2 as the first step and the formation of Th_4H_{15} as the second step, the formation of Th_4H_{15} through the reaction of ThH_2 with H_2 is found to be responsible for the pulverization of metallic thorium. This reaction is accompanied by the transformation of the crystal structure

from fct of ThH_2 to bcc of Th_4H_{15}.

2) The reaction of formation of Th_4H_{15} by the reaction of ThH_2 with H_2 should be performed at lower temperatures so as to ensure the complete conversion of ThH_2 into Th_4H_{15} for the purpose of production of powdered thorium.
3) The pressure-composition-temperature relationships for Th-H system are determined at 200, 300, 350 and 800°C. From these results, a tentative equilibrium diagram for the binary Th-H system is proposed.
4) The equilibrium hydrogen pressure in the two-phase region of ThH_2 and Th_4H_{15} varies very sensitively with temperature. In other words, the isotherm in this region varies very markedly as temperature changes.

REFERENCE

[1] P.Chiotti and B.A.Rogers, Metal Progress, 60(1951)60.
[2] S.Ozaki, M.Kanno and T.Mukaibo, J.Nucl.Sci.Technol., 8(1971)41.
[3] R.E.Rundle and E.U.Wollan, Acta Cryst., 5(1952)22.
[4] W.H.Zachariasen, Acta Cryst., 6(1953)393.
[5] H.E.Flotow and D.W.Osborne, J.Chem.Thermodyn., 10(1978)537.
[6] D.T.Peterson and J.Rexer, J.Less-Common Met., 4(1962)92.
[7] M.W.Mallett and I.E.Campbell, J.Am.Chem.Soc., 73(1951)4850.

Table 2-1 Impurities in the starting thorium metal

Element	p.p.m.
Al	100
B	0.2
Cd	<0.2
Co	<1
Cr	10
Cu	5
Mg	20
Mn	10
Ni	10
Fe	100
Mo	<5
H	271
C	<250
U	<5
Cl	<10
Dy	<0.1
Eu	<0.1
Sc	<0.1
Sm	<0.1

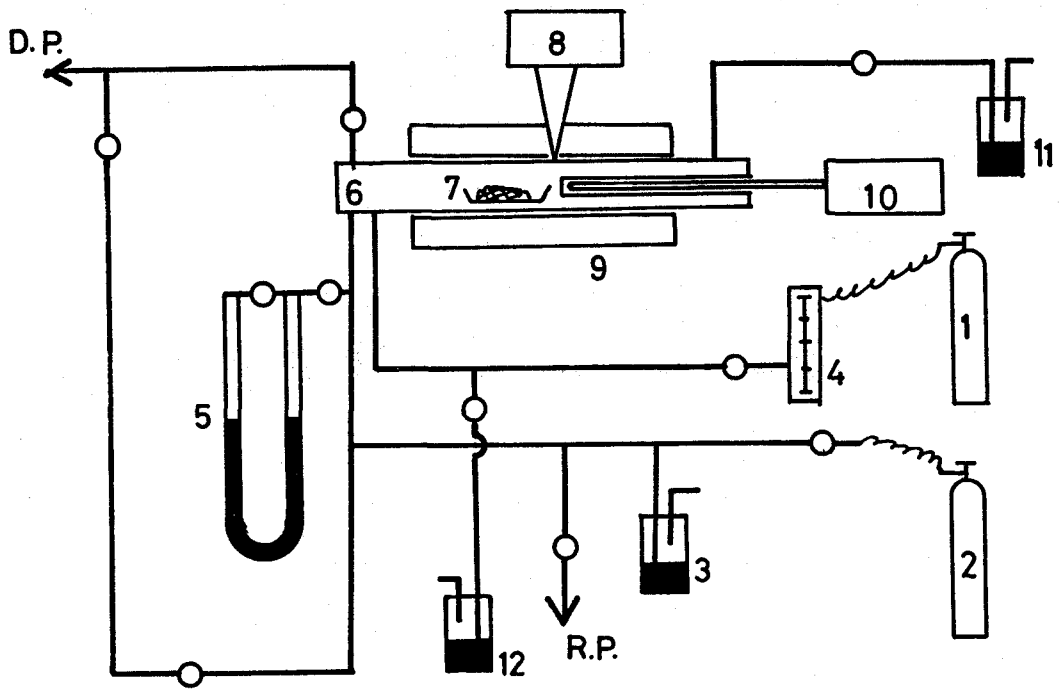

1. Nitrogen cylinder
2. Hydrogen cylinder
3. 12. Hg bubbler
4. Flow meter
5. Hg manometer
6. Reaction tube
7. Specimen
8. Thermoregulator
9. Furnace
10. Thermometer
11. Oil bubbler

Fig. 2-1 Apparatus for pulverization of metallic thorium

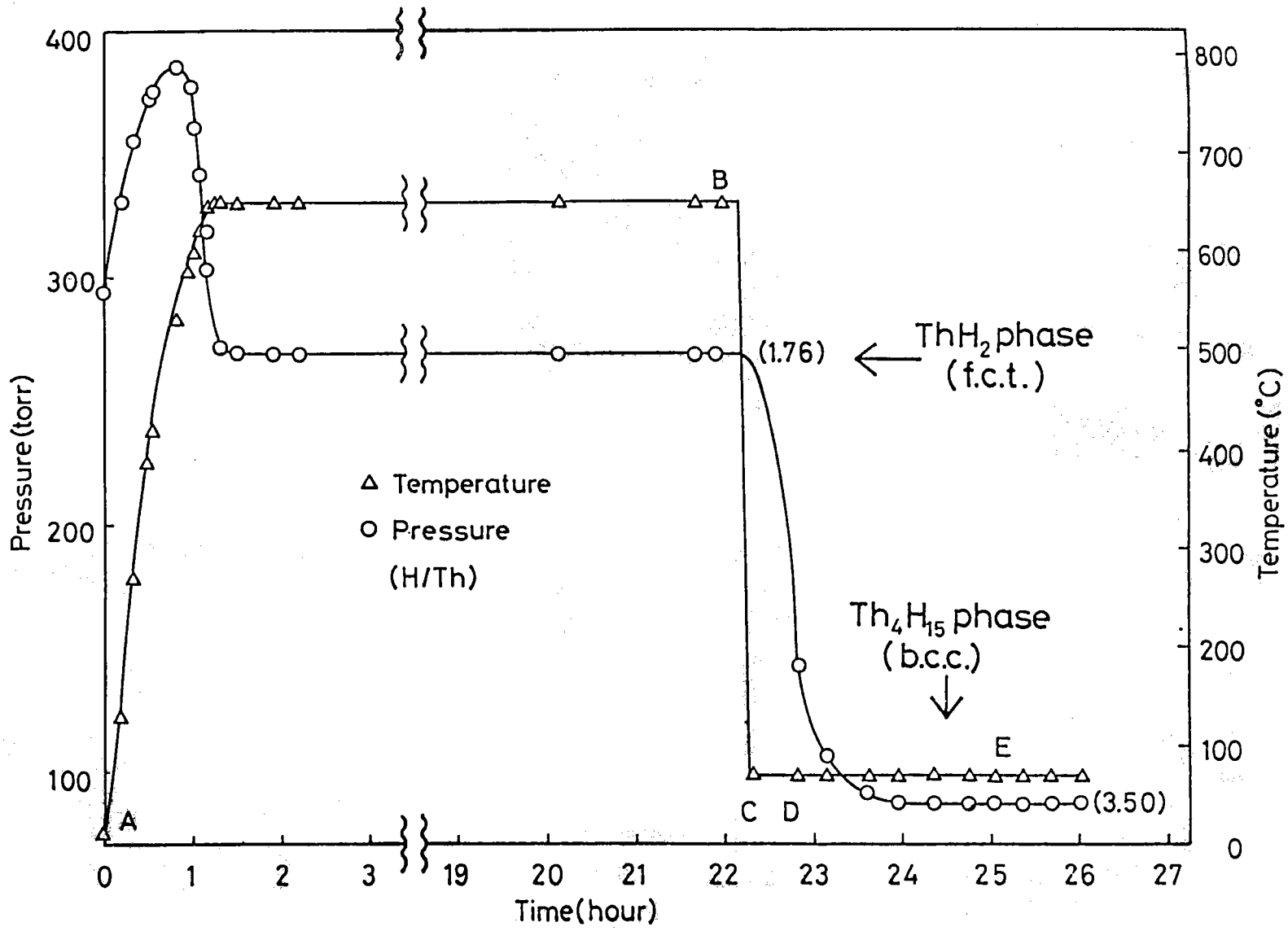

Fig. 2-2 Hydrogen absorption behavior at an experimental run (in a closed system consisting of thorium and H_2)

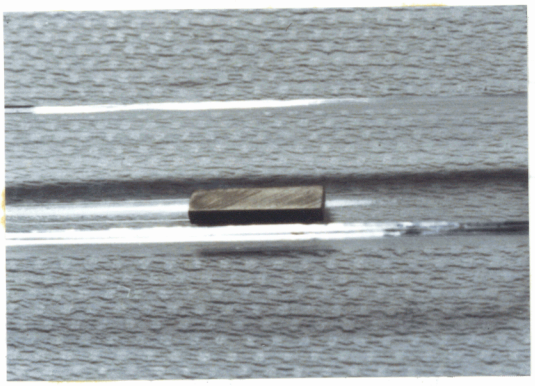

Photo. 1 The specimen at the point A

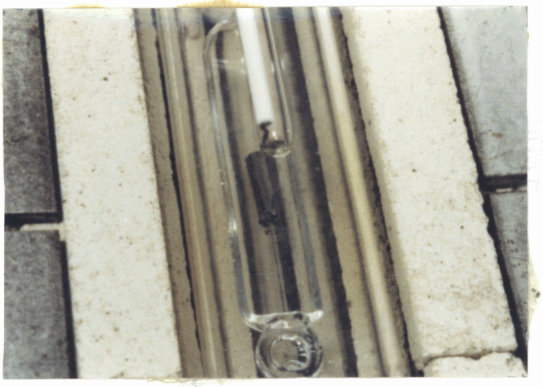

Photo. 2 The specimen at the point B

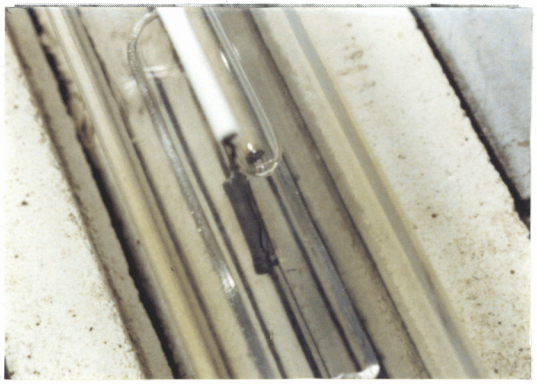

Photo. 3 The specimen at the point C

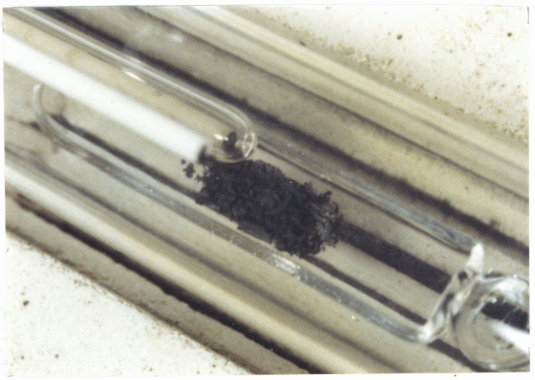

Photo. 4 The specimen at the point D

Photo. 5 The specimen at the point E

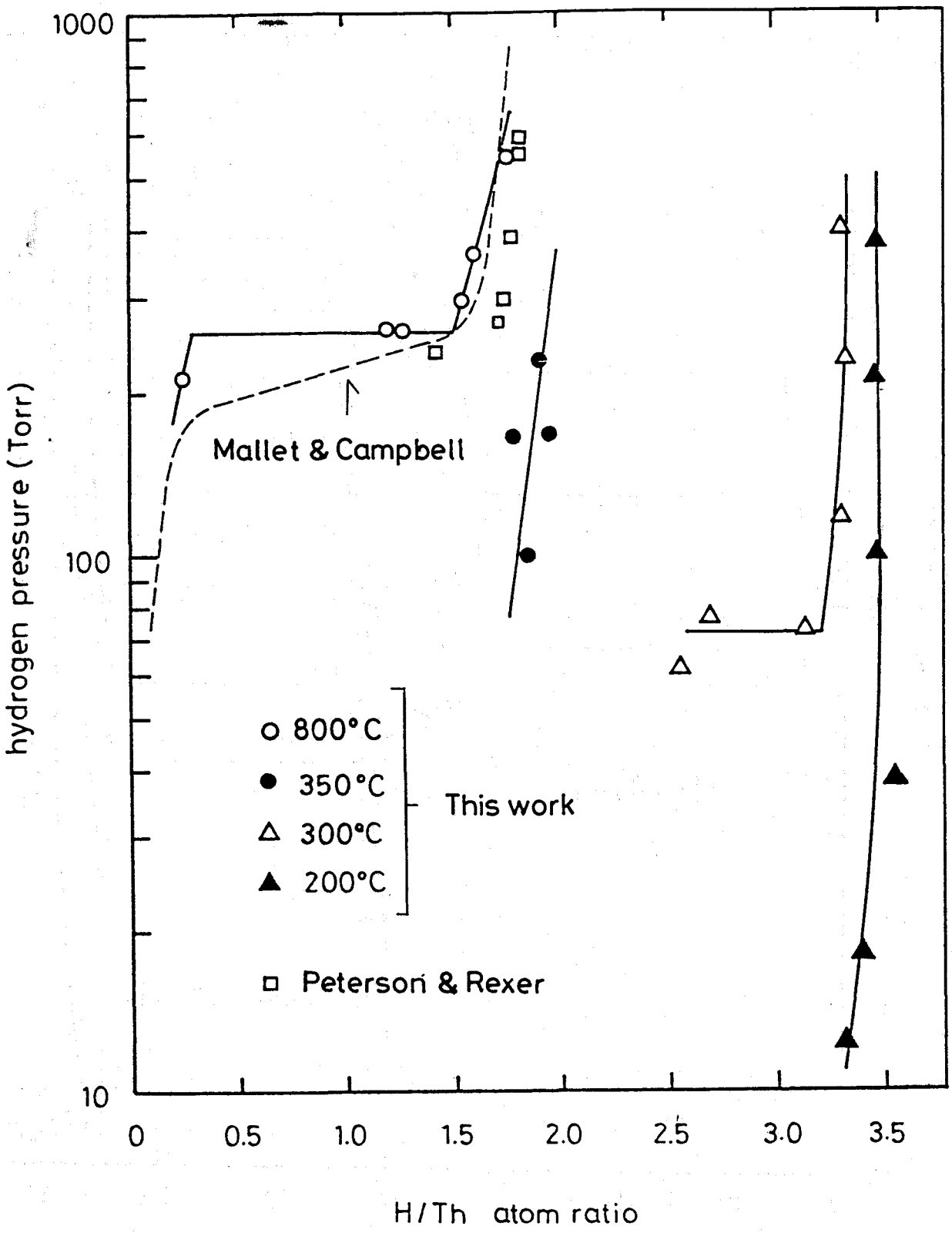

Fig. 2-3 Pressure-composition-temperature relationships in the Th-H system

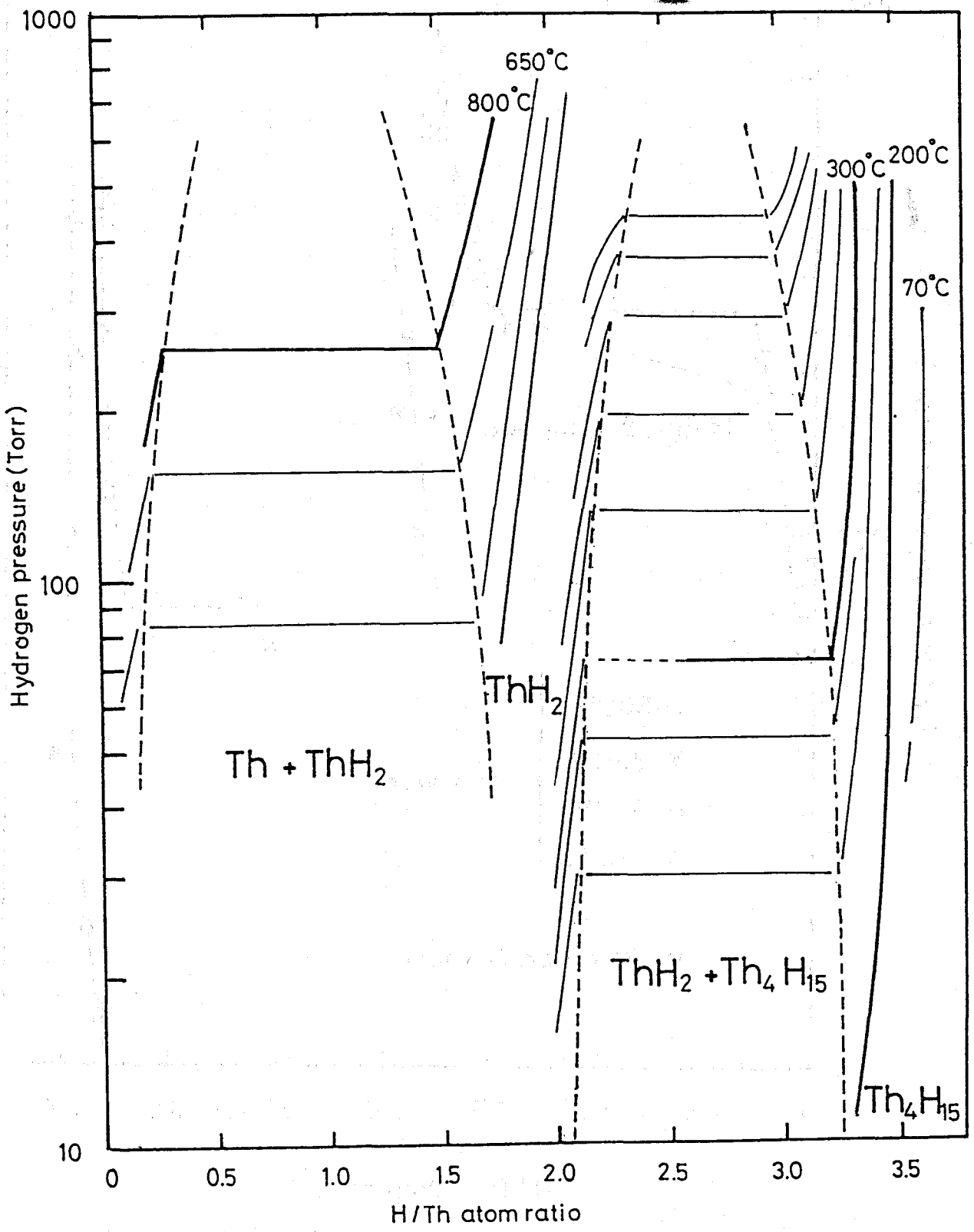

Fig. 2-4 Tentative phase diagram for Th-H system.

3 PREPARATION OF THORIUM NITRIDES

3-1 INTORDUCTION

As already mentioned in Chapter 2, the pulverization method of metallic thorium has been established. The hydriding process consists of the formation of ThH_2 at 650°C as the first step and the formation of Th_4H_{15} at 70°C as the second step. The second step is responsible for pulverization. Powdered metallic thorium can be obtained by thermal decomposition of powdered Th_4H_{15} into thorium powder and hydrogen gas at temperatures above 900°C. The next step is preparation of thorium nitrides using thus obtained Th_4H_{15} powder or thorium powder.

Several methods for the preparation of Th_3N_4 have been reported. Chiotti[1] prepared Th_3N_4 by passing NH_3 or N_2 over thorium metal powder at temperatures between 400 and 940°C. Aronson and Auskern[2] produced Th_3N_4 by heating thorium powder in N_2 under 1 atm at 900°C for about one hour. Benz et al.[3] converted thorium hydride to Th_3N_4 in a stream of N_2 at temperatures from 200 to 900°C. Ozaki et al.[4] prepared Th_3N_4 powder by the reaction of thorium hydride with N_2 under 1 atm at 900°C for about 3 hours.

Thorium mononitride, ThN, can be made in the following two ways: (1) the direct reaction of Th metal with N_2 at high temperatures, say 2000°C, and (2) the thermal decomposition of Th_3N_4. Olson and Mulford[5] obtained ThN containing only 400 p.p.m. oxygen by weight through the direct nitriding of Th metal under 2 atm. N_2 at 2000°C. Ozaki et al.[4] prepared ThN by the thermal decomposition of Th_3N_4 in vacuum at 1450-1550°C. Benz et al.[3] obtained ThN by heating Th_3N_4 in vacuum at 1500°C. Their X-ray diffraction examinations revealed the presence of ThO_2 as an impurity in the products. Although the method (1) usually provides a pure ThN free from ThO_2, one of the main purposes of this work is to establish the method of preparing ThN containing no ThO_2 by the thermal decompsition.

In the present study, a large amount of experimenal work

has been expended to prepare Th_3N_4 and some of the representative results will be discussed in terms of conditions of nitriding process. Moreover, the crystal structure of Th_3N_4 has been re-examined with the X-ray diffraction pattern of Th_3N_4 without impurity phase.

For the preparation of ThN, thermal decomposition of Th_3N_4 has been performed under various conditions and the products have been examined as a function of temperature and time. In the Th-N-O system there exits ThN, Th_3N_4, ThO_2 and Th_2N_2O as solid phases, and gaseous O_2 and N_2. The thermodynamic stability of these solid compounds has been evaluated as a function of $P(O_2)$ and $P(N_2)$ and compared with the experimental results.

3-2 PREPARATION OF Th_3N_4

3-2-1 EXPERIMENTAL

Powdered thorium or Th_4H_{15} produced as described in Chapter 2 was nitrided in an atmosphere of nitrogen or NH_3 at temperatures from 700 to 900°C. To avoid exposure of thorium or Th_4H_{15} to air, this nitriding following hydriding was performed in the same apparatus used for the hydriding.

Nitrogen and thorium contents of each sample prepared were determined by combustion to ThO_2 at 800°C in an oxygen filled furnace connected to a gas chromatograph (Sumigraph NC-80; Sumitomo chemical Industry Co.Ltd.).

X-ray diffraction powder patterns for the samples were obtained at room temperature with a diffractometer (Rigaku Denki; Geiger flex rad-rA) using nickel-filtered CuKα radiation. The widths of both the divergence slit and scatter slit were 1° and that of the receiving slit was 0.15 mm. A step scanning width at an interval of $2\theta = 0.02°$ and a counting period of 0.4 sec. were adopted. Each Th_3N_4 sample was embedded in an aluminum sample holder with epoxy resin in order to minimize oxidation during the X-ray diffraction neasurement. This procedure is

shown in Fig. 3-1 and 3-2.

3-2-2 RESULTS AND DISCUSSION

The results of the chemical analysis of Th_3N_4 from three representative runs are shown in Table 3-1 together with the conditions of hydriding, dehydriding and nitriding processes. In run 1, the chemical analysis shows that the [N]/[Th] mol ratio of the product is 1.23 ± 0.03, which is rather lower than the value of 1.33 corresponding to the theoretical value of Th_3N_4. In run 2, the application of NH_3, instead of nitrogen, yields little increase in the nitrogen content of the resulting Th_3N_4, judging from the chemical analysis. In order to obtain homogeneous Th_3N_4 powder, it is desirable to use thorium or Th_4H_{15} in the form of fine powder (as fine as possible), since with these fine powders, nitrogen can diffuse deeper into the inner part of the particles. It has been observed that sintering occurs to some extent during the dehydriding process at 900°C. This may partly explain the difficulty in obtaining a Th_3N_4 phase with an [N]/[Th] ratio close to 1.33 encountered in run 1 and 2. In run 3, the reaction of Th_4H_{15} powder with flowing nitrogen at 800°C was adopted. The [N]/[Th] ratio of 1.30 ± 0.03 obtained by chemical analysis is close to the theoretical value. (Since the combustion of Th_3N_4 by oxygen for chemical analysis always results in the formation of a very small amount of NO_2 gas in addition to nitrogen , the true values of [N]/[Th] determined by the chemical analysis may have slightly higher values than those given in Table 3-1.) The above chemical analytical results, together with those for the other samples which are not described here, suggest that the reaction of Th_4H_{15} with a stream of nitrogen at 800°C gives the highest possible nitrogen content.

The X-ray diffraction pattern for Th_3N_4 produced by the reaction of thorium powder with nitrogen in a closed system is shown in Fig. 3-3(pattern (a)). Although no peaks corresponding to ThO_2 were detected, the separation of the (211)

and (333) peaks of Th_3N_4 is unsatisfactory. Pattern(b) is the X-ray diffraction pattern of Th_3N_4 obtained by the reaction of Th_4H_{15} with flowing nitrogen at 800°C. The separation of the (211) and (333) peaks is excellent showing the formation of Th_3N_4 with a high degree of crystallinity. In addition to the results presented here, a considerable amount of work has been carried out in an effort to find the optimum conditions for preparing pure and homogeneous Th_3N_4 with a high degree of crystallinity. From all of the results, it may be concluded that the reaction of Th_4H_{15} with flowing nitrogen at about 800°C is most suitable for preparing pure Th_3N_4 with a high degree of crystallinity.

As already described in Chapter 1, the structure of Th_3N_4 was first studied by Benz and Zachariasen [6] who concluded that Th_3N_4 is rhombohedral with $a = 9.398 \pm 0.002$Å and $\alpha = 23.78 \pm 0.001°$. Since their description is only one that has been reported, a re-examination of the structure of Th_3N_4 was made in this work using Th_3N_4 obtained by the reaction of Th_4H_{15} with flowing nitrogen at 800°C. The observed intensities of the X-ray diffraction peaks are summarized in Table 3-2, together with those calculated based on the description that the three thorium atoms per rhombohedral cell are in positions (000) and $\pm$(zzz) with z=2/9. This arrangement of thorium atoms is shown in Fig. 3-4. The intensity I is calculated from the expression;

$$I = \frac{1+\cos^2\theta}{\sin^2\theta\cos\theta} \times P \times |F|$$

where θ is the Bragg angle, P is the multiplicity and F is the structure factor. Atomic scattering factors f used in the calculation of F were taken from the International Tables [7]. As seen from Table 3-2, the present result shows that the strongest peak is the (211) peak, which agrees well the theoretical result. However, Benz and Zachariasen reported that the strongenst line was the (333) peak. Thus, observed values in this work agree fairly well with the calculated ones although some fainter peaks cannot be detected.

3-3 PREPARATION OF ThN

3-3-1 EXPERIMENTAL

Thermal decomposition of Th_3N_4 was performed in an alumina reaction tube in which a molybdenum tube was inserted in order to avoid the reaction of samples with oxygen released from the reaction tube. The reaction tube could be evacuated up to $1x10^{-4}$ Pa with an oil diffusion pump and be heated up to 1400°C by means of a furnace with a SiC heater. The schematic diagram of the apparatus is shown in Fig. 3-5.

Th_3N_4 was prepared by the reaction of Th_4H_{15} with flowing nitrogen at 800°C, as described in section 3-2. The Th_3N_4 powder in a molybdenum boat was placed in the center of the alumina reaction tube and then it was heated up to a desired temperature in a vacuum or in flowing gas(H_2 or He) at a flow rate of 100 ml/min. After the temperature was maintained for the desired period of time, the sample was cooled to room temperature. The product was taken out of the reaction tube and transferred to an Ar-filled glove box for analysis.

The X-ray diffraction measurements and the determination of thorium and nitrogen contents of the decomposition products were performed in the same way as described in section 3-2-1.

3-3-2 RESULTS AND DISCUSSION

Thermal decomposition in a vacuum

The phases identified by X-ray diffraction measurements and the [N]/[Th] mol ratios determined by chemical analysis for the products obtained by thermal decomposition in a vacuum are summarized in Table 3-3, where the conditions for the thermal decomposition are also given. The product obtained on heating at 1400°C for 2 hours contained ThN as a major phase and ThO_2

as a minor phase. According to the Th-ThO_2 phase diagram reported by Benz[8](Fig. 1-1), ThO_2 is stoichiometric at the temperatures examined in the present study. Thus, from the value of 0.95 for the [N]/[Th] mol ratio, it follows that the product contains 95 mol % of ThN.

Decreasing the temperature from 1400 to 1300°C(Run 2), the minor phases changed from ThO_2 to a mixture of ThO_2 and Th_2N_2O but the amounts of these impurities decreased, judging from the X-ray diffraction patterns. With decreasing time at the fixed temperature(Run 2 and 3), the [N]/[Th] ratio became higher although little significant difference in the X-ray diffraction patterns could be observed.

The thermal decomposition on heating at 1250°C for 1 hour yielded the product containing ThN as a major phase and only Th_2N_2O as a trace. The [N]/[Th] ratio of the product was 0.98. Thus, it is seen that a decrease in time and temperature of the heat treatment reduces undesirable oxidation of the sample.

It should be noted that the product in Run 6 did not contain the oxdie phases(ThO_2 and Th_2N_2O) even though a time as long as 14 hours was allotted to the thermal decomposition. From these results it is expected that pure ThN phase may be prepared by choosing suitable conditions between those of Run 5 and Run 6.

Thermal decomposition in flowing gas

The experimental results for the thermal decomposition of Th_3N_4 in flowing gas are summarized in Table 3-4. No appreciable difference in the results was observed whether H_2 gas or He gas was employed.

In order to know the effect of reaction time on the type of products, three experiments were performed at 1400°C(Run 7-9). It is seen from the results given in Table 3-4 that the amounts of oxide phases ThO_2 and Th_2N_2O decrease with decreasing time. Thus, a decrease in the time reduces the oxidation of the sample.

In order to clarify the effect of temperature on the kind

of reaction products, four experiments were made(Run 8, 10-12). The reaction time was kept constant 2 hours. On decreasing the temperature of the heat treatment, the Th_2N_2O content decreased and the Th_3N_4 content increased. In other words, a decrease in temperature suppresses the undesirable oxidation of the sample, although the complete thermal decomposition cannot be established.

Th-N-O phase stability diagram

According to studies on the preparation of ThN by thermal decomposition of Th_3N_4 performed by Benz et al.[3] and Ozaki et al.[4], ThO_2 always exists as the impurity phase together with ThN. They did not mention the occurrence of Th_2N_2O as the impurity phase. However, the present study shows that the impurity oxide changes from ThO_2 to Th_2N_2O with decreasing reaction temperature and time. Therefore, it may be important to consider the phase stability of the Th-N-O system, including Th_2N_2O as well as ThO_2, ThN and Th_3N_4 as the solid phases.

For this purpose, phase stability diagrams for the Th-N-O system have been prepared. The system considered in the present study contains solid phases ThN, Th_3N_4, ThO_2 and Th_2N_2O and gaseous N_2 and O_2. The equilibria in such a multiphase, multicomponent system can be treated as follows[9].

First, the following four equilibria will be considered:

$$Th + 1/2N_2 = ThN \quad \text{----- (1)}$$
$$3Th + 2N_2 = Th_3N_4 \quad \text{----- (2)}$$
$$Th + O_2 = ThO_2 \quad \text{----- (3)}$$
$$2Th + N_2 + 1/2O_2 = Th_2N_2O \quad \text{----- (4)}$$

Then the element, Th, which is not considered as being present in the system is eliminated by several combinations of these equilibria.

$$Th_3N_4 + 3O_2 = 3ThO_2 + 2N_2 \quad \text{----- (5)}$$

$ThN + O_2 = ThO_2 + 1/2N_2$ ----- (6)

$2Th_3N_4 + 3/2O_2 = 3Th_2N_2O + N_2$ ----- (7)

$Th_2N_2O + 3/2O_2 = 2ThO_2 + N_2$ ----- (8)

$2ThN + 1/2O_2 = Th_2N_2O$ ----- (9)

$Th_3N_4 = 3ThN + 1/2N_2$ ----- (10)

In each of equilibria (5)-(10), the degree of freedom is 2(F=C-P+2). If temperarture, T, is fixed, and the second degree of freedom is chosen as $P=P_{N_2}+P_{O_2}$, then, for example, in the equilibrium (5) the values of P_{N_2} and P_{O_2} are fixed by the following two relations;

$$P = P_{O_2} + P_{N_2} \text{ and } K_{(5)} = P_{N_2}^{\ 2}/P_{O_2}^{\ 3}$$

where $K_{(5)}$ is equilibrium constant for the equilibrium (5), and

$$\ln K_{(5)} = -\Delta G^\circ_{(5)} = \Delta G^\circ_{(Th_3N_4)} - 3\Delta G^\circ_{(ThO_2)}$$

$$= \Delta G^\circ_{(2)} - 3\Delta G^\circ_{(3)}$$

From the reported values of ΔG°[10] for the reactions, (2) and (3), the following expression can be obtained

$$\ln P_{N_2}^{\ 2}/P_{O_2}^{\ 3} = 566910 - 50.45T \text{ [for the equilibium(5)]}$$

Thus, the conditions of the phase equilibrium (5) can be represented on an isothermal diagram, the coordinates of which are P_{O_2} and P_{N_2}. The variation of P_{O_2} and P_{N_2} for the equilibium at 1400°C is shown as the line AB in Fig. 3-6. If ThN and Th_2N_2O were not involved, Th_3N_4 would be stable with respect to ThO_2 below the line AB and the reverse would be the case above the line AB.

Equilibia (6), (7) and (8) can be determined in the similar way and the variations of P_{O_2} and P_{N_2} are shown as lines CD, EF and GH for (6), (7) and (8), respectively. For equilibria (9), P_{O_2} is constant and given as $P_{O_2}^{\ -1/2} = K_{(9)}$. Similarly for (10), P_{N_2} is constant and given as $P_{N_2}^{\ 1/2} = K_{(10)}$. These are

represented by the lines IJ and KL.

It is seen from Fig. 3-6 that the lines EF, IJ and KL cross at the point M, the lines CD, GH and IJ cross at the point N and the lines AB and IJ cross at the point O. Since there must be four stable single-phase fields, some of these lines represent metastable equilibria. It is a property of such phase diagrams that the lines of metastable and stable equilibria radiate alternatively from points such as M, N and O. Thus, one set of lines MK, MN and MF are stable equilibrium lines. Similary, NM, NC and NH, and OM and ON are stable equiribium lines. The final phase diagram is shown in Fig. 3-7.

Figure 3-7 is the Th-N-O phase stability diagram at 1400°C. constructed by the above mentioned method. In this figure ThN is stable in the segment AFEB, Th_3N_4 in the segment BEC, Th_2N_2O in the segment CEFD and ThO_2 in the segment AFD. As seen from this Figure, thorium nitrides are stable with respect to thorium oxides only at very low oxygen pressure. And at such a low oxygen pressure, if the nitrogen pressure is lower than about $1x10^{-2}$ atm($1x10^{3}$ Pa), ThN is stable with respect to Th_3N_4. Thus, in order to prepare ThN with no other phases, thermal decomposition of Th_3N_4 at 1400°C must be performed at a nitrogen pressure lower than about $1x10^{-2}$ atm. However, the oxygen pressure required is so low, e.g. $1x10^{-30}$ atm., that it cannot be attained easily under ordinary experimental conditions. Even in a vacuum which can normally be achieved in a laboratory, for example, $1x10^{-9}$ atm($1x10^{-4}$ Pa), ThO_2 is very stable with respect to ThN.

Figure 3-8 shows the phase stability diagrams at 800, 1100, 1400 and 2000°C obtained by the similar way as for 1400°C. The stable region of ThN, which corresponds to the segment BEFA in Fig. 3-7, moves downwards with decreasing temperature. Thus, the oxygen and nitrogen pressures required for preparation of pure ThN become lower with decreasing temperature. It can therefore be concluded that it is very difficult to prepare ThN by thermal decomposition of Th_3N_4 at a low temperature, say 1400°C, from the thermodynamic point of view.

Nevertheless, the products containing ThN together with ThO_2 and/or Th_2N_2O could be prepared experimentally. The ratio

of ThN to the oxides varied according to the experimental conditions, in particular temperature and time. This means that both the thermal decomposition of Th_3N_4 and the oxidation of thorium nitrides take place simultaneously. It is, therefore, a kinetic matter whether ThN containing no oxide phases can be prepared or not. Judging from the experimental results which showed products containing more than 95 mol % ThN could be obtained, it may be possible to prepare the ThN phase without the oxide phase by choosing suitable conditions of temperature and time, in such a way that only the decomposition of Th_3N_4 occurs without the oxidation of nitrides.

The comparison between the results of thermal decomposition in a vacuum and those in flowing gas suggests that the thermal decomposition in a vacuum is more favorable than that in flowing gas. An explanation of the results may be that the nitrogen gas resulting from the reaction $Th_3N_4 = 3ThN + 1/2N_2$ may be removed more rapidly in a vacuum than in flowing gas.

3-4 CONCLUSION

1) Of all the experiments carried out, the reaction of Th_4H_{15} with flowing N_2 at 800°C yields Th_3N_4 with the highest nitrogen content and the highest degree of crystallinity.
2) Material containing more than 95% ThN could be obtained by thermal decomposition of Th_3N_4.
3) The Th-N-O phase stability diagrams were constructed from thermodynamic calculations.
4) Although ThN is extremely unstable from a thermodynamic point of view, the present experimental results suggest that the kinetics play an important role in preparing ThN containing no thorium oxide phases.

REFERENCE

[1] P.Chiotti, J.Am.Ceram.Soc., 35(1952)123.

[2] S.Aronson and A.B.Auskern, J.Phys.Chem., 70(1966)3937.
[3] R.Benz, C.G.Hoffman and G.N.Rupert, J.Am.Chem.Soc., 89(1967)191.
[4] S.Ozaki, M.Kanno and T.Mukaibo, J.Nucl.Sci.Tech., 8(1971)41.
[5] W.M.Olson and R.N.R.Mulford, J.Phys.Chem., 69(1965)1223.
[6] R.Benz and W.H.Zachariasen, Acta Cryst., 21(1966)838.
[7] International Tables for X-ray Crystallography, vol.3 Kynoch Press, Birminghan 1962.
[8] R.Benz, J.Nucl.Mat., 29(1968)43.
[9] D.R.Gaskel, "Introduction to Metallurgical Thermodynamics", McGraw-Hill, New York, 1973, pp.410.
[10] M.H.Rand, O.von Golobeck, R.Ferro. K.Girgis and A.L.Dragoo, in O.Kubaschewski (ed.), "Thorium: Physico-Chemical Properties of its Compounds and Alloys", I.A.E.A., Vienna, 1975.

Table 3-1 Preparation of Th_3N_4

Run No.	1	2	3
Hydriding process	650°C $P(H_2)$=300torr 20h Quenching to 70°C 70°C $P(H_2)$=100torr 4h		
Dehydriding process	900°C $P(H_2)=1\times10^{-5}$torr 1h		No dehydriding process
Nitriding process	In a closed system $P(N_2)$=450torr 700°C 22h 900°C 2h 700°C 3h	In flowing NH_3 300ml/min. 900°C 10h	In flowing N_2 100ml/min. 800°C 10h
N/Th mol ratio	1.23±0.03	1.22±0.03	1.30±0.03

Table 3-2 X-ray diffraction data of Th_3N_4

hkl	Relative intensity Obs.	Cal.	Benz et al. [6]
100	43	37	w
110	31	15	vw
333	60	24	vs
211	100	100	m
322	-	8	vw
332	7	15	w
433	-	11	w
443	-	4	vvw
101	36	20	m
544 321	25	23	m
554	21	19	w
111 222	-	7	vw
432 220	33	41	s

Table 3-3 Analyses of the thermal decomposition products of Th_3N_4 in a vacuum

Thermal decomposition Run NO.	Temp. (°C)	Time (h)	N/Th mol ratio	Phases Th_3N_4	ThN	Th_2N_2O	ThO_2
1	1400	2	0.95	-	+++	-	++
2	1300	2	0.96	-	+++	+	+
3	1300	1	0.97	-	+++	+	+
4	1300	1/3	0.97	-	+++	+	+
5	1250	1	0.98	-	+++	+	-
6	1100	14	1.12	+++	+++	-	-

+++; major phase, ++; minor phase, +; trace, -; not detected

Table 3-4 Analyses of the thermal decomposition products of Th_3N_4 in flowing gas

Thermal decomposition Run NO.	Temp. (°C)	Time (h)	N/Th mol ratio	Phases Th_3N_4	ThN	Th_2N_2O	ThO_2
7†	1400	5	1.01	-	+++	++	+
8*	1400	2	1.04	-	+++	++	-
9#	1400	0.5	1.12	+++	+++	+	-
8*	1400	2	1.04	-	+++	++	-
10*	1350	2	1.19	+++	+++	+	-
11*	1300	2	1.25	+++	-	-	-
12*	1250	2	1.24	+++	-	-	-

+++; major phase, ++; minor phase, +; trace, -; not detected
†;Thremal decomposition in flowing H_2.
*;Thermal decomposition in flowing He.
#;Thermal deocmposition was done in both atmospheres but the resut corresponds to that in flowing He.

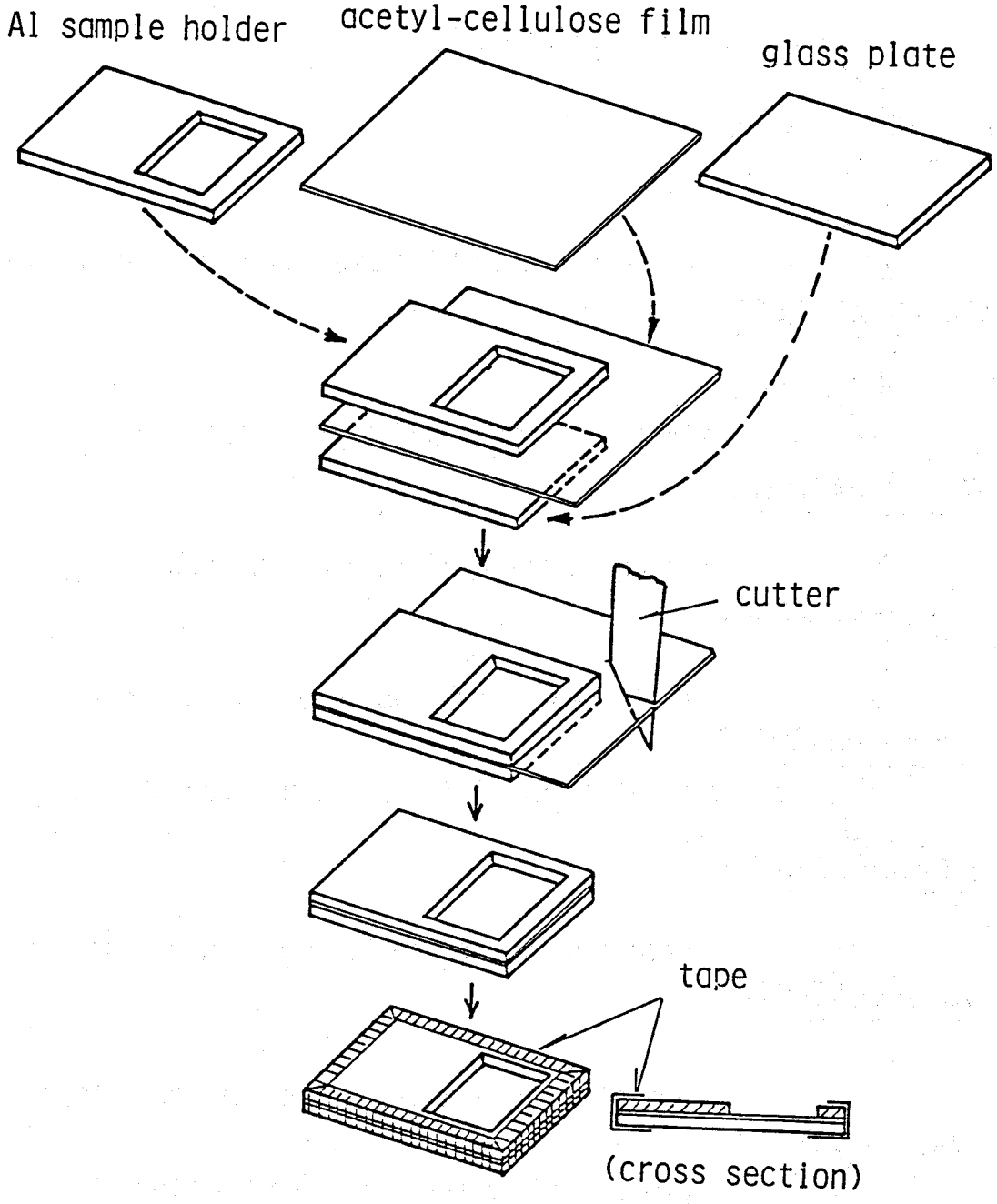

Fig. 3-1 Preparation of the sample holder for X-ray diffractometry

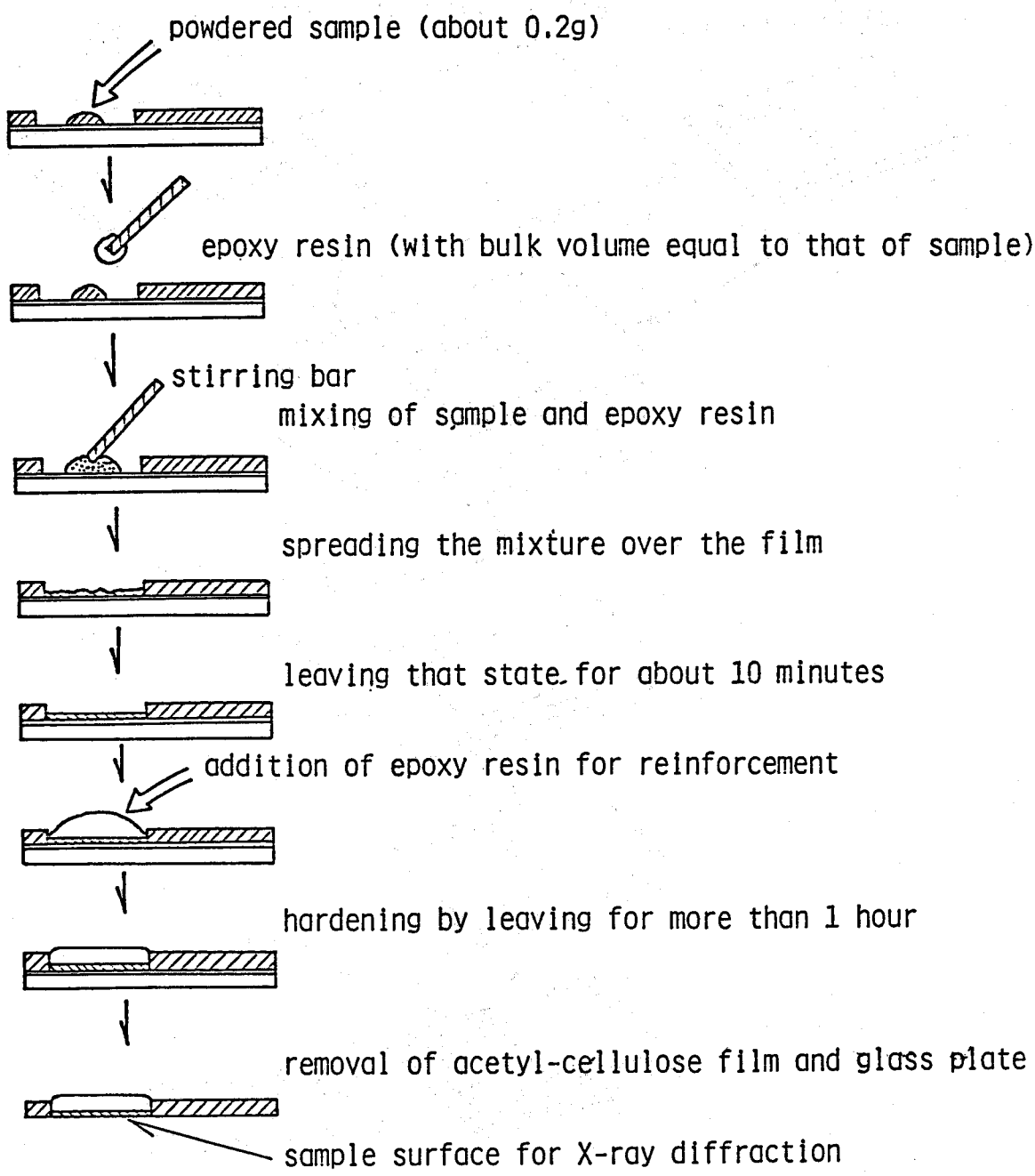

Fig. 3-2 Preparation of the sample for X-ray diffractometry

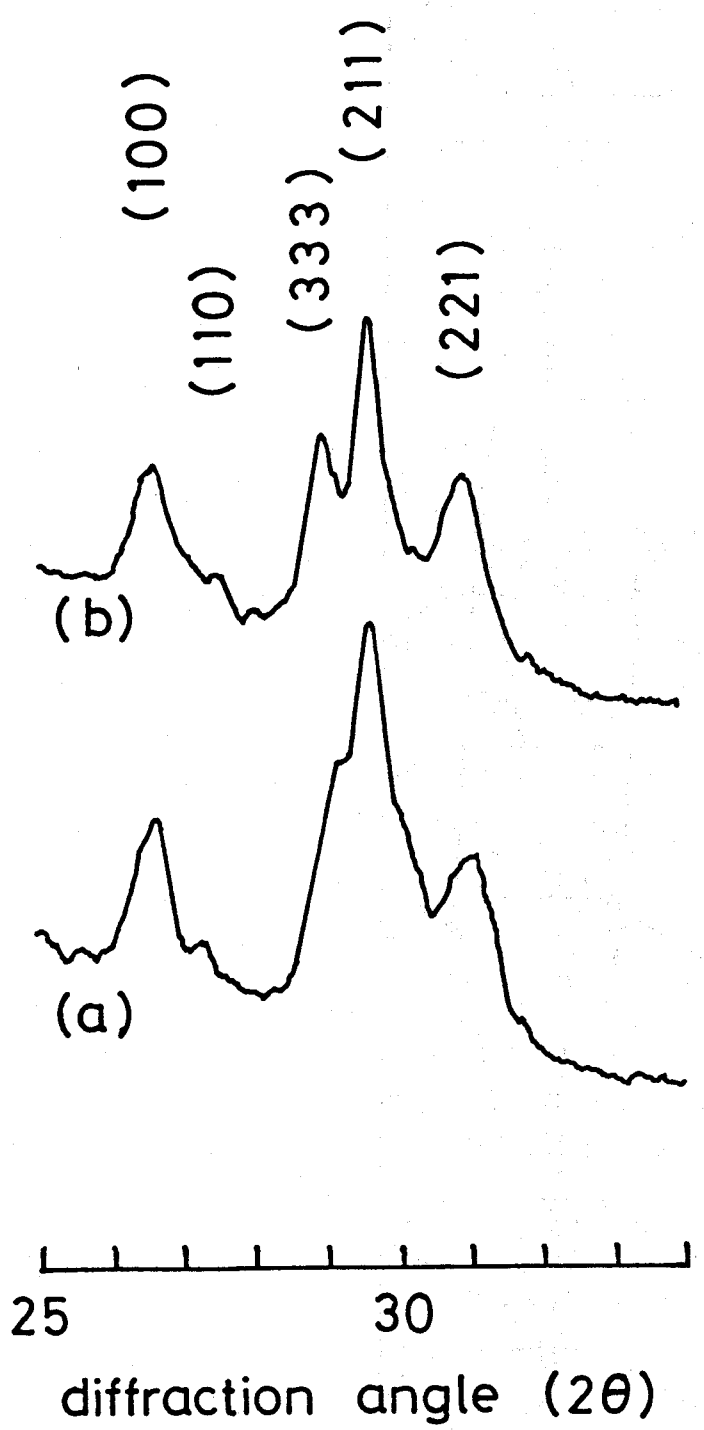

Fig. 3-3 X-ray diffraction patterns for Th_3N_4:
(a) obtained by the reaction of thorium with nitrogen
(b) obtained by the reaction of Th_4H_{15} with flowing N_2

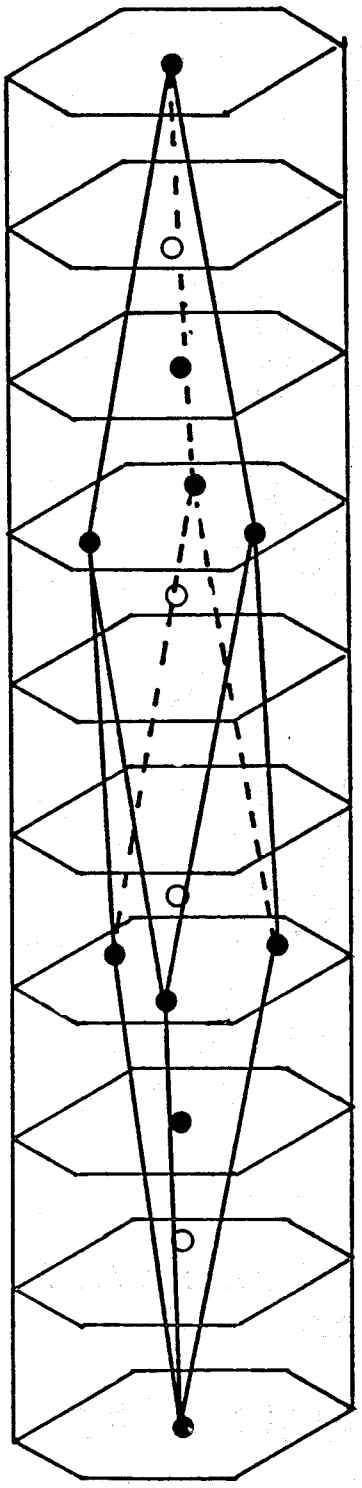

Fig. 3-4 The structure of Th_3N_4
Filled circles denote thorium atoms.
Open circles denote nitrogen atoms.

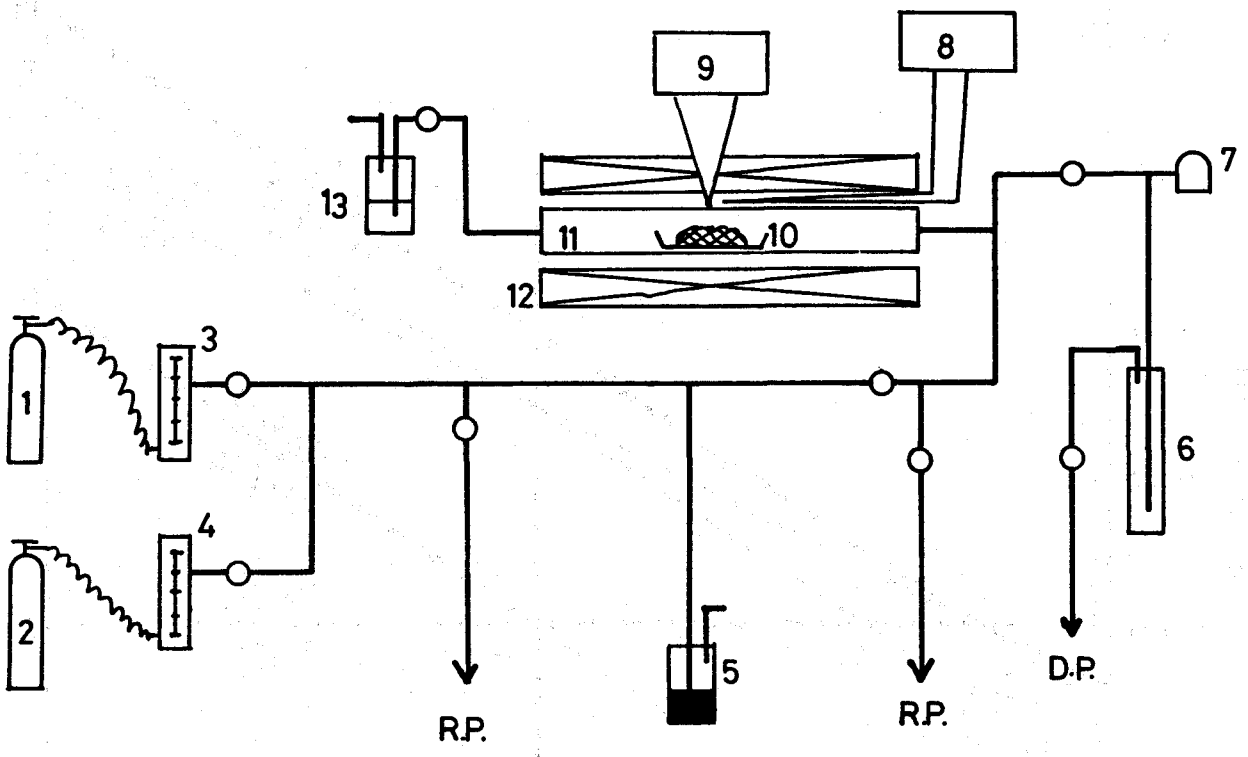

1. Hydrogen cylinder
2. Argon cylinder
3. 4. Flow meter
5. Hg bubbler
6. Cold trap
7. Ionization vacuum gauge
8. Thermometer
9. Thermal regulator
10. Specimen
11. Reaction tube
12. Furnace
13. Oil bubbler

Fig. 3-5 Experimental apparatus for thermal decomposition of Th_3N_4

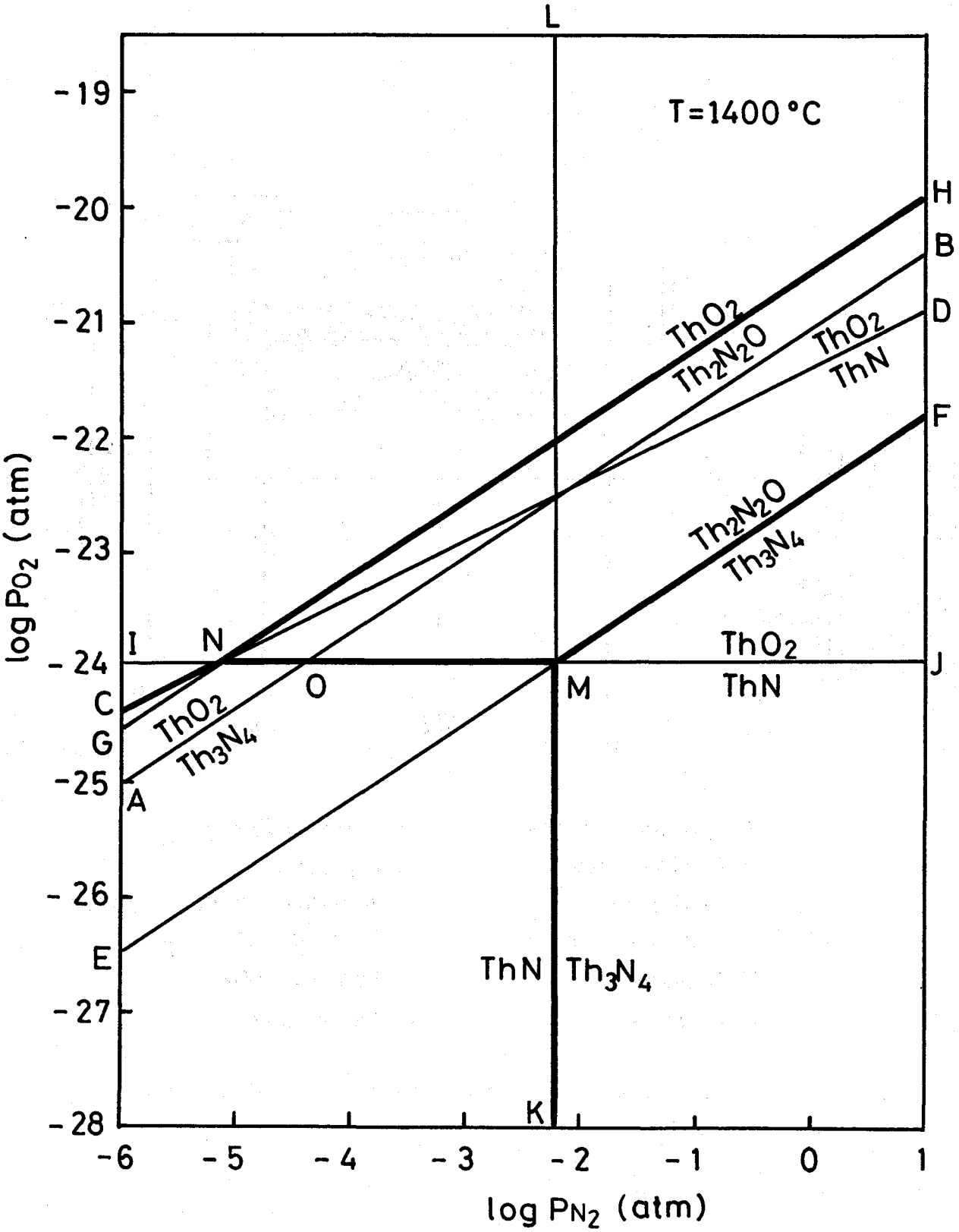

Fig. 3-6 The Th_3N_4-ThO_2, ThN-ThO_2, Th_3N_4-Th_2N_2O, Th_2N_2O-ThO_2, ThN-Th_2N_2O and Th_3N_4-ThN equilibria in O_2-N_2 atomsphere at 1400°C.

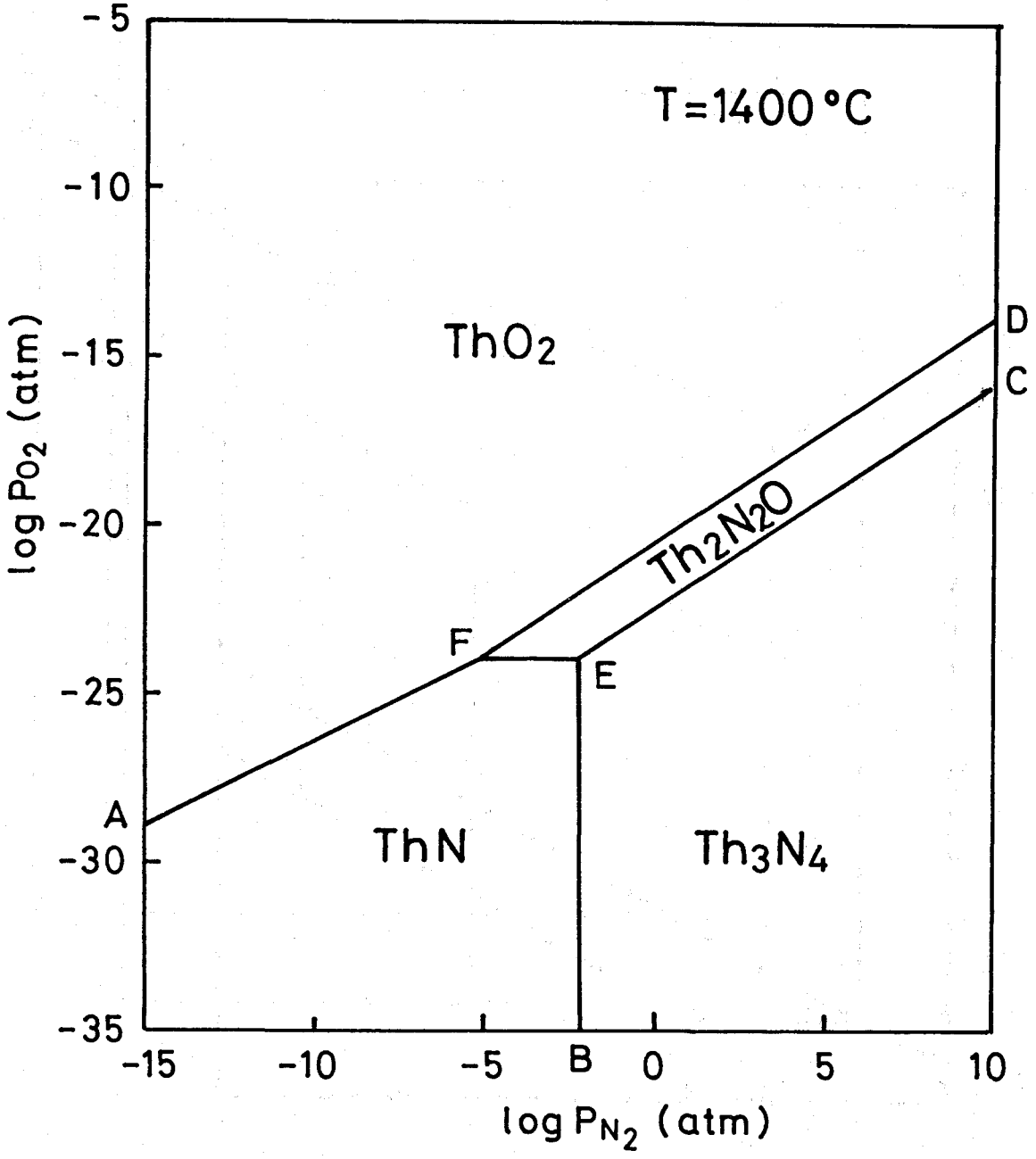

Fig. 3-7 The Th-N-O phase stability diagram at 1400°C.

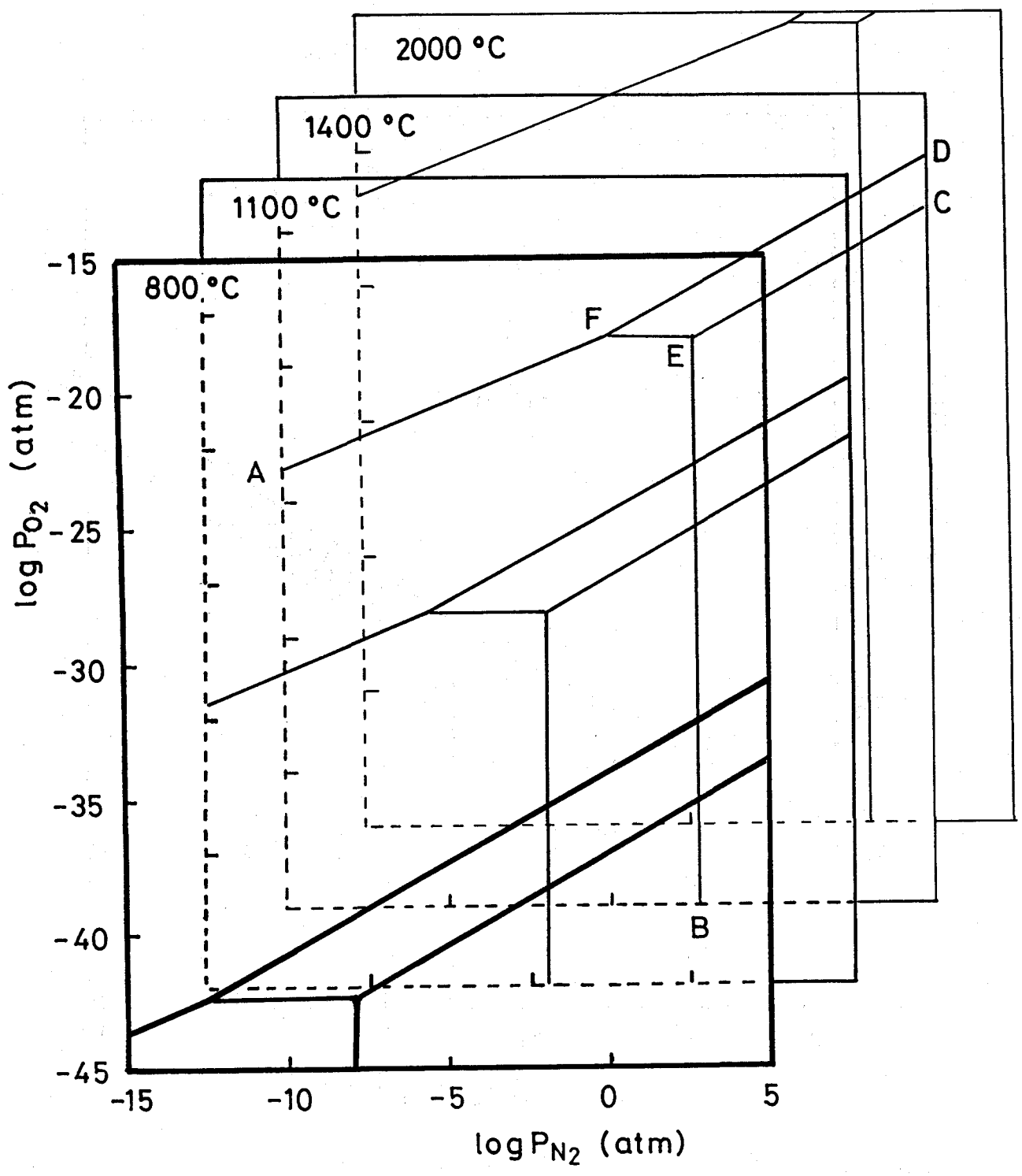

Fig. 3-8 The Th-N-O phase stability diagram at 800, 1100, 1400 and 2000°C

4 OXIDATION BEHAVIOR OF THORIUM NITRIDES

4-1 INTRODUCTION

As already described in Chapter 3, ThN free from ThO_2 has not yet been obtained. Thus in order to obtain pure ThN by thermal decomposition of Th_3N_4, it is necessary to know the oxidation behavior of thorium nitrides. Ozaki et al.[1] carried out a kinetic study on the oxidation of Th_3N_4 at temperatures of 340-480°C with an oxygen pressure of 0.2 atm and found a linear oxidation rate law.

One of the main aims in this work is to explore the oxidation behavior of thorium nitrides. In the preliminary experiment, both oxidation of ThN and oxidation of Th_3N_4 gave the same result. Further study of the oxidation of thorium nitrides has been mainly investigated for Th_3N_4 since Th_3N_4 free from oxide can be easily obtained as the starting material.

4-2 EXPERIMENTAL

Th_3N_4 prepared by the reaction of Th_4H_{15} with flowing nitrogen gas at 800°C as described in Chapter 3 was divided into three portions in a glove-box with an argon atmosphere. One portion was exposed to air for one week in Dewar flask held at 0°C. The second portion was placed in an electric incubator and held at 50°C with a relative humidity of $20\pm5\%$ for one week. The last portion was exposed to air in a furnace maintained at 100°C for one week.

X-ray diffraction powder patterns of the exposed portions were obtained at room temperature with the same diffractometer as that described in Chapter 3. As ThO_2 is stable with respect to air, a glass sample holder was used for the ThO_2 powder sample.

Infrared absorption spectra were obtained as Nujol mulls. The Nujol mull samples were dispersed between TlI plates. The

instrument used was a grating IR spectrophtometer, Hitachi Perkin-Elmer Model 225.

4-3 RESULTS AND DISCUSSION

From a preliminary study of the air oxidation of Th_3N_4, it was found that the oxidation product obtained close to room temperature exhibited only one or more diffuse reflections in its X-ray diffraction patterns, suggesting that the product may be of a poor crystalline nature. In order to reveal the dependence of the crystallinity of the products on the oxidation temperature, powdered Th_3N_4 was exposed to air for one week at 0, 50 and 100°C and the product was examined by X-ray diffraction. The X-ray diffraction patterns obtained are shown in Fig. 4-1, and the detected peaks are listed in Table 4-1. As can be seen from pattern(a) in Fig. 4-1, the product obtained after the exposure of Th_3N_4 to air at 0°C generates only two broad diffuse halos, which may correspond to (111) and (220) peaks for ThO_2. In the diffraction pattern of the product obtained at 50°C(pattern(b) in Fig. 4-1), two additional broad halos appeared, together with the (111) and (220) peaks. They may be considered to be the (200) and (311) peaks for ThO_2. The (111) and (220) peaks are somewhat sharper than those of pattern(a) in Fig. 4-1. In the diffraction pattern of the product obtained at 100°C(pattern(c) in Fig. 4-1), there exist five peaks of ThO_2 in the angular range 2θ = 20-60°. In this case, however, two more additional peaks, (331) and (442), can be observed in the angular range higher than 60°. Comparison of the X-ray diffraction pattern for the product obtained at 100°C with those obtained at 0 and 50°C shows that each peak at 100°C is sharper than that at 0 or 50°C. It follows from the above results that the degree of crystallinity increases with temperature in the range examined, although even the product obtained at 100°C still exhibits a rather low crystallinity.

All of the products prepared by oxidizing the maroon-brown Th_3N_4 in air acquired a white color which is characteristic

of ThO_2. Chemical analysis of the sample oxidized at 50°C gave a value of less than 0.003 for the [N]/[Th] mol ratio, its value being within the limit of detection. Thus nitrogen component in Th_3N_4 was almost completely removed by the air oxidation.

In order to confirm the stoichiometry of the oxidation products of Th_3N_4, i.e. ThO_2, the powder sample prepared by air oxidation of Th_3N_4 at 50°C was heat treated at 1400°C in vacuum($1x10^{-4}$Pa). Practically no appreciable amount of oxygen is considered to be transferred into the solid sample during the heat treatment in vacuum. Moreover, heat treatment in a reducing atmosphere, i.e. in flowing hydrogen(flow rate, 100ml/min) was also carried out in order to completely remove the supply of oxygen. In both cases, the X-ray diffraction patterns were essentially identical and the lattice parameters caluculated therefrom gave the same value. These results suggest that the heat treatment of the poorly-crystallized ThO_2 leads to the well-crystallized stoichiometric ThO_2, irrespective of the atmosphere of the heat treatment. The X-ray diffraction pattern for the sample heat-treated in flowing hydrogen is shown in Fig. 4-2, together with the starting material (the oxidation product of Th_3N_4 at 50°C), and detected peaks are given in Table 4-1. The diffraction pattern of the sample heat-treated at 1400°C consists of the same 15 peaks appearing in the pattern for ideally-crystallized ThO_2 when Cu Kα radiation is used. The reported values of relative intensities of these 15 peaks are also given in Table 4-1[2]. All the peaks are sharp and Kα doublets are well-resolved in the higher angular range. The calculated lattice parameter is 5.597Å, in excellent agreement with the reported values[3,4]. The thorium dioxide, ThO_2, is the only stable oxide in the solid state in the Th-O system and its fluorite-type structure does not undergo any polymorphic transformation up to its melting point of 3390°C, the highest of the oxides[3]. According to Ackermann and Tetenbaum[4], no measurable deviation from stoichiometry was revealed by lattice parameter and weight gain studies at temperatures below 2600K. Therefore, it can be concluded that the sample heat-treated at 1400°C was well-crystallized stoichiometric ThO_2. These consid-

erations provide evidence for the suggestion that the air oxidation products of Th_3N_4 at 0, 50, and 100°C possess the stoichiometric composition of ThO_2.

The patterns of the samples oxidized at 0 and 50°C are compared with that of the well-crystallized sample obtained by heat treatment at 1400°C in Fig. 4-2. The (111) and (220) peaks, which are the strong peaks in the case of the well-crystallized ThO_2, are diffuse in the patterns for the samples oxidized at 0 and 50°C. Some fainter peaks, e.g. (400) and (420), of the two latter patterns were unresolved and peaks at the higher angles were not detected. In other words, these ThO_2 powders generate only one or at most a few broad diffuse reflections, which is a characteristic feature of amorphous substances. However, the broad peaks can also result from polycrystalline aggregates, composed of a large number of individual crystals of very small size, even though a long-range order exists in the individual crystals. The crsytallite sizes of these samples will be discussed later.

The oxidation of Th_3N_4 may be perceived as a kind of phase transformation from a rhombohedral structure to an f.c.c. structure, as far as the configuration of thorium atoms is concerned, through the chemical reaction: $Th_3N_4 + 3O_2 = 3ThO_2 + 2N_2$.

Oxidation of Th_3N_4 in air at 50°C was examined as a function of time. The X-ray diffraction patterns at several stages of the oxidation are shown in Fig. 4-3. The starting material was Th_3N_4 powder with a high degree of crystallinity. It can be seen from Fig. 4-3 that the diffraction pattern of the sample exposed for 1 hour shows the (111) peak of ThO_2 as well as the (211) and (221) peaks of Th_3N_4, although the latter peaks for Th_3N_4 are much broader than those for the starting Th_3N_4 sample. After 2 hours, neither the (211) nor the (221) peaks of Th_3N_4 can be recognized and the whole pattern spreads around the (111) peak of ThO_2. After 5 hours, only the (111) and (200) peaks of ThO_2 can be distinguished, and the diffraction pattern obtained for the sample after 200 hours oxidation does not differ essentially from that obtained for the sample after 5 hours

oxidation. Therfore, it can be concluded that oxidation of Th_3N_4 in air at 50°C is complete in 5 hours.

The rhombohedral structure of Th_3N_4 must be transformed into the f.c.c. structure of ThO_2 as a result of oxidation. As pointed out by Magini et al.[5], regular tetrahedra of thorium atoms can be recognized in the ThO_2 structure, as illustrated in Fig. 4-4(c), where two types of fragments of the ThO_2 structure, thorium tetrahedra sharing corners or edges, are shown. The shortest Th-Th distance in ThO_2(3.97Å) is the length of the edge of the tetrahedra. In the rhombohedral unit cell of Th_3N_4 in Fig. 4-4(a), a distored tetrahedron can be distinguished, where the shortest Th-Th distance is 3.75Å and the distance of the other edges is 3.85Å (Fig. 4-4(b)). These values differ only by a factor of less than 10% from the Th-Th distance(3.97Å) in the ThO_2 structure so that the distorted tetrahedra could be changed with relative ease into tetrahedra as shown in Fig. 4-4(c) by enlarging the Th-Th distance as a result of oxidation.

The IR absorption spectra in the region of 1000 to 200 cm^{-1} for poorly- and well-crystallized ThO_2 are shown in Fig. 4-5. The X-ray diffraction pattern for the former is shown in Fig. 4-2. The latter was obtained by heat treatment of poorly-crystallized sample at 1400°C in vacuum($1x10^{-4}$Pa). As can be seen in Fig. 4-5, both the specimens show a broad, very strong absorption at about 350 cm^{-1} as well as a less strong absorption band at about 720 cm^{-1}.

According to Shimanouchi and Tsuboi[6], the CaF_2 crystal, which belongs to the space group O_h^5, has only one F_{1u} type IR active vibration. For such a lattice, to which ThO_2 also belongs, only one IR active lattice vibration is expected and the broad and strong band observed at 270 cm^{-1} is assigned to this vibration. The frequency of this vibration depends only on the Th-O distance.

The tetrahedral XY_4 molecule vibration may provide the basis for the interpretation of IR absorption since there are a large number of aspects of molecular vibration which closely correspond to crystal vibration. In the case of the tetrahedral

XY_4 molecule, which belongs to the point group T_d, two triply degenerate vibrations which are IR active exist; ν_3 and ν_4 of species F_2. The two absorption bands in Fig. 4-5 could be explained by the behavior of XY_4 molecule stretching.

As already stated, a thorium tetrahedron with one oxygen atom in its center exists in both types of fragments of ThO_2 (Fig. 4-4) and this tetrahedron may be resposible for the two absorption bands in the IR absorption spectrum(Fig. 4-5). It is interesting to note that both well- and poorly- crystallized ThO_2 exhibit two absorption bands which may reflect the similarity between the vibration modes of the ThO_2 crystal and the tetrahedron as its unit molecule.

However, scanning electron microscopy (SEM) observation suggests a morphological difference between the poorly-crystallized ThO_2 powder and the well-crystallized powder, as shown in Fig. 4-6. Poorly-crystallized ThO_2 powders obtained by the oxidation of Th_3N_4 at 50°C (Fig. 4-6(a)) are irregularly shaped particles which are aggregates of small crystallites. Well-crystallized ThO_2 (Fig. 4-6(b)) obtained from heat treatment at 1400°C in vacuum are round particles. This may arise from internal sintering of aggregate particles during the heat treatment. This change of morphology is very similar to that reported by Palmer et al.[7] in which crystal growth of ThO_2 powders was described. Their X-ray line broadening measurements showed that the crystallite size of ThO_2 increased by about a factor of eight during heat treatment at 1000°C.

The respective crystallite sizes of ThO_2 powders prepared by air oxidation at 0, 50, and 100°C have been evaluated roughly to be 13.6, 33.5, and 76.0Å, using the Scherrer formula;

$$t=0.9\lambda/B\cos\theta$$

where t is the crystallite size and B is the half-width value of the (111) peak. It should be emphasized that the oxidation products obtained at 0 and 50°C are ThO_2 powders with a crystallite size of a few unit cell sizes and even the product obtained at 100°C only possesses a size of about ten times the

unit cell size of ThO_2.

Broad diffuse halos developed in the X-ray diffraction patterns of poorly-crystallized ThO_2 samples are likely to be ascribed to their small crystallite sizes. Although no information on the formation of glass ThO_2 has yet become available, the possibility that the amorphous ThO_2 has been formed by the air oxidation of Th_3N_4 cannot be ruled out. Glass is an amorphous solid and in principle any substances can be made into a glass state by quenching it well below the melting point, from the liquid state, rapidly enough to suppress the crystallization. It should be emphasized that when thermodynamically very unstable Th_3N_4 is oxidized to very stable ThO_2 at low temperature, ThO_2 of a poor crystalline nature can be obtained. In other words, the oxidation of metal nitrides can provide a new preparation method for obtaining non-crystalline metal oxides.

However, more detailed studies are necessary to confirm whether the broad X-ray diffraction peaks of ThO_2 prepared in this work are due to small crystallite sizes or to an amorphous character.

4-4 CONCLUSION

1) Oxidation of Th_3N_4 close to room temperature produces poorly-crystallized ThO_2, whose degree of crystallinity increases with oxidation temperature.
2) Broad diffuse reflections in the X-ray diffraction patterns for ThO_2 as obtained by air oxidation of Th_3N_4 are suggested to be due to small crystallite size, which SEM observations seem to support.
3) The tetrahedral units, of which the fragments of ThO_2 are composed, might be responsible for the absorptions at 350 and 720 cm^{-1} in the IR absorption spectra for both poorly- and well-crystallized ThO_2.

REFERENCE

[1] S. Ozaki, M. Kanno and T. Mukaibo, J. Mucl. Sci. Technol., 8(1971)41.

[2] JCPDS Cards No. 4-0556.

[3] R. Benz, J. Am. Chem. Soc., 89(1967)197.

[4] J. Ackermann and M. Tetenbaum, High. Temp. Sci., 13(1980)91.

[5] M. Magini, A. Cabrini, G. Scibona, G. Johansson and M. Sandström, Acta Chem. Scand., A,30(1976)437.

[6] T. Shimanouchi and M.Tsuboi, J. Chem. Phys., 35(1961)1597.

[7] B.J.F. Palmer, J.A. Scoberg and A.Y.H. Gin, Am. Ceram. Soc. Bull., 62(1982)627.

Table 4-1 X-ray diffraction data for ThO_2

Miller index	Diffraction angle 2θ(degree)	Oxidation temperature(°C) 0	50	100	Relative intensity well-crystallized ThO_2*	JCPDS Cards[2]
(111)	27.580	+	+	+	100	100
(200)	31.962	-	+	+	39	35
(220)	45.852	+	+	+	50	58
(311)	54.363	-	+	+	43	64
(222)	56.997	-	-	+	11	11
(400)	66.857	-	-	-	7	8
(331)	73.781	-	-	+	16	26
(420)	76.025	-	-	-	13	17
(422)	84.825	-	-	+	14	20
(511)	91.325	-	-	-	14	19
(440)	102.217	-	-	-	6	6
(531)	108.984	-	-	-	15	18
(600)	111.293	-	-	-	9	8
(620)	120.978	-	-	-	9	14
(533)	128.930	-	-	-	8	9

Note: +=detected
-=not detected

*This ThO_2 was obtained by heat-treating a poorly-crystallized ThO_2, which was obtained by air oxidation of Th_3N_4 at 50°C.

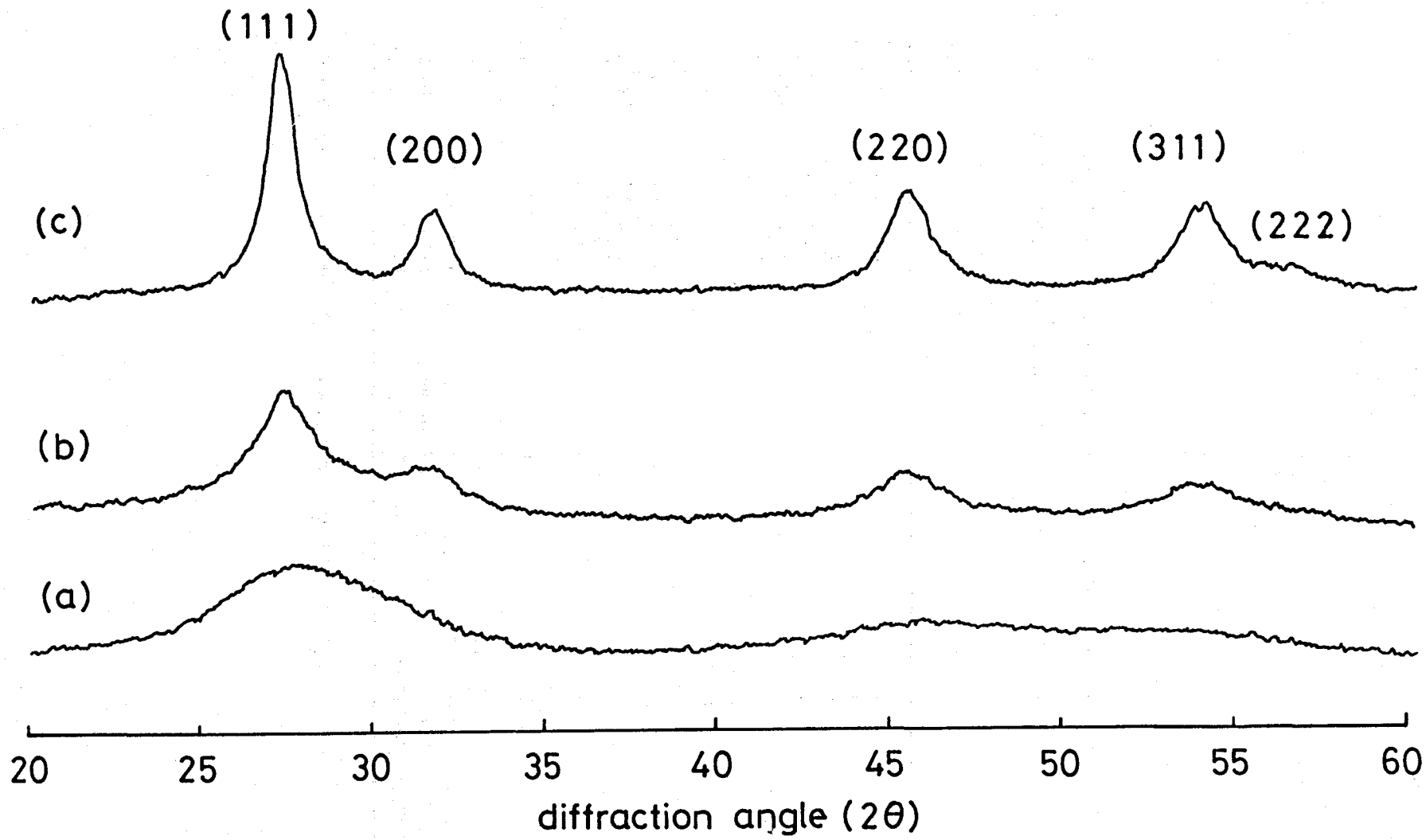

Fig. 4-1 X-ray diffraction patterns for the products obtained by the oxidation of Th_3N_4: (a) at 0°C; (b) at 50°C; (c) at 100°C.

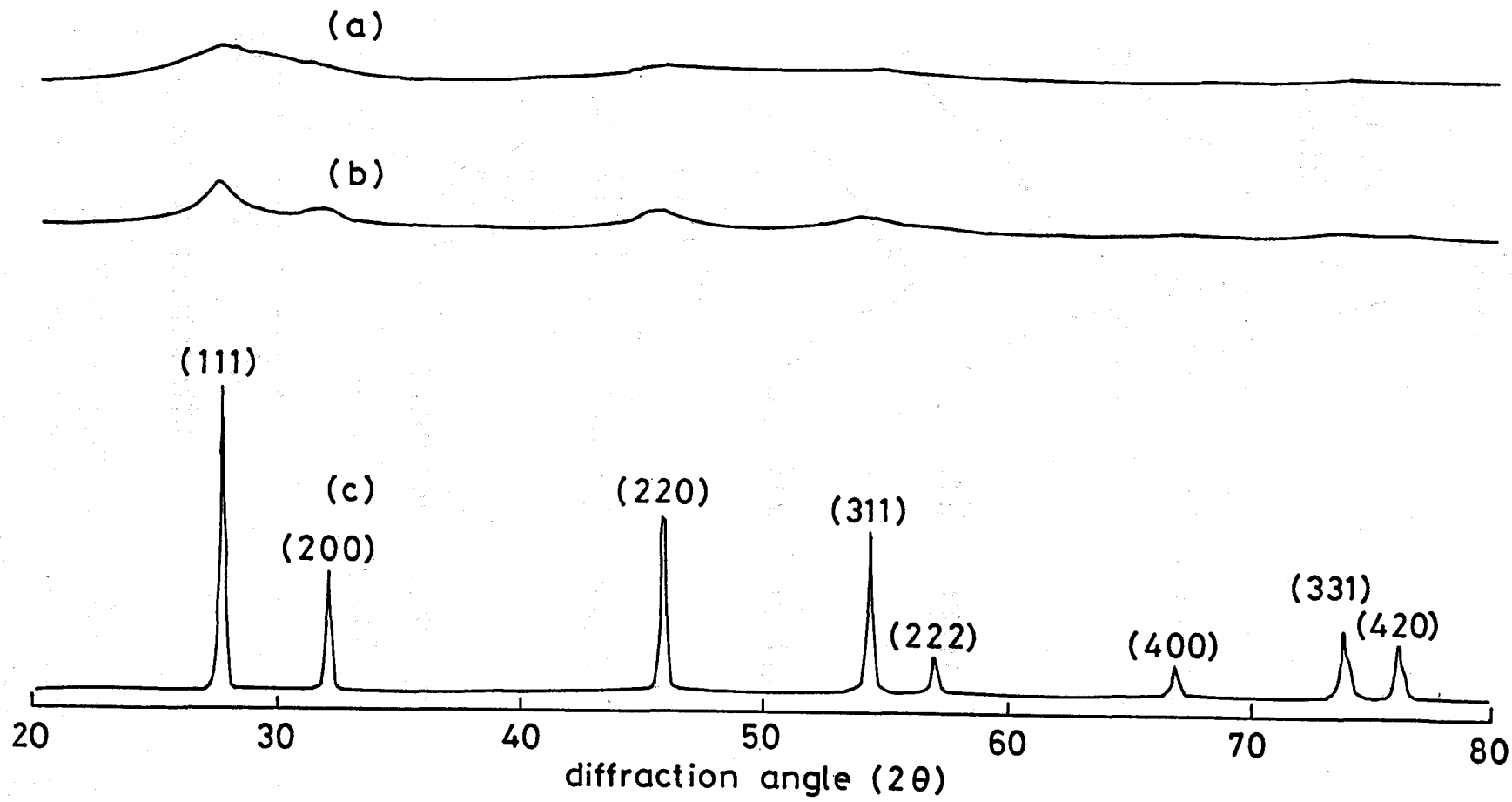

Fig. 4-2 X-ray diffraction patterns for pooly-crystallized ThO_2 obtained by the oxidation of Th_3N_4 (a) at 0°C and (b) at 50°C in air and (c) well-crystallized ThO_2 obtained by heat treatment of the poorly crystallized ThO_2 at 1400°C in flowing H_2

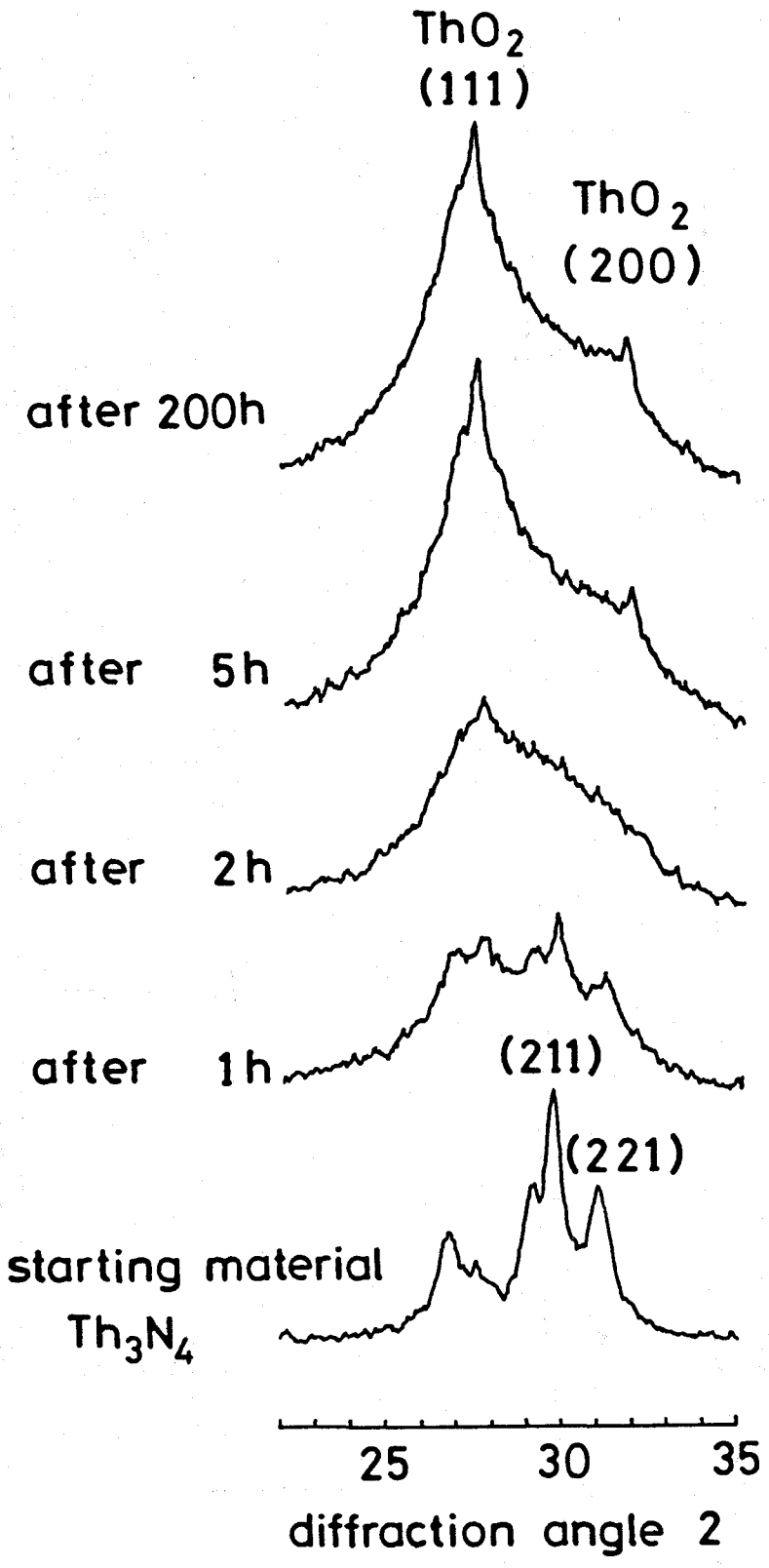

Fig. 4-3 Oxidation behavior of Th_3N_4 at 50°C; the change of X-ray diffraction pattern due to oxidation as a function of time.

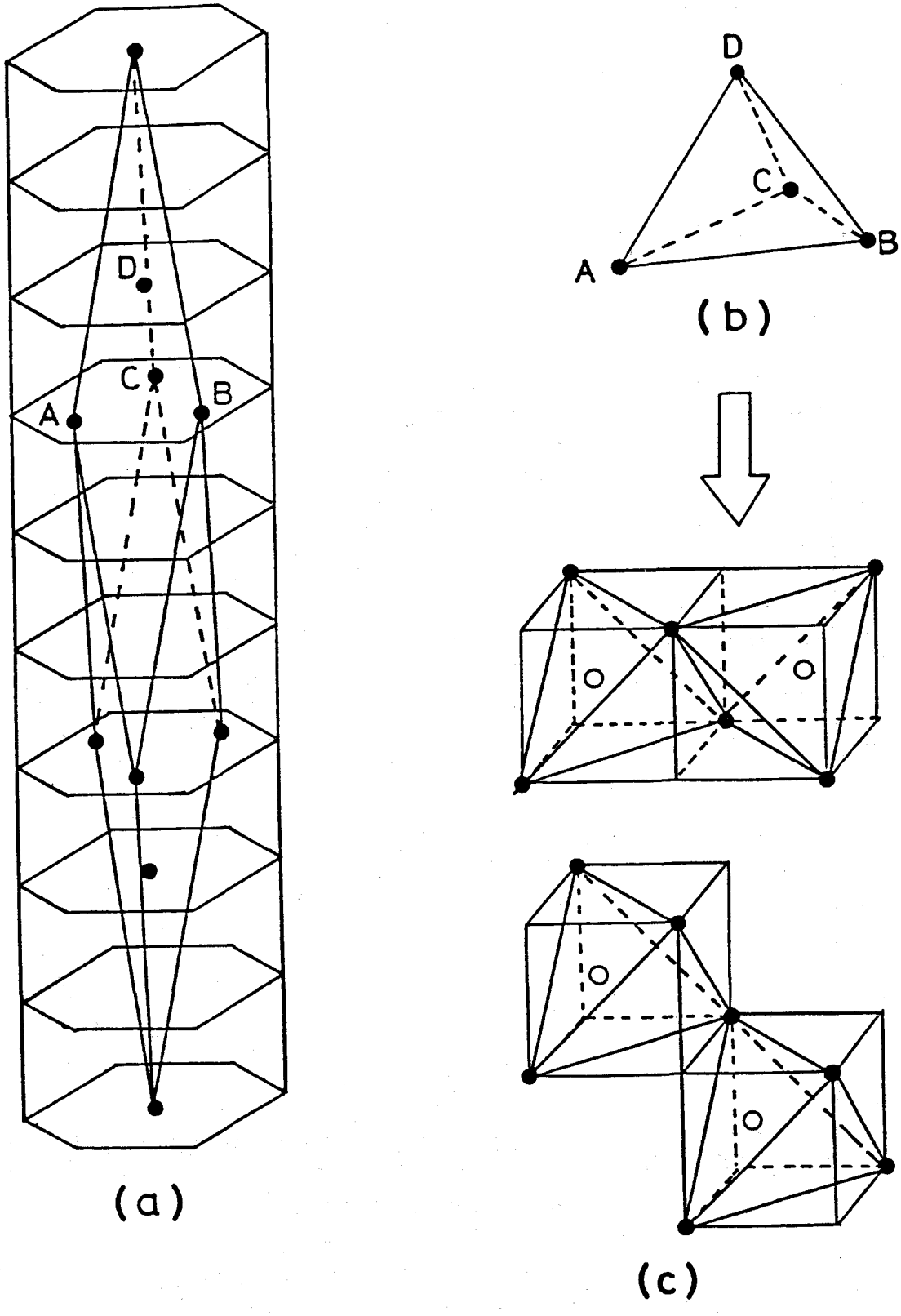

Fig. 4-4 (a) The structure of Th_3N_4; (b) fragment of the Th_3N_4 structure(AB=BC=CA=3.85Å, AD=BD=CD=3.75Å);
(c) fragment of the ThO_2 structure.
Filled circles denote thorium atoms and open circles denote oxygen atoms.

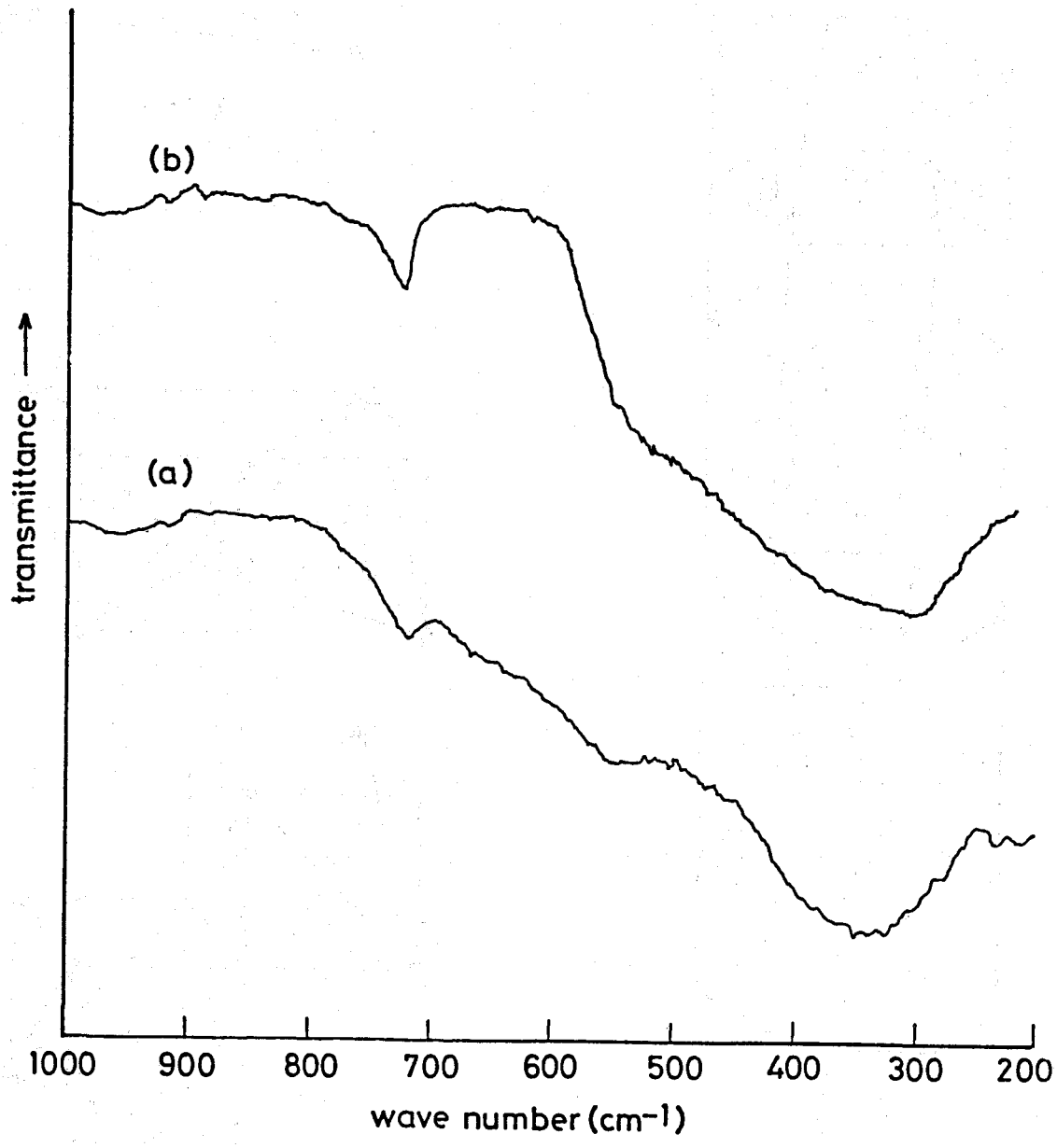

Fig. 4-5 IR spectra for: (a) poorly-crystallized ThO_2 ; (b) well-crystallized ThO_2.

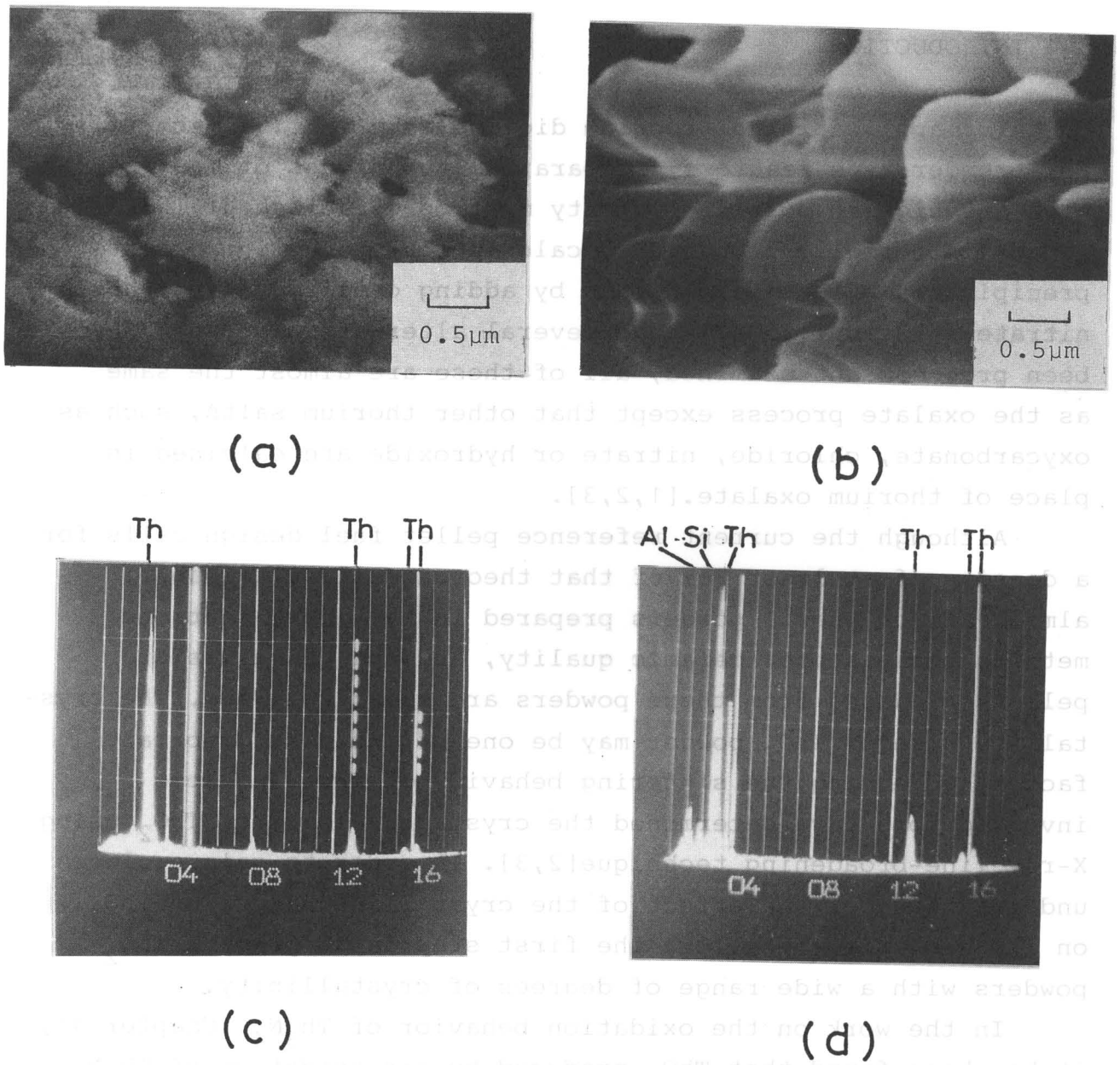

Fig. 4-6 SEM micrographs of: (a) poorly-crystallized ThO_2; (b) well-crystallized ThO_2; and energy dispersive X-ray analysis(EDXA) profiles of: (c) poorly-crystallized ThO_2; (d) well-crystallized ThO_2. Well-crystallized ThO_2 contains a little aluminum and silicon which seems to come from an alumina boat used for the heat treatment.

5 THE DEGREE OF CRYSTALLINITY OF ThO_2

5-1 INTRODUCTION

For application of thorium dioxide as a fertile material for breeder-type reactors, preparation techniques of ThO_2 pellets with the highest possible density must be established. Thoria powder is normally prepared by calcination of thorium oxalate precipitates which are obtained by adding oxalic acid to thorium nitrate solution[1]. Although several alternative methods have been proposed and examined, all of these are almost the same as the oxalate process except that other thorium salts, such as oxycarbonate, chloride, nitrate or hydroxide are calcined in place of thorium oxalate.[1,2,3].

Although the current reference pellet fuel design calls for a density of at least 96% of that theoretically attainable, almost all of thoria powders prepared in the above mentioned methods possess poor ceramic quality, and the densities of pellets produced from these powders are relatively low. The crystallite size of ThO_2 powder may be one of the most important factors governing the sintering behavior of ThO_2 and some investigators have determined the crystallite size of ThO_2 using X-ray line-broadening technique[2,3]. In order to gain a clear understanding of the effect of the crystalline nature of ThO_2 on its sintering behavior, the first step is to prepare ThO_2 powders with a wide range of degrees of crystallinity.

In the work on the oxidation behavior of Th_3N_4 (Chapter 4), it has been found that ThO_2 produced by air oxidation of Th_3N_4 close to room temperature exhibits a very broad X-ray diffraction pattern, indicating that ThO_2 obtained in this way may be of poor crystalline nature.

One of the purpose of this investigation is to prepare ThO_2 with a wide variety of degrees of crystallinity by heat treatment of poorly-crystallized ThO_2, which is produced by the air oxidation of Th_3N_4 at 50°C. The degree of crystallinity of ThO_2 heat-treated at and below 1000°C is discussed in terms of the number of detected peaks in the X-ray diffraction

patterns, and above 1100°C in terms of the Kα doublet resolution of detected peaks. When the degree of crystallinity progressively decreases, the X-ray diffraction lines progressively broaden. The integral breadth furnishes a direct criterion for the extent of line broadening. Therefore, the integral breadth is also used as one of the criteria for the degree of crystallinity of ThO_2.

Not only the smallness of the crystallite size but also some distortions from the regular crystalline arrangement may cause the line broadening of an X-ray diffraction peak. The most popular distortion may be non-uniform strain in the crystallite. In an effort to calculate the crystallite size and strain parameters separately from the integral breadth values, a line broadening technique proposed by Hall[4] is applied. Radial distribution analysis of ThO_2 samples with various degrees of crystallinity is also performed, and the local order of atoms is examined.

5-2 ANALYTICAL METHOD FOR THE DEGREE OF CRYSTALLINITY

5-2-1 X-RAY LINE BROADENING TECHNIQUE

The following development follows closely the treatment proposed by Hall[4]. If the broadening is due to only small crystallite size, the integral breadth β_c is expressed by the equation

$$\beta_c=\lambda/(\varepsilon\cos\theta) \qquad (1)$$

where ε is the crystallite size, λ is the wavelength of the X-ray, and θ is the Bragg angle. If the broadening is due to only strain, the integral breadth, β_s, is expressed by the equation

$$\beta_s=2\eta\tan\theta \qquad (2)$$

where η is the strain. When both size and strain broadenings

are simultaneously present, it becomes necessary to make assumption as to the shapes of the two contributing peak profiles. The two most commonly assumed peak shapes are Gaussian and Cauchy forms. If the two peak profiles arising from size and strain are assumed to be the Cauchy form, the observed integral breadth is the sum of breadths of these peak profiles, that is, $\beta=\beta_c+\beta_s$. According to Hall, the Cauchy form is also assumed here. Thus, from Eq.(1) and (2),

$$\beta\cos\theta/\lambda=1/\varepsilon+2\eta\sin\theta/\lambda \qquad (3)$$

As can be seen from Eq.(3), when $\beta\cos\theta/\lambda$ is plotted against $\sin\theta/\lambda$ for more than two peaks and straight line is drawn through these points, the reciprocal of intersect of the line with the vertical axis is ε and slope of the line is 2η.

5-2-2 RADIAL DISTRIBUITON ANALYSIS

The following development follows closely the treatment by Klug and Alexander[5]. According to Debye[6], the X-ray intensity, I, in electron units scattered by a noncrystalline array of atoms is given by

$$I=\sum_{m}\sum_{n} f_m f_n (\sin Sr_{mn}/Sr_{mn}) \qquad (4)$$

where f_m and f_n are the respective atomic scattering factors of the m th and n th atoms and r_{mn} is the distance between these two atoms. The double summation is taken over all pairs in the assemblage. Although the intensity can be expressed as a function of any angular variable such as θ, 2θ or $\sin\theta$, it is useful to specify its dependence on $S=(4\pi\sin\theta/\lambda)$ or $s=\sin\theta/\lambda$ in the study of radial distribution analysis.

(1) Material consisting of one kind of atom

In the case of a material consisting of only one kind of atom, since the environment of one atom is the same as that of any other atom, equation (4) can be written as follows

$$I=Nf^2\sum_m(\sin Sr_{mn}/Sr_{mn}) \tag{5}$$

where N is the number of the atoms in the material.

Considering the interaction of each atom with itself, since in the limit as $r_{mn}\longrightarrow 0$, $(\sin Sr_{mn}/Sr_{mn})\longrightarrow 1$, equation (5) may be written as

$$I=Nf^2[1+\sum_{m'}(\sin Sr_{mn}/Sr_{mn})] \tag{6}$$

where the summation excludes the origin atom.

Now regarding the distribution of atoms about any reference atom as being continuous, the summation can be replaced by an integral,

$$I=Nf^2[1+\int_0^\infty 4\pi r^2\rho(r)\cdot(\sin Sr/Sr)dr] \tag{7}$$

where $\rho(r)$ is the atom-density function at a distance r from the reference atom, and $4\pi r^2\rho(r)dr$ is the number of atoms contained in a spherical shell of radius r and thickness dr.

Using ρ_0, the average density of atoms in the sample, equation (7) may be written as

$$I=Nf^2\{1+\int_0^\infty 4\pi r^2[\rho(r)-\rho_0](\sin Sr/Sr)dr + \int_0^\infty 4\pi r^2\rho_0(\sin Sr/Sr)dr\} \tag{8}$$

The integral of the last term represents the scattering by a hypothetical object of the same form as the specimen but of rigorously uniform electron density. This scattering occurs at such small angles as to be unresolvable from the direct beam. Since the attention may be limited to experimentally observable

intensities, equation (8) can be simplified to the form

$$I/Nf^2-1=\int_0^\infty 4\pi r^2[\rho(r)-\rho_0](\sin Sr/Sr)dr \qquad (9)$$

By means of the Fourier integral theorem, this expression can be transformed to

$$r[\rho(r)-\rho_0]=1/(2\pi^2)\int_0^\infty Si(S)\sin rSdS$$

or

$$4\pi r^2\rho(r)=4\pi r^2\rho_0+(2r/\pi)\int_0^\infty Si(S)\sin rSdS \qquad (10)$$

where

$$i(S)=I/Nf^2-1 \qquad (11)$$

(2) Material consisting of more than one kind of atom

In the case of a material consisting of more than one kind of atom, it is necessary to consider some appropriate units of structure (such as one molecule) of which the entire specimen is regarded as being composed. If p denotes the kind of atoms in a unit and the number of such units is N, equation (4) can be written as

$$I=N\sum_p f_p^2+\sum_m^{m\neq n}\sum_n f_m f_n(\sin Sr_{mn}/Sr_{mn}) \qquad (12)$$

The first term is due to the interaction of each atom with itself. The first summation is to be taken over all the atoms in a unit(in the case of ThO_2, one thorium atom and two oxgen atoms). The second summation is to be taken over every pair of atoms regardless of which units they are in.

The second term of the equation (12) is treated as follows. Letting an atom of type m be the reference atom, $\sum_m f_m$ for the reference atom can be expressed in terms of N and p in the form

$$\sum_m f_m=N\sum_p f_p \qquad (13)$$

The distribution of atoms about any reference atom is once

the average number of atom of type p, lying in a spherical shell of radius r and thickness dr is a_p. If a weighted density function $\rho_p(r)$ is defined as

$$4\pi r^2\rho_p(r)dr=\Sigma a_p f_p, \tag{14}$$

the summation of the second term of equation (12) is replaced by an integral

$$I=N[\sum_p f_p{}^2+\sum_p f_p\int_0^\infty 4\pi r^2\rho_p(r)\cdot(\sin Sr/Sr)dr] \tag{15}$$

Since both f_p and $\rho_p(r)$ are functions of S, this expression cannot be directly inverted by using the Fourier integral theorem. Thus, the following approximation is employed using f_e, the scattering factor of a single electron. First, the scattering factor of atom p can be expressed in the form

$$f_p=f_e f_p^\circ \tag{16}$$

where f_p° is the value of f_p at S=0.

Secondly, the atomic density function $\rho_p(r)$ can now be expressed as

$$\rho_p(r)=f_p^\circ g_p(r), \tag{17}$$

where $g_p(r)$ is the electron density function.

Substitution of equation (16) and (17) in equation (15) gives

$$I=N[\sum_p f_p{}^2+4\pi f_e{}^2\int_0^\infty\sum_p f_p g_p(r)r^2(\sin Sr/Sr)dr] \tag{18}$$

By proceeding in the same way as in deriving equation (9) from (7), equation (18) can be transformed to the expression

$$I/N-\sum_p f_p{}^2=4\pi f_e{}^2\int_0^\infty\sum_p f_p^\circ[g_p(r)-g_\circ]r^2(\sin Sr/Sr)dr \tag{19}$$

Application of the Fourier integral theorem yields

$$4\pi r^2 \sum_p f_p^{\circ} g_p(r) = 4\pi r^2 g_o \sum_p f_p^{\circ} + (2r/\pi) \int_0^{\infty} Si(S) \sin rS dS \quad (20)$$

where

$$i(s) = \sum_p [f_p^{\circ 2}/f_p^{\ 2}][I/N - \sum_p f_p^{\ 2}] \quad (21)$$

The determinaiton of radial-distribution function, with the aid of expression (11) or (20) comprieses two main steps; first the numerical evaluation of the function i(s) from experimental scattering data and, second, numerical computation of the intergral $\int_0^{\infty} Si(S) \sin rS dS$.

5-3 EXPERIMENTAL

5-3-1 PREPARATION OF ThO_2 WITH VARIOUS DEGREES OF CRYSTALLINITY

As described in Chapter 4, poorly-crystallized ThO_2 was prepared by the oxidation of Th_3N_4 at 50°C in air for more than one week.

Heat treatments at temperatures at and below 1000°C were performed using the apparatus described in Chapter 2. The poorly-crystallized ThO_2 powder in a quartz boat was heated to a desired temperature within 1 hour either in air or in vacuum(about 1×10^{-4} Pa.). After the specimen was kept at the temperature for 5 hours, it was cooled to room temperature in about 5 minutes. Heat treatments at temperatures above 1100°C were performed with the apparatus used for the preparation of ThN. The specimen was heated to a desired temperature up to 1400°C in about 2.5 hours. An alumina boat was used for the heat treatments in air and a molybdenum boat for those in vacuum(about 1×10^{-4}Pa) because Mo is oxidized in air at such high temperatures. After the temperature was maintained for 5 hours it was decreased to room temperature in about 12 hours.

After the desired heat treatment the specimen was embedded in a glass sample holder and the X-ray diffraction powder patterns for estimation of the degree of crystallinity were obtained at room temperature in the same manner as described in Chapter 4.

For determination of lattice parameters, a step scanning

width at an interval of $2\theta=0.004°$ and a counting period of 4 sec. were adopted. The X-ray diffraction was carried out at $20\pm1°C$. The angle corresponding to the middle point of line drawn at half-maximum intensity parallel to the background was adopted as the diffraction angle. These angles were calibrated with silicon ($a=5.4306\text{Å}$) used as an internal standard. The lattice parameter was determined by plotting a values of (440), (531), (600), (620), and (533) reflections against $\cos^2\theta$ and extrapolating to $\cos^2\theta=0$.

5-3-2 ANALYSIS BY X-RAY LINE BROADENING TECHNIQUE

X-ray diffraction measurement

In employing the Hall method, the integral breadth values for the X-ray diffraction peaks are needed. The integral breadth is defined by the integrated intensity divided by the peak maximum, that is, the width of the rectangle having the same area and height as an X-ray diffraction peak. The integrated intensity and peak maximum were measured with the same X-ray diffractometer as described in Chapter 2. The conditions for the diffractometry was the same as that employed in determination of lattice parameters.

Data treatment

The peaks of the same lattice direction must be selected for application of the line broadening technique since both crystallite size and strain may vary with lattice direction. The [(200),(400),(600)], [(220),(440)], and [(111),(222)] combinations of peaks of ThO_2 satisfy this condition. But, since the (600) and (222) peaks for the ThO_2 samples examined overlap with the neighboring peaks, the [(200),(400)] and [(220),(440)] pairs of peaks are selected for the application.

Before applying the Eq.(3), two corrections must be made

to the observed breadths since they are influenced, in addition to small crystallite size and nonuniform strain, by the following two factors; the Kα doublet broadening and the instrumental broadening. Correction for Kα doublet broadening was made by a method established by Jones[7] who made a correction curve as shown in Fig. 5-1. In this figure, d is the angular separation of the Kα doublet, b_o is the observed breadth and b is the corrected breadth. Correction for the instrumental broadening was made using α-quartz as a standard in a manner proposed by Alexander[8]. The correction curve reported by Alexander is shown in Fig. 5-2, where b is the observed breadth and B is the breadth of the standard and β is the corrected breadth. The α-quartz heat-treated at 800°C for 40 hours is assumed to have no strain and sufficiently large crystallite size. The instrumental broadening of the (200), (400) and (220) peaks of ThO_2, were corrected with the integral breadths of the (110) Kβ, (113) and (201) peaks of α-quartz, respectively. For the correction of the (440) peak of ThO_2, the average of the integral breadths of the (223) and the (321) peaks of α-quartz was used. After the above two corrections, the Eq.(3) was applied to the observed breadths.

5-3-3 RADIAL DISTRIBUTION ANALYSIS

In order to determine radial-distribution function with the aid of expression (20), it is necessary to evaluate the function i(S) by calculation of $[I/N-\sum_p f_p^2]$ from experimental scattering data. The procedure is shown in Fig. 5-3.

Intensity measurement

The integration of equation (20) may require that the intensity measurement is extended to very large S value. However, as S becomes large, the integration of equation (15) approaches zero, and hence I approaches $N\sum_p f_p^2$. For many noncrystalline

substances, this state is attained for S between 8 and 10. Since $S=4\pi\sin\theta/\lambda$, a radiation of short wave length is commonly employed to supply intensity data at large S values, and a radiation of longer wave length is preferable in order to resolve the intensity details for smaller values of S.

Thus, CuKα radiation was used to cover the S range from 0.156 to 4.663$\mathring{A}^{-1}$ corresponding to the 2θ range from 2 to 70° and MoKα radiation was employed to cover the S range from 4.307 to 10.116$\mathring{A}^{-1}$ corresponding to the 2θ range from 28 to 70°. Measurements were performed at discrete points with intervals of 2θ=0.5° for CuKα and 0.2° for MoKα.

Correction for air scattering

Equation (20) can apply only to the coherent scattering by the specimen. Therefore, it is necessary to exclude the intensity of the scatter due to air from the observed intensity.

Since the geometrical arrangement in diffractometry of the apparatus used in the present study is symmetrical reflection, the ratio of the air scattered intensity received with and without the sample in place is given by Ergun[9]

$$a_r=1/2+[1/2-(T\cos\theta/R\beta)]\exp(-2\mu T/\sin\theta) \qquad (22)$$

In this equation T is the thickness of a flat specimen, R is the goniometer radius, β is the equotorial angle subtended at the specimen by the detector slit and μ is the linear absorption coefficient. Since μ for ThO_2 and T are sufficiently large, equation 22 is simplified to the form

$$a_r=1/2 \qquad (23)$$

Thus, the correction for air scatter was done by substracting the half value of intensity measured in the absence of the specimen from the intensity scattered by the specimen.

Correction for polarization and absorption

The observed intensity cannot be employed in the calculation of equation (21) since it has some distortions that vary with the scattering angle. The main factors of this kind are polarization and absorption by the sample.

When a monochrometer is used, the polarization effect makes the intensity scattered by the sample be diminished by the factor

$$P=(1+\cos^2 2\theta'\cos^2 2\theta)/(1+\cos^2 2\theta') \qquad (24)$$

where θ' is the Bragg angle for the reflecting planes of the monochromatizing crystal. Thus, the intenisty corrected for polarization was obtained by multiplying the observed intensity by the reciprocal of equation (24). In the present study, the intensity scattered by the sample was monochromatized by reflection from the (002) planes of graphite.

In the symmetrical-reflection technique, the effect of the absorption by the sample on the intensity is independent of θ if the thickness of the specimen is sufficiently large[10]. The thickness of the sample in the present study are so large that the effect of the absorption by the sample is postulated to be independent of θ.

Normalization and correction for incoherent scattering

The next step for evaluation of the function, i(S) is to exclude the incoherent scattering from the obsereved scattering and, as seen from the inspection of equation (21), to express I in the same units as $N\sum_p f_p^2$.

These two treatments have been accomplished by fitting the obsereved curve corrected for the above three factors to the theoretical total independent scattering curve at large values of S where I approaches $N\sum_p f_p^2$. This is illustrated in Fig. 5-4. The total independent scattering(B) is the sum of independent scattering(C) and incoherent scattering(D). Independ-

ent scattering is defined as the hypothetical scattered intensity from an assemblage of atoms when each one scatters independently of the others so that no interference effects are provided. Intensity of independent scattering for one ThO_2 is given

$$I_{ind}=\sum_p f_p^2 \qquad (25)$$

The atomic scattering factors, f_p, given by Cormer and Waber[11] for neutral Th and O atoms were used. The intensity of the incoherent scattering of an atom of atomic number Z is expressed

$$I_{inc}=R(Z-\sum_n f_n^2) \qquad (26)$$

where f_n is the scattering factor of the nth electron in the atom, and R is the Breit-Dirac recoil factor which can be expressed

$$R=(1+0.0486\sin^2\theta/\lambda)^2 \qquad (27)$$

The incoherent intensity, $(Z-\sum_n f_n^2)$, for Th and O was obtained from Cormer[12].

The normalization was done, first by fitting the corrected MoKα intensity curve to the total independent scattering curve in the S range around 10Å^{-1} and then, fitting the corrected CuKα intensity curve to the normallized MoKα intensity curve in the S range of 4.4 to 4.7Å^{-1}. The normalized experimental curve was obtained by the combination of these two curves. The total independent scattering was, finally substracted from the experimental intenity curve, leaving the desired coherent scatter, $I/N-\sum_p f_p^2$.

5-4 RESULTS AND DISCUSSION

5-4-1 THE DEGREE OF CRYSTALLINITY

Poorly-crystallized materials exhibit only one or more faint and broad reflections in the low angle region of the X-ray diffraction patterns, and the back-reflection lines do not appear. The progressive increase of the degree of crystallinity can be estimated by the fact that low angle peaks become sharper, middle and high angle peaks first become to be detected, then become sharper and ultimately Kα doublets of high angle peaks are resolved. However, as the degree of crystallinity falls below some level, the sharpness of back reflection lines is first affected, and the Kα doublet eventually ceases to be resolved.

Fig. 5-5 shows the variation of (111) and (200) peaks (low angle peaks) of the x-ray diffraction patterns for ThO_2 heat-treated at temperatures at and below 1000°C for 5 hours. From visual inspection of the pattern in Fig. 5-5, it is clear that the degree of crystallinity of the samples increases with temperature of heat treatment.

A typical example of the variation of higher angle peaks with the heat treatment temperature is shown in Fig. 5-6, where the X-ray diffraction patterns for ThO_2 samples heat-treated in vacuum at 600, 1000 and 1400°C as well as the starting material are shown.

The change in the degree of crystallinity of ThO_2 was evaluated under following three criteria; the number of detected peaks, Kα doublet resolution and integral breadth values.

The number of detected peaks

First, the degree of crystallinity of the samples heat-treated at and below 1000°C was evaluated in terms of the number of detected peaks. The results are summarized in Table. 5-1. For well-crystallized ThO_2 15 peaks can be detected using nickel-

filtered Cu Kα radiation by the diffractometer employed in the present study, which can scan in the diffraction angle region from 2θ=0 to 2θ=130 degrees. The reported values of relative intensity (I/I_o) of these 15 peaks for an ideally-crystallized ThO_2 are also shown in the last column of Table 5-1.[13]

Similar to that of the starting material, only the four peaks from the lowest angle peak, (111) to the fourth-lowest angle peak, (311) are detected in the X-ray diffaction pattern for ThO_2 heat-treated at 200°C, although each of the four individual peaks at 200°C is sharper than each of the four corresponding ones of the starting material. Ten peaks are detected at 400°C and (531) peak is detected at 600°C, in addition to these ten peaks. However, the (440) peak is not detected. This may arise from the fact that the relative intensity of this peak is essentially weaker than that of the (531) peak, as shown in Table 5-1. As the temperature of heat treatment increases from 200 to 1000°C, higher angle peaks become observable. At 1000°C, all of the 15 peaks are observed.

Judging from the number of detected peaks, the degree of crystallinity increases with temperature, and there is no difernce between those of ThO_2 heat treated in air and in vacuum, if the comparison is made at the same temperature.

Above 1000°C, the degree of crystallinity of ThO_2 heat-treated cannot be discussed in terms of the number of detected peaks since all the 15 peaks are detected at these temperatures.

Kα doublet resolution

The degree of crystallinity of the samples heat-treated above 1100°C is discussed in terms of Kα doublet resolution. Variation of (400), (531) and (600) peaks of the X-ray diffraction patterns for ThO_2 heat-treated at temperatures above 1000°C are shown in Fig. 5-7. As seen from this figure, as the temperature increases the peaks become higher and sharper up to 1400°C. At 1200°C each Kα doublet of the (600) peaks is partially resolved and each Kα doublet is clearly resolved at

1400°C. No significant difference between the results of heat treatments in air and in vacuum can be recognized.

Integral breadth values

Integral breadth value defined as the integrated intensity divided by the peak maximum may be employed as a quantitative description of peak sharpness. Line broadening may arise not only from small cryatallite size and nonuniform strain but also Kα doublet broadening and instrumental broadening. In order to evaluate extra breadth, or broadening due to size and strain effects alone, the corrections for Kα doublet and instrumental broadening must be made. Corrected integral breadth values of the peaks are listed in Table 5-2. In order to illustrate the variation of the values clearly, those of the (200) and (400) peaks are shown in Fig. 5-8. This figure clearly shows that the integral breadth values decrease with increasing temperature.

According to the Th-ThO_2 phase diagram reported by Benz[14], ThO_2 is the only stable oxide in the condensed state and only stoichiometric ThO_2 exists below 1754°C. Foex[15] reported that ThO_2 suffers no weight change when the atmosphere is changed from an oxidizing (O_2) to a reducing (H_2 or CO) one below 1400°C. As reported in Chapter 4, all the ThO_2 samples heat-treated in this work should have stichiometric composition unless any effects such as contamination from boat substance occurred.

Lattice parameteres of ThO_2 heat-treated at 1300 and 1400°C in the both atmospheres were calculated. The lattice parameter of ThO_2 heat-treated in vacuum, 5.597 ± 0.001Å, is in excellent agreement with reported one, 5.597 ± 0.001Å[14]. However, those of ThO_2 heat-treated in air, 5.595 ± 0.001Å, are slighly smaller than reported one.

According to E.C. Subbarao et al.[16], Y_2O_3 dissolved in ThO_2 up to about 20 mol% $YO_{1.5}$ at 1400°C and the solid solution had the CaF_2-type structure with a filled cation sublattice

and anion vacancies. They reported also that its lattice parameter decreased with increasing the concentration of Y_2O_3. The decrease of lattice parameters of the samples heat treated at 1300 and 1400°C in air might be due to the contamination of Al_2O_3 used as a boat since aluminum in Al_2O_3 is trivalent cation as yittrium in Y_2O_3 although no data about the solubility of Al_2O_3 in ThO_2 have been reported. Another explanation might be contamination of CaO as a possible impurity in Al_2O_3 boat since CaO is known to form extensive solid solution with ThO_2. However, more detailed studies are needed to clarify these points.

5-4-2 EVALUATION OF CRYSTALLITE SIZE AND NONUNIFORM STRAIN BY X-RAY LINE BROADENING TECHNIQUE

Harada et al.[2] prepared ThO_2 powders by calcining the oxycarbonate, chloride, nitrate, and oxalate of thorium in air at temperatures ranging from 400 to 1200°C. The crystallite size of thus obtained ThO_2 increases with the calcinaiton temperature. Palmer et al.[3] prepared ThO_2 powders by hydrothermally denitrating hydrated thorium nitrate crystals at 480°C. The ThO_2 prepared in this way was heat-treated at 750 and 1000°C. The crystallite size increases with heat treatment temperature. Although Harada et al. and Palmer et al. used X-ray line broadening technique in determining the crystallite size, they did not refer to nonuniform strain. In the present study, in an effort to calculate the crystallite size and nonuniform strain parameters separately, a line broadening technique proposed by Hall[4] is applied to the integral breadth values shown in Table 5-2.

The crystallite size and strain in the [100] direction for the samples heat-treated below 600°C and those in the [110] direction for the samples heat-treated below 1000°C cannot be estimated since the corresponding peaks are not observable. For the samples heat-treated at 1300 and 1400°C, the integral breadth is so small that the difference between integral breadth

of ThO_2 and that of α-quartz as a standard is extremely small. This fact may suggest that ThO_2 samples heat treated at 1300 and 1400°C have so large crystallite sizes and small strains that the present method cannot be applied.

Table 5-3 summarizes the evaluated crystallite size and nonuniform strain parameters in the [100] and [110] directions, which were calculated by applying the expression (3), to the corrected integral breadths of the (200) and (400) peaks for [100] direction and those of the (220) and (440) peaks for the [110] direction, respectively. These crystallite size and strain parameters in both the directions are plotted against temperature in Fig. 5-9 and Fig. 5-10, respectively.

From Fig. 5-9, it is seen that the crystallite sizes in the both directions increase with increasing temperature of heat treatment. Fig. 5-10 shows that the strain value in the [100] direction seems to reach its maximun at about 1000°C.

Increase in crystallite size causes the decrease in integral breadth, and decrease in strain causes decrease in integral breadth. The line broadening at low temperatures, say, between 200 and 400°C, may arise mainly from small crystallite size and the strain contribution seems not to be great. At temperatures between 600 and 1200°C, both small size and strain effects make a contribution to the line broadening, and the contribution of strain in the [100] direction is at a maximum around 1000°C. The ThO_2 samples heat-treated at 1300 and 1400°C have sufficiently large crystallite size and negligibly small strain.

5-4-3 ESTIMAITON OF LOCAL ORDER BY RADIAL DISTRIBUTION ANALYSIS

Regular arrangement of atoms in the ThO_2 structure.

In thorium dioxide, which has the fluorite-type structure, thorium atoms are on corner sites and face-center sites of the unit cell(a=5.60Å) and oxygen atoms are surrounded by four thorium atoms as the center of the regular tetrahedron as shown

in Fig. 5-11(a). In ideally crystallized ThO_2, where infinite number of unit cells are assembled, the number of neighbors and distances up to 10Å from the reference atom are summarized in Table 5-4.

Radial distribution curves for ThO_2 with various degrees of crystallinity

Radial distribution curve for ThO_2 heat-treated at 1400°C, which is confirmed to have very high degree of crystallinity from the X-ray diffraction pattern, is shown in Fig. 5-12. This curve shows clearly that this ThO_2 sample exhibits a high degree of local order. Vertical broken lines in this figure indicate the positions and relative areas anticipated from the ideally crystallized ThO_2, as summarized in Table 5-4.

The first peak at 2.4Å corresponds to the nearest Th-O bond. The second peak at about 4.0Å can be divided into two peaks, as indicated by broken curves. The area of the larger broken peak (A in Fig. 5-12) at 3.96Å correponds to the fact that Th atom has about 12 nearest Th neighbors at this distance, and that of the smaller broken peak(B in Fig. 5-12) at 4.64Å indicates that each Th atom is surrounded by 24 oxygen atoms at the distance. These results agree well with the regular arrangements of thorium and oxygen atoms in the ThO_2 structure. It is difficult, however, to do such a treatment for the peaks at higher r values, since several peaks arising from some Th-Th and Th-O interactions are superposed. The interactions between oxygen atoms cannot be estimated from the curve since the area of the peak due to the interaction of this type is much smaller than those of the peaks due to the other types of interactions.

Radial distribution curves for ThO_2 samples heat-treated at temperatures lower than 1400°C are given, together with that of ThO_2 heat-treated at 1400°C, in Fig. 5-13, where the curves for ThO_2 heat-treated at 200, 600 and 1000°C are shown as representative results. These three curves have peaks at the same positions as those of the peaks in the curve for ThO_2 heat-

treated at 1400°C although each peak becomes sharper with increasing temperature. Thus, it is seen that ThO_2 heat-treated at temperatures lower than 1400°C also exibits local order. The area of the peak at about 4.0Å at each temperature indicates that the number of the first nearest neighbor at 3.96Å (Th-Th) is 12 and that each Th atom is surrounded by 24 oxygen atoms at 4.64Å. It should be noted, however, that the first peak corresponding to the nearest Th-O bond and the third peak corresponding to the second nearest Th-Th bond become sharper with increasing temperature. These facts may suggest that the degree of local order increases with temperature.

Radial distribution curves for ThO_2 obtained by air oxidation of Th_3N_4 at 0, 50 and 100°C are shown in Fig. 5-14. These curves have peaks at about 4.0Å, which corresponds to the shortest Th-Th distance, but approach the average atomic distribution(broken curve) as r increses. Thus, ThO_2 obtained by air oxidation of Th_3N_4 close to room temperature exibits a low degree of local order.

The area of the peak at 4.0Å indicates that each Th atom is surrounded by only about 6 other Th atoms at this distance. This fact shows that these ThO_2 samples do not comprise the CaF_2 type unit cell.

According to Benz and Zachariasen[17], Th_3N_4, is rhombohedral and the tetrahedron of thorium atoms can be distinguished in the Th_3N_4 structure, as pointed out in Chapter 4. The length of the longer edge of the tetrahedron is 3.85Å and that of the shorter one is 3.75Å. On the other hand, regular tetrahedron of thorium atoms, ABCD, as illustrated in Fig. 5-11(a), the length of the edge of which is 3.96Å, can be recognized in the ThO_2 structure. Since the lengths of the edges of the tetrahedron in the Th_3N_4 structure are not much different from the length of the edge of regular tetrahedron in the ThO_2 structure, it can be considered that the latter is easily formed from the former during the oxidation. The existence of the regular tetrahedra in poorly-crystallized ThO_2 obtained by oxidizing Th_3N_4 at 50°C as well as well-crystallized ThO_2 obtained by heat treating this poorly-crystallized ThO_2 at 1400°C has been

also supported by the IR absorption spectroscopy as described in Chapter 4. The shortest Th-Th distance is 3.96Å and the number of the neighbours is much less than 12 for both the tetrahedra sharing corners(Fig. 5-11(b)) and tetrahedra sharing edges(Fig 5-11(c)). This agrees well with the results of the radial distribution analysis. Thus, in the ThO_2 obtained by the oxidation of Th_3N_4 close to room temperature, the regular tetrahedra have been formed but the CaF_2 type unit cells have not been formed. These ThO_2 samples may comprise the fragments of the two tetrahedra as shown in Fig. 1-11(b) and (c). This fact suggests that ThO_2 obtained by the air oxidation of Th_3N_4 close to room temperature may be considered to be amorphous.

5-5 CONCLUSION

ThO_2 with a wide range of degrees of crystallinity was prepared by heat treatment of poorly-crystallized ThO_2, which was obtained by air oxidation of Th_3N_4 at 50°C, in the temperature region of 200 to 1400°C in air and in vacuum.

1) The degree of crystallinity was discussed in terms of number of the detected peaks, the Kα doublet resolution and integral breadth values. The degree of crystallinity increases with temperature of heat treatment.
2) The crystallite size and nonuniform strain were estimated separately by the line broadening technique. Although the crystallite size increases with temperature, both crystallite size and strain effects contribute to line broadening, and the strain value reaches its maximum at about 1000°C as far as the [100] direction is concerned.
3) The local order of atoms was estimated by radial distribution analysis. ThO_2 obtained by the air oxidation of Th_3N_4 at 0, 50 and 100°C exibits a low degree of local order and may comprise not the CaF_2 type unit cells but the fragments consisting of the regular tetrahedra of thorium atoms. ThO_2 samples heat-treated at temperatures from 200 to 1400°C exhibit a high degree of local order, the degree of which

increases with temperature. The radial distribution analysis strongly suggests that ThO_2 obtained by the air oxidation of Th_3N_4 at 0, 50 and 100°C may be of amorphous nature.

REFERENCE

[1] J.M.Pope and K.C.Radford, J.Nucl.Mater., 52(1974)241.

[2] Y.Harada, Y.Baskin and J.H.Hadwerk, J.Am.Ceram.Soc., 45(1962) 253.

[3] B.J.F.Palmer, J.A.Scoberg and A.Y.H.Gin, Am.Ceram.Soc.Bull., 62(1982)627.

[4] W.H.Hall, Proc.Roy.Soc.London, A62(1949)741.

[5] H.P.Klug and L.E.Alexander, "X-ray Diffraction Procedure", 2nd ed., Wiley, New York, 1974, pp.791-859.

[6] P.Debby, Ann. Phys., 46(1915)809.

[7] F.W.Jones, Proc.Roy.Soc.London, A166(1938)16.

[8] L.Alexander, J.Appl.Phys., 25(1954)155.

[9] S.Ergun, "Chemistry and physics of carbon", Vol.3 in P.L.Waker,Jr (ed.), Marcel Dekker, New York, 1968, pp.211-288.

[10] L.E.Alexander, and H.P.Klug, Anal. Chem., 20(1948)886.

[11] D.T.Cormer and J.T.Waber, Acta Cryst., 18(1965)104.

[12] D.T.Cormer, J.Chem.Phys., 50(1969)4857.

[13] JCPDS Cards No. 4-0556.

[14] R.Benz, J.Nucl.Mater., 29(1969)43.

[15] M.Foex, C.R.Acad.Sci.Paris., 215(1942)534.

[16] E.C.Subbarao, P.H.Sutter and J.Hrizo, J.Am.Ceram.Soc., 48(1965)443.

[17] R.Benz and W.H.Zachariasen, Acta Cryst., 21(1966)838.

Table 5-1 Detected peaks in the X-ray diffraction patterns

(hkl)	staring material	heat treatment in air temperature (°C) 200	400	600	800	1000	heat treatment in vac 200	400	600	800	1000	I/I_o
(111)	+	+	+	+	+	+	+	+	+	+	+	100
(200)	+	+	+	+	+	+	+	+	+	+	+	35
(220)	+	+	+	+	+	+	+	+	+	+	+	58
(311)	+	+	+	+	+	+	+	+	+	+	+	64
(222)	-	-	+	+	+	+	-	+	+	+	+	11
(400)	-	-	+	+	+	+	-	+	+	+	+	8
(331)	-	-	+	+	+	+	-	+	+	+	+	26
(420)	-	-	+	+	+	+	-	+	+	+	+	17
(422)	-	-	+	+	+	+	-	+	+	+	+	20
(511)	-	-	+	+	+	+	-	+	+	+	+	19
(440)	-	-	-	-	-	+	-	-	-	-	+	6
(531)	-	-	-	+	+	+	-	-	+	+	+	18
(600)	-	-	-	-	-	+	-	-	-	-	+	8
(620)	-	-	-	-	+	+	-	-	-	+	+	14
(533)	-	-	-	-	-	+	-	-	-	-	+	9

note: +=detected
-=not detected

Table 5-2 Corrected integral breadth ($x10^{-3}$radian)

(a) Heat-treatment in air

hkl	Temperature(°C)								
	200	400	600	800	1000	1100	1200	1300	1400
200	+	+	10.8	8.04	6.76	5.18	3.80	1.50	0.242
400	-	+	15.3	13.7	11.7	7.79	6.11	1.87	0.927
220	+	+	+	+	8.86	6.69	4.47	1.37	0.245
440	-	-	-	-	18.2	13.1	10.0	1.40	1.04

(b) Heat-treatment in vacuum

hkl	Temperature(°C)								
	200	400	600	800	1000	1100	1200	1300	1400
200	+	+	11.5	8.12	6.63	5.19	3.57	1.87	0.564
400	-	+	16.6	14.0	12.5	10.3	6.55	3.51	1.38
220	+	+	+	+	10.5	18.0	4.82	2.14	0.718
440	-	-	-	-	21.8	18.3	11.3	5.35	1.26

note -;The peak is not detected.
+;The peak is so broad that it overlaps with the neighbouring peak.

Table 5-3 Crystallite size and strain

(a) Heat-treatment in air

Temp. (°C)	[100] size (Å)	[100] strain (10^{-3})	[110] size (Å)	[110] strain (10^{-3})
1200	700	2.6	790	2.8
1100	440	2.8	370	2.6
1000	480	6.0	280	3.4
800	380	6.7	---	---
600	190	4.2	---	---

(b) Heat-treatment in vacuum

Temp. (°C)	[100] size (Å)	[100] strain (10^{-3})	[110] size (Å)	[110] strain (10^{-3})
1200	1100	3.7	850	3.4
1100	1100	6.5	460	5.2
1000	670	7.4	270	5.1
800	390	7.1	---	---
600	190	5.1	---	---

Table 5-4 Numbers of neighbors and distaces in ThO_2 structure

Th-Th		Th-O		O-O	
number of neighbors	distance (Å)	number of neighbors*	distance (Å)	number of neighbors	distance (Å)
12	3.96	8	2.42	6	2.82
6	5.60	24	4.64	12	3.96
24	6.86	24	6.10	8	4.85
12	7.92	32	7.27	6	5.60
24	8.85	48	8.28	24	6.26
8	9.69	24	9.18	24	6.86
		48	10.0		

*A thorium atom is taken as a reference atom.

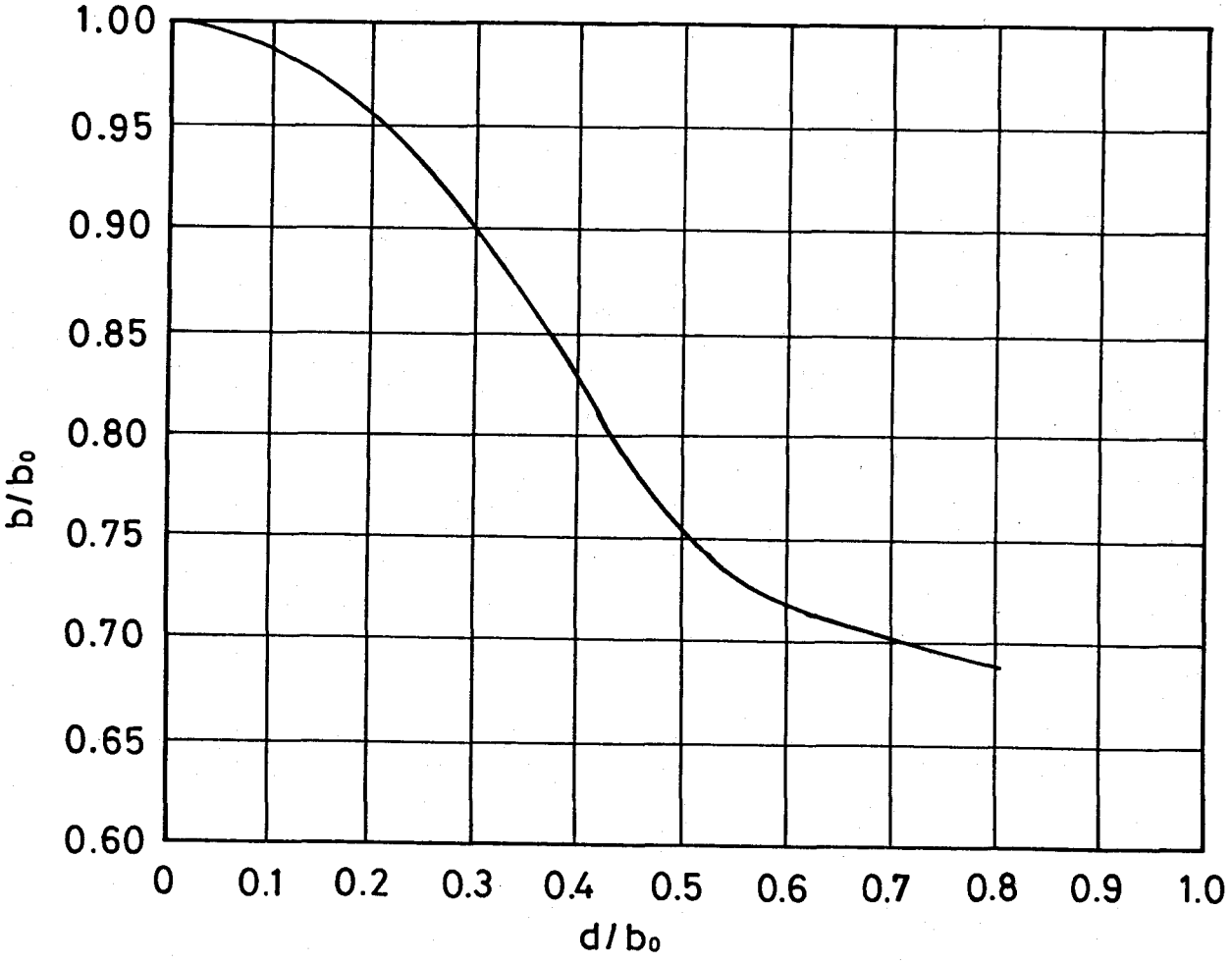

Fig. 5-1 Curve for correcting line breadths for Kα doublet broadening[7]

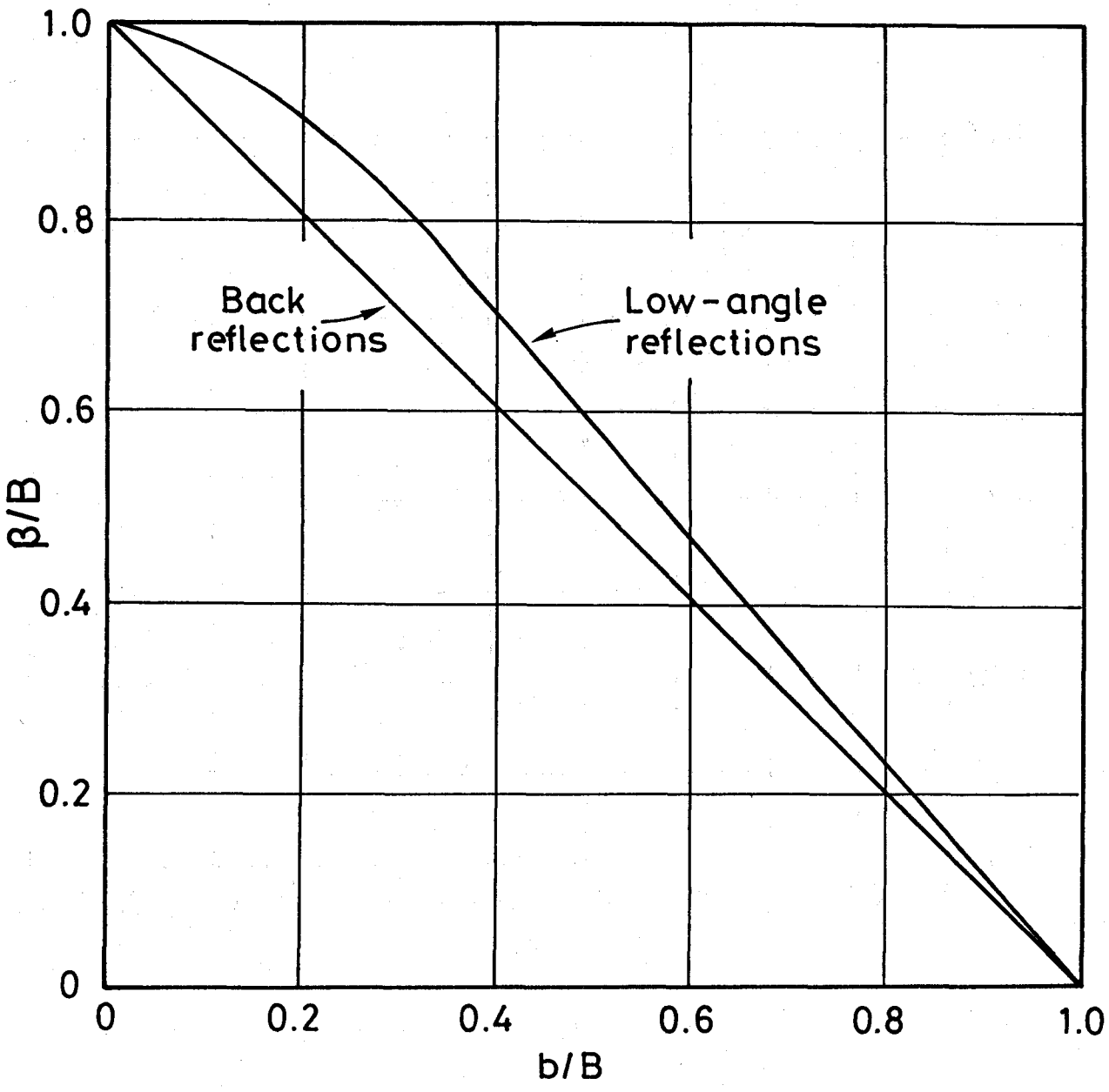

Fig. 5-2 Curves for correcting X-ray diffractometer line breadths for instrumental broadening[8].

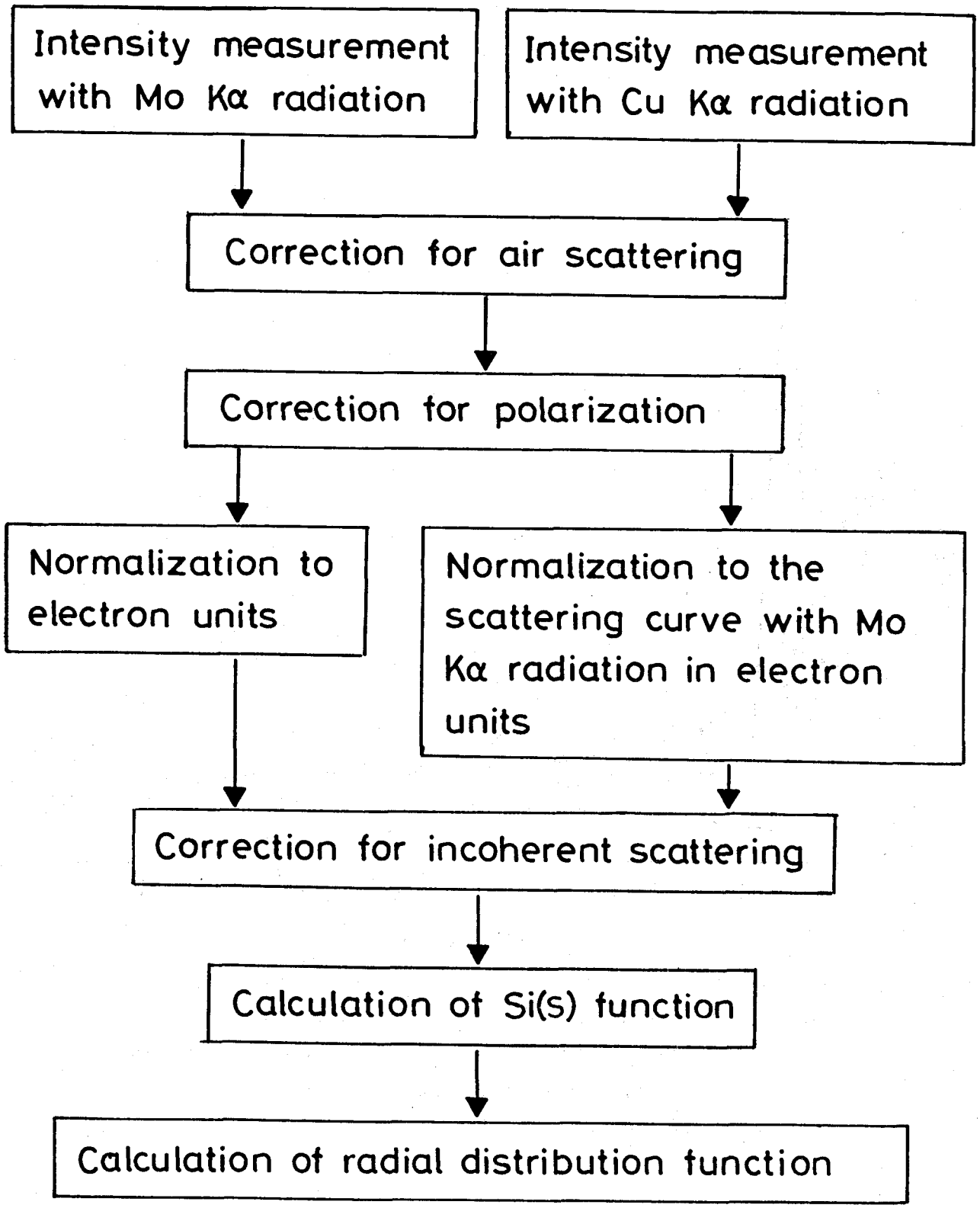

Fig. 5-3 Procedure for calculation of radial distribution function.

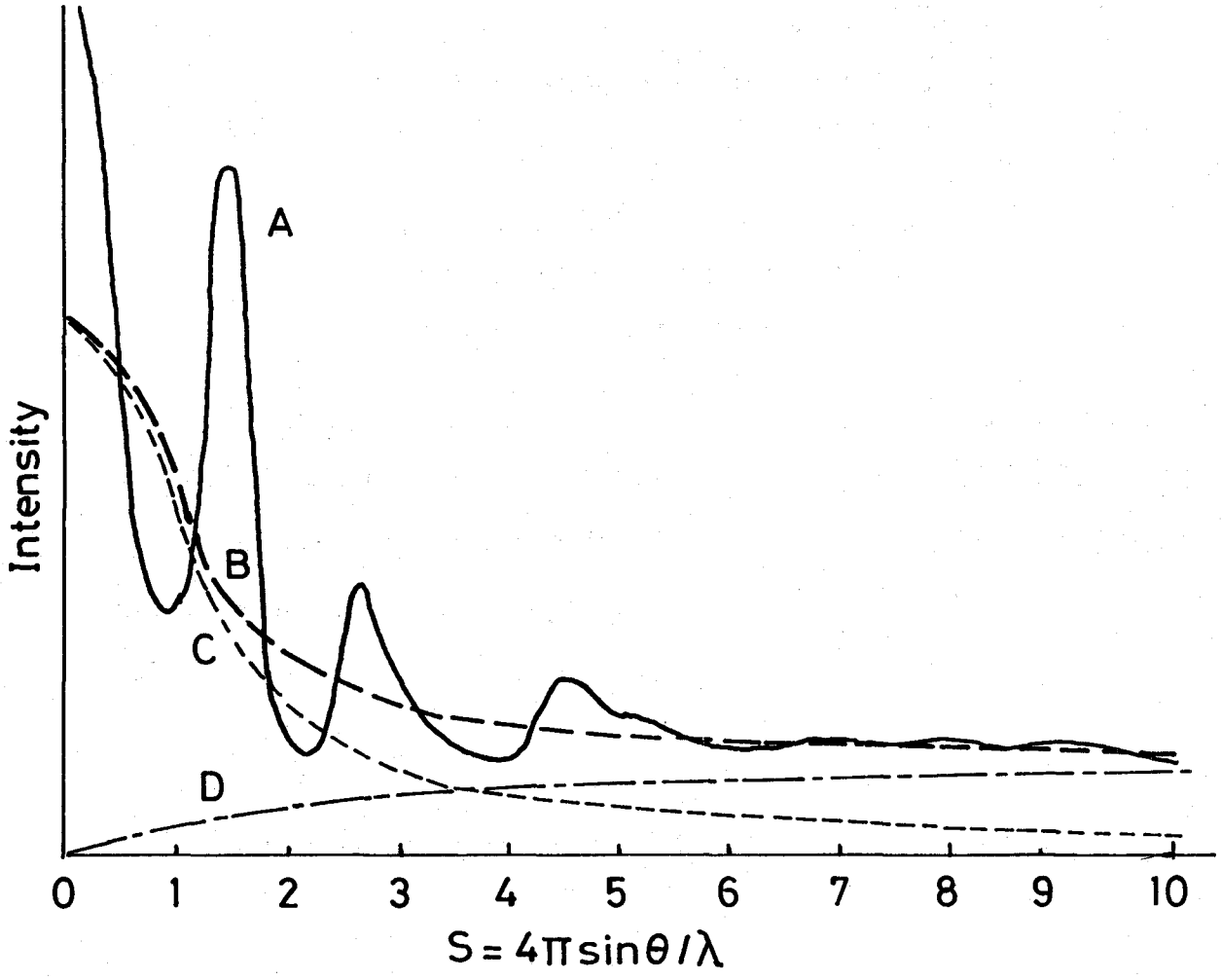

Fig. 5-4 Normalized scattering curve(A) compared with theoretical independent scattering curves; independent scattering(C), incoherent scattering(D) and total independent scattering(B).

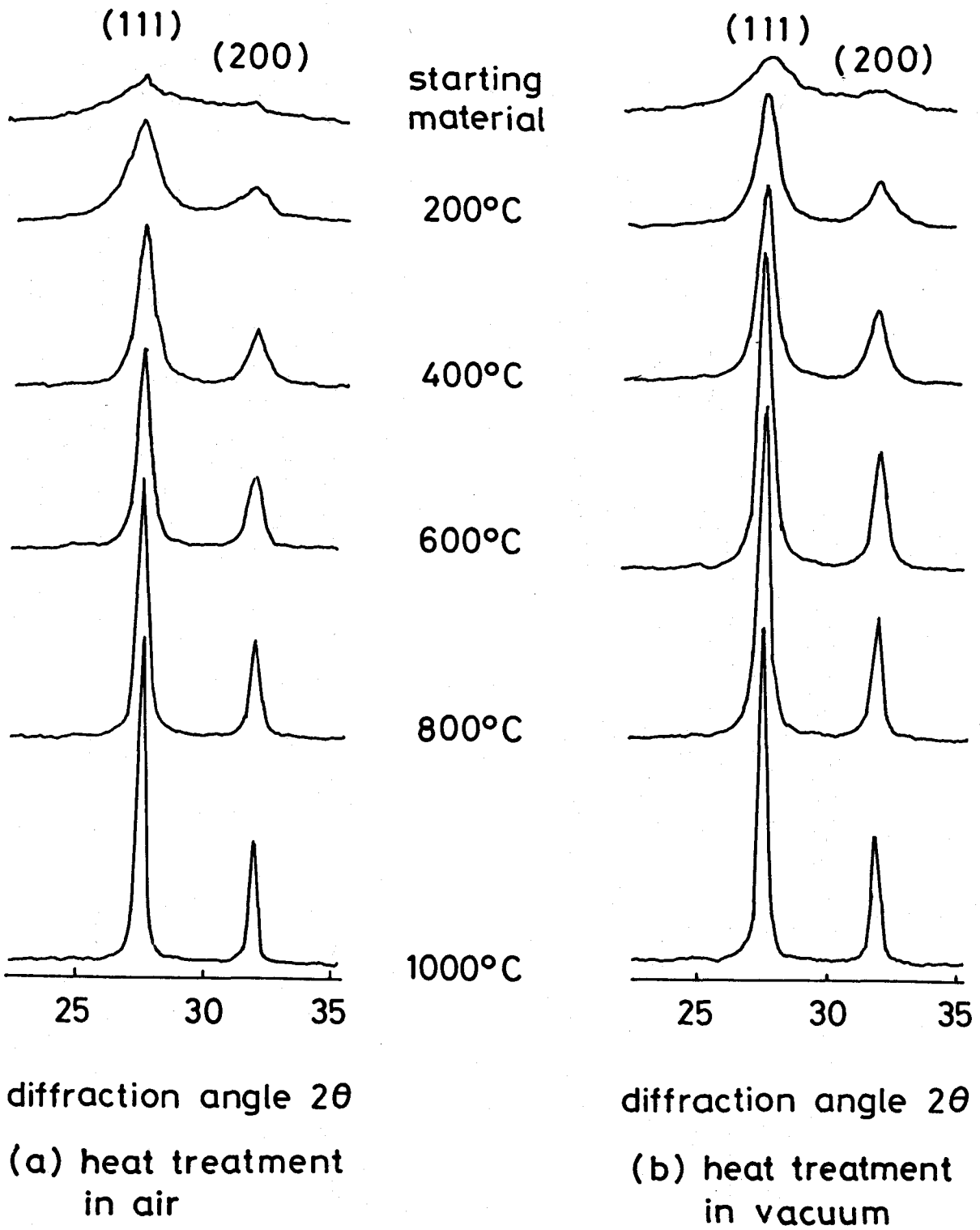

Fig. 5-5 Variation of X-ray diffraction pattern for ThO_2 with temperature of heat treatment.

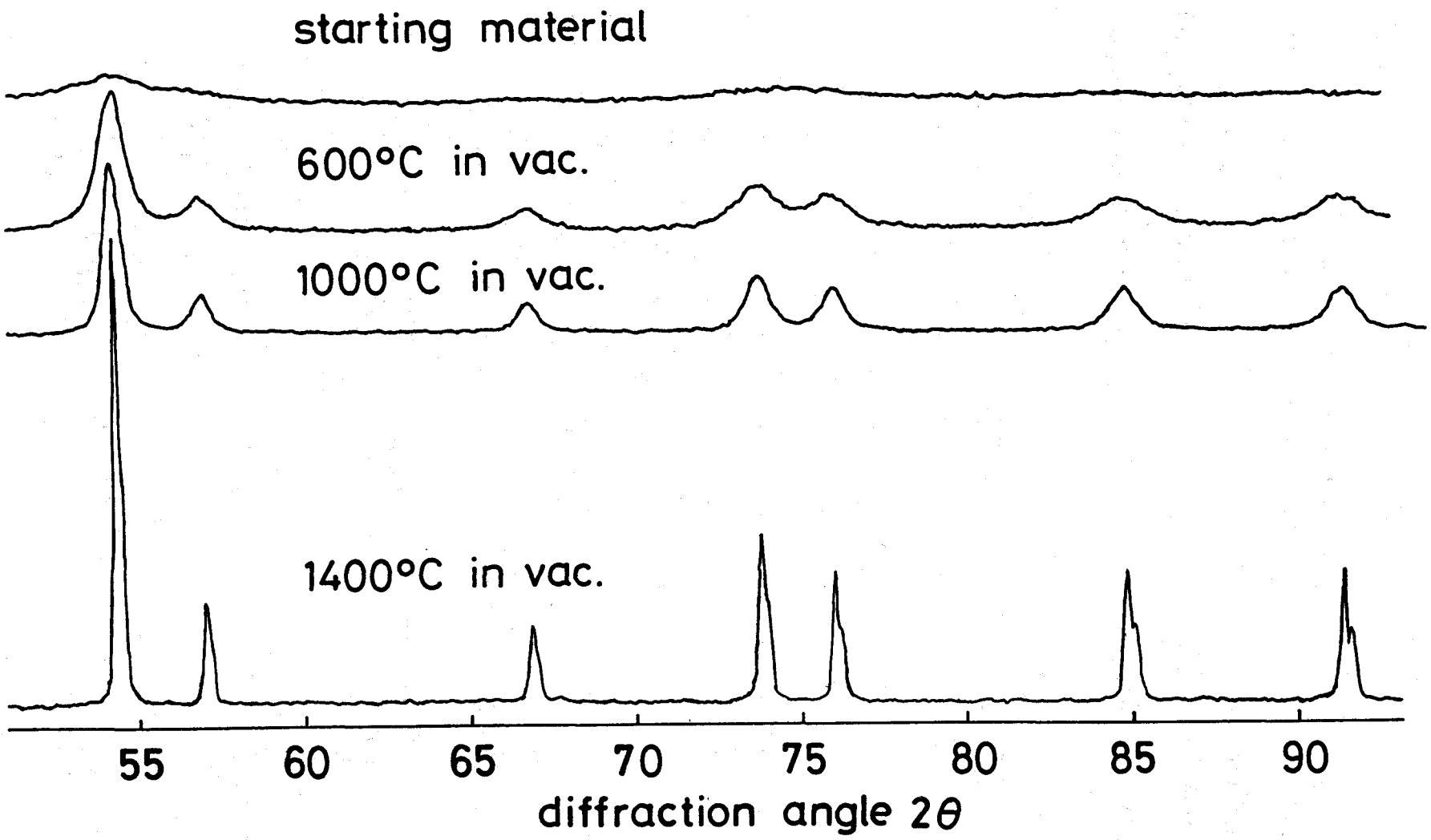

Fig. 5-6 X-ray diffraction patterns for ThO_2 with various degrees of crystallinity.

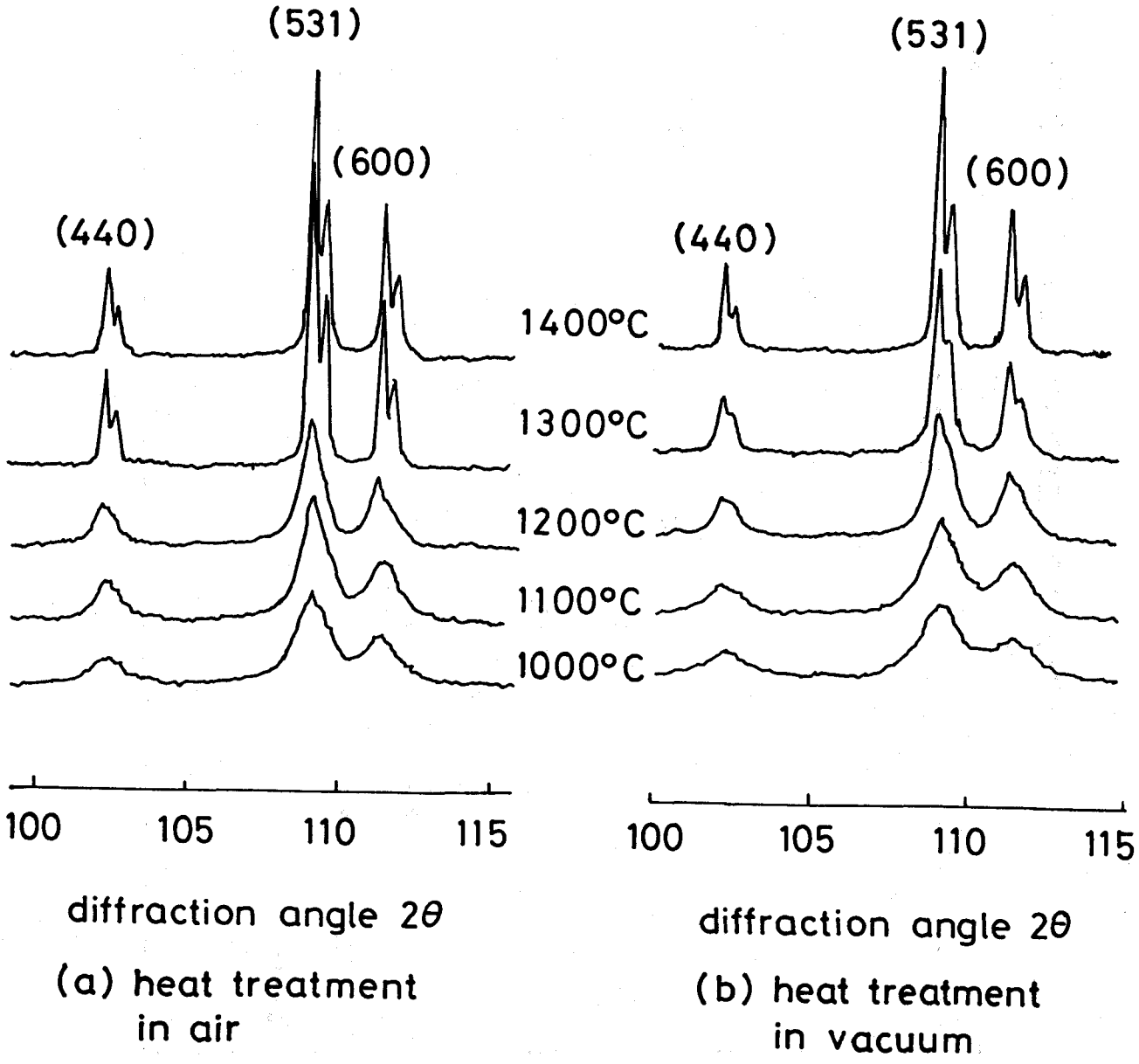

Fig. 5-7 Variation of X-ray diffraction pattern for ThO_2 with temperature of heat treatment.

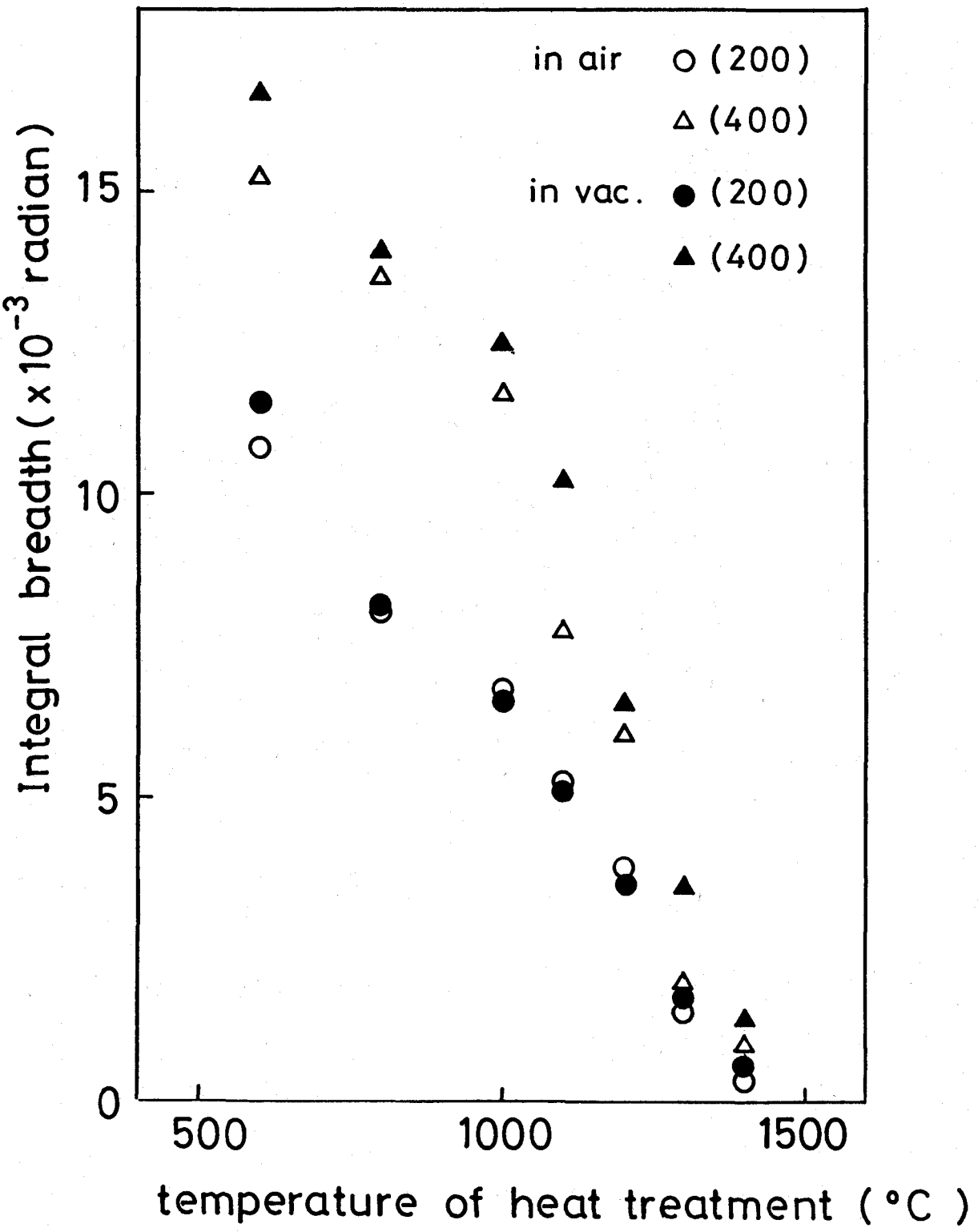

Fig. 5-8 Variation of integral breadth values of diffraction peaks of ThO_2 with temperature of heat treatment.

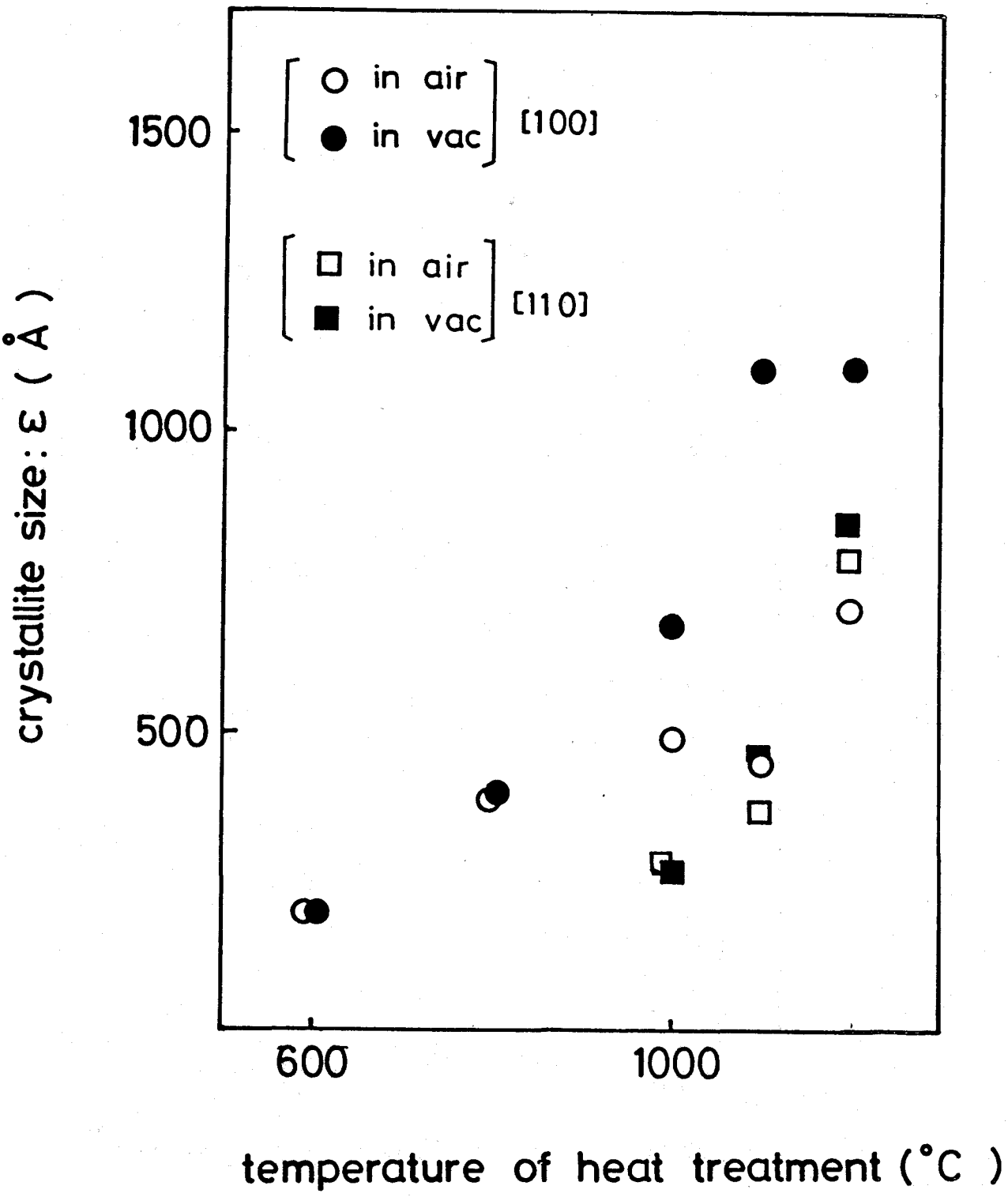

Fig. 5-9 Variation of crystallite sizes with temperature of heat treatment.

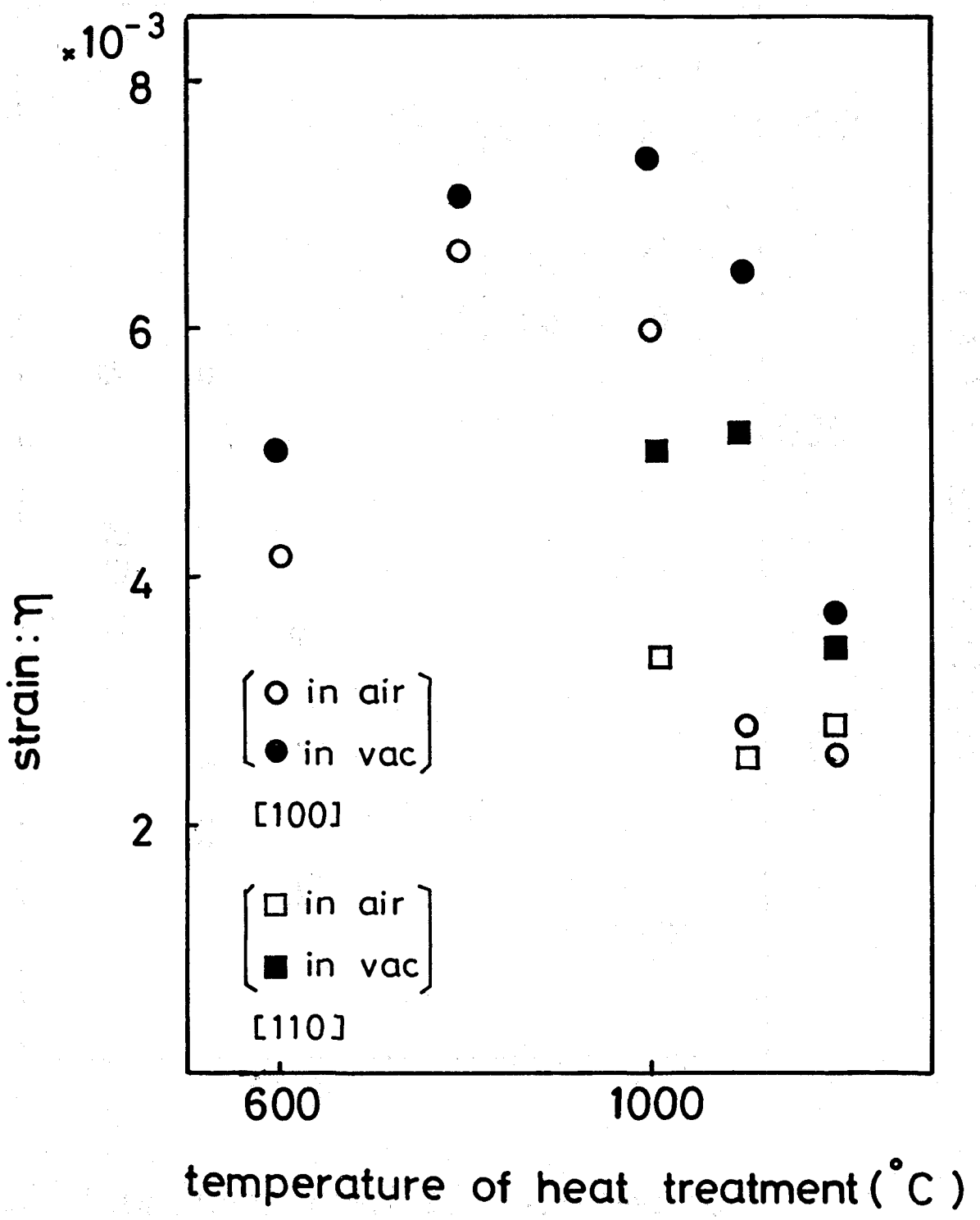

Fig. 5-10 Variation of strain values with temperature of heat treatment.

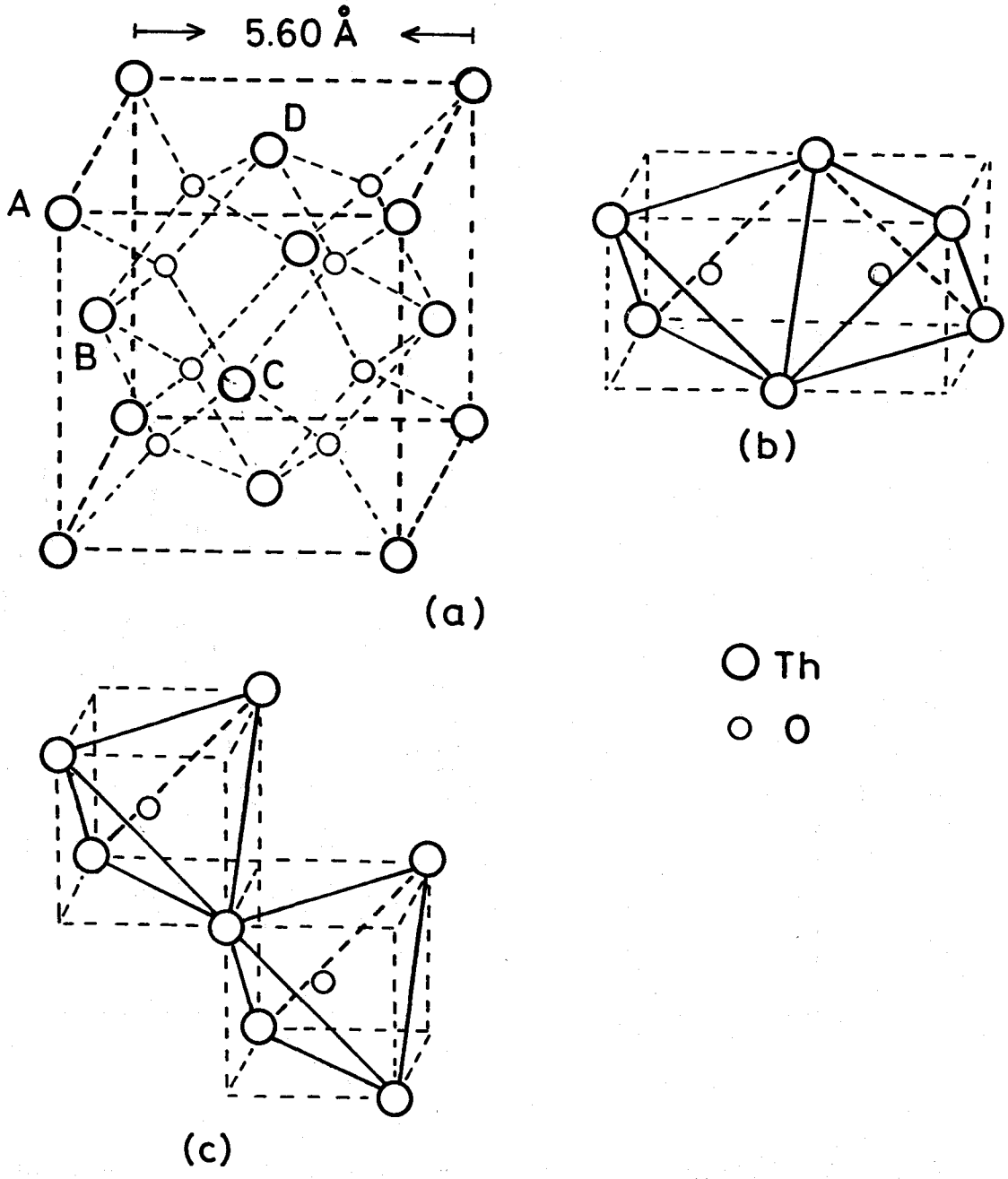

Fig. 5-11 (a) Arrangement of the atoms in the unit cell of ThO_2.
(b) Fragment of the tetrahedra sharing edges.
(c) Fragment of the tetrahedra sharing corners.

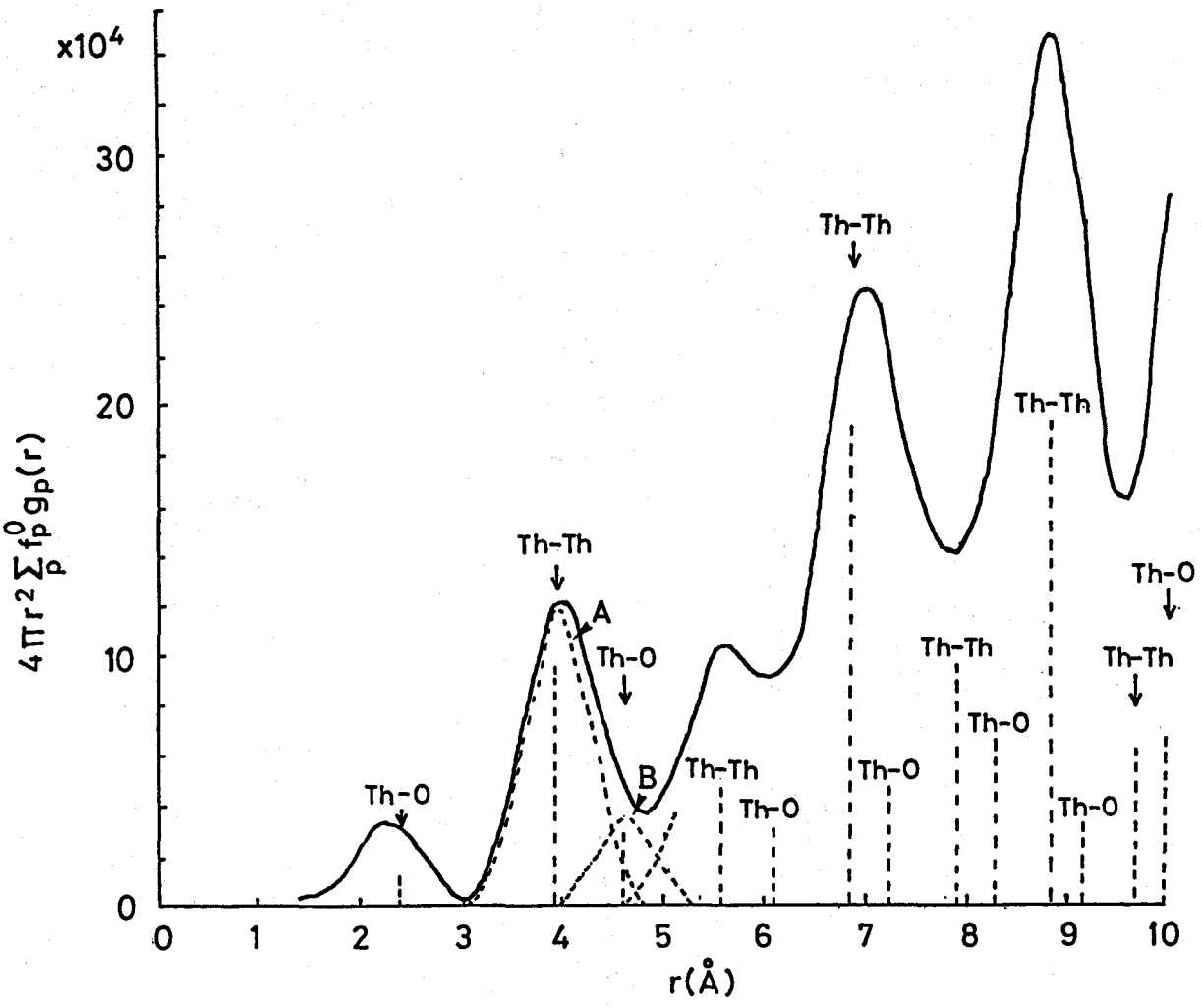

Fig. 5-12 Radial distribution curve for ThO_2 heat-treated at 1400°C.

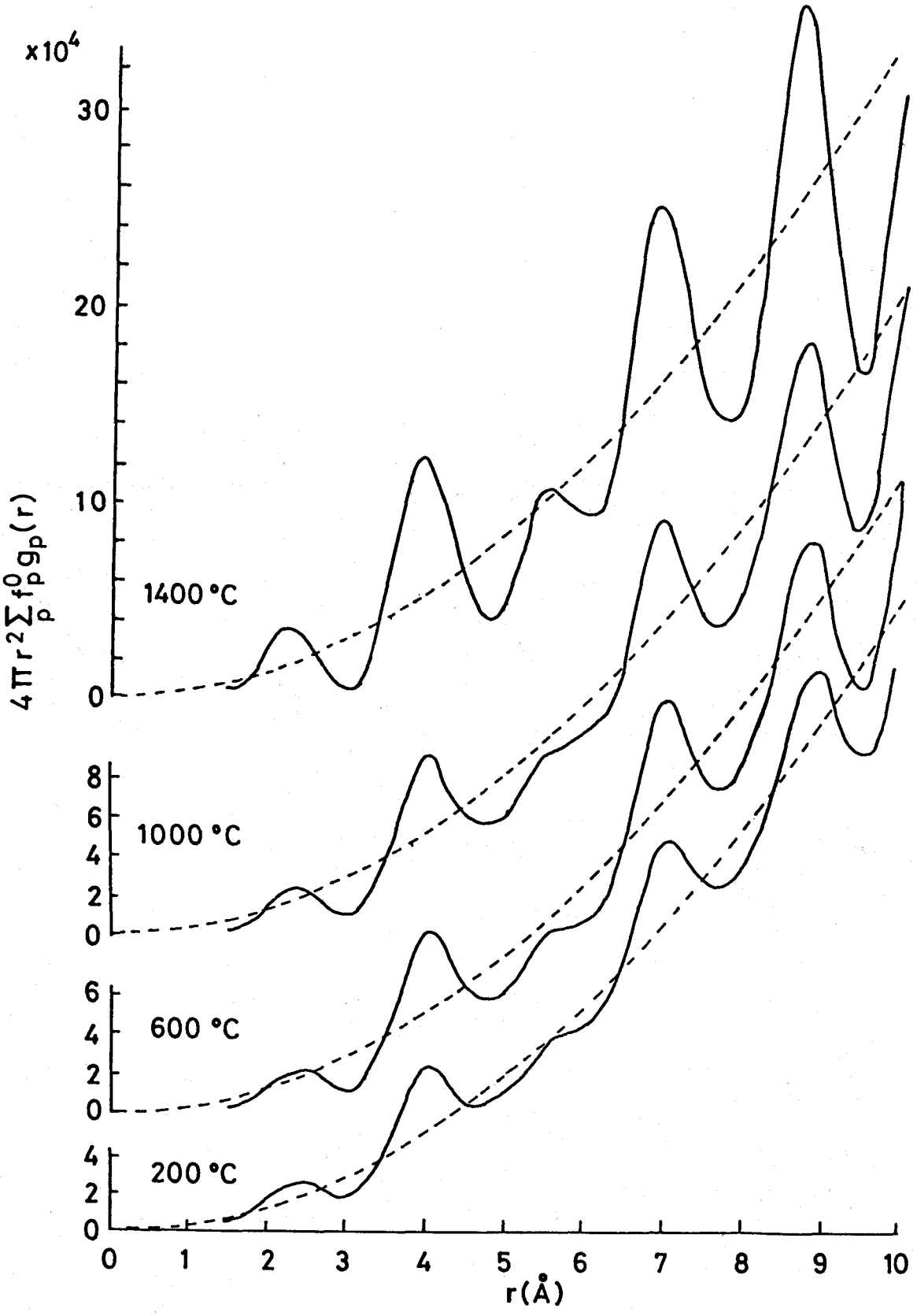

Fig. 5-13 Radial distribution curves for ThO_2 samples heat-treated at various temperatures.

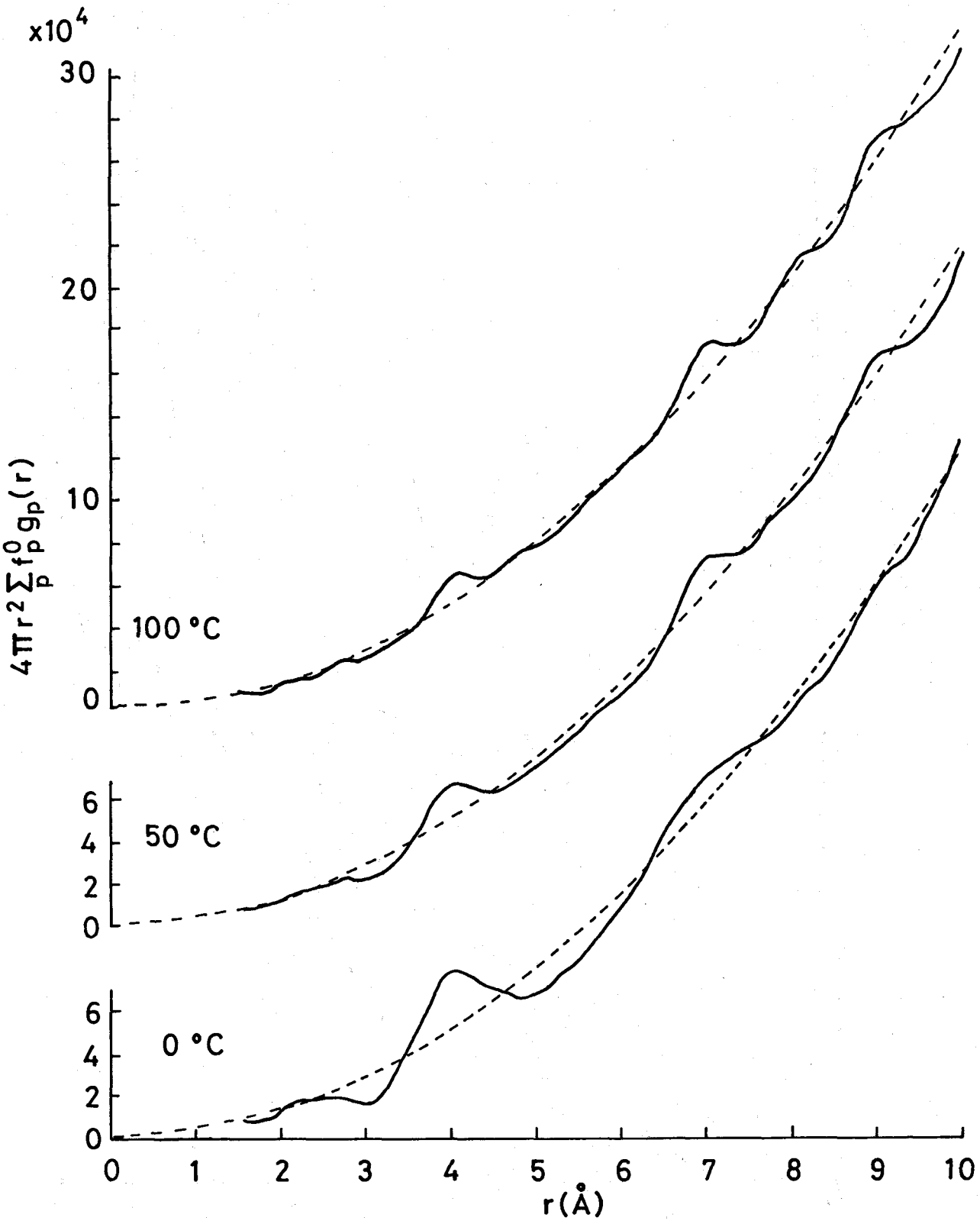

Fig. 5-14 Radial distribution curves for ThO_2 samples obtained by the oxidation of Th_3N_4 close to room temperature.

6 CONCLUSION

One of the main purposes of this work is to study basic problems in preparing pure ThN. Particularly, on account of the instability of thorium nitrides with respect to ThO_2, efforts had to be expended on the study of oxidation behavior of Th_3N_4.

In Chapter 1, the present status of the knowledge on thorium dioxide and thorium nitrides has been reviewed.

In Chapter 2, the pulverization method of metallic thorium thorough hydridng process, which is the initial step of the preparation of ThN, has been discussed. This process consists of the formation of ThH_2 at 650°C as the first step and formation of Th_4H_{15} at 70°C as the second step. The formation of Th_4H_{15} through the reaction of ThH_2 with H_2 is found to be responsible for the production of powdered thorium. The pressure-composition-temperature relationships for Th-H system have been determined, and a tentative equilibrium diagram for the binary Th-H system has been proposed. The equilibrium hydrogen pressure in the two-phase region of ThH_2 and Th_4H_{15} varies very sensitively with temperature.

In Chapter 3, the results obtained from the study on the preparation of thorium nitrides have been given. Of all the experiments carried out, the reaction of Th_4H_{15} with flowing N_2 at 800°C yields Th_3N_4 with the highest nitrogen content and the highest degree of crystallinity. Thermal decomposition of Th_3N_4 has been performed under various conditions. Material containing more than 95% ThN can be obtained. Moreover, the thermodynamic stability of the solid compounds in the Th-N-O system has been evaluated. The comparison of the thermodynamic consideration with the experimental results suggest that the kinetics play an important role in preparing ThN containing no oxide phase.

In Chapter 4, oxidation behavior of Th_3N_4 has been studied. Oxidation of Th_3N_4 close to room temperature produces poorly-crystallized ThO_2, whose degree of crystallinity increases with oxidation temperature.

In Chapter 5, ThO_2 with a wide range of degrees of

crystallinity has been prepared by heat treatment of poorly-crystallized ThO_2 at temperatures ranging from 200 to 1400°C in air and in vacuum. The degree of crystallinity increases with temperature of heat treatment, and both crystallite size and strain effects contribute to the line broadening. Radial distribution analysis suggests that poorly-crystallized ThO_2 obtained by the air oxidation of Th_3N_4 close to room temperature may be of amorphous nature.

As concluding remarks and further works;

(A) Thorium nitrides containing a very small amount of oxide can be obtained. It is strongly hoped that the reliable chemical, physical and the other properties will be measured with ThN prepared in this way.

(B) ThO_2 with various degrees of crystallinity is obtained, which has not been reported in the literature. The results in the present study also must serve the study on the fabrication of high density ThO_2 pellets.

ACKNOWLEDGEMENT

The author would like to express the sincere appreciation to Professor M.Miyake for his precious guidance, valuable discussion, warm encouragement and for everything kindly extended to the author.

The author is indebted to Prof. S.Imoto, Prof. T.Sekiya, Prof. K.Sumita, Prof. T.Yamamoto and Prof. T.Okada.

The author is also indebted to Assoc. Prof. M.Katsura for his kind and helpful advice without which this work could never be accomplished.

The author would like to express his appreciation to Dr. P.Son and Mr. Y.Yamanaka for their hospitality and encouragement.

Thanks are also due to the other members of the laboratory for their kindness.

LIST OF PAPERS BY THE AUTHOR

(1) "HYDRIDING OF METALLIC THORIUM"
M.Miyake, M.Katsura, Y.Matsuki and M.Uno
Technol.Rep.Osaka Univ., 33(1983)239.

(2) "PREPARATION OF THORIUM NITRIDES AND THEIR OXIDATION BEHAVIOR"
M.Uno, M.Katsura and M.Miyake, J.Less-Common Met., 121(1986)615.

(3) "PREPARATION OF Th_3N_4 AND ITS OXIDATION BEHAVIOR"
M.Uno, M.Katsura and M.Miyake, J.Less-Common Met., 135(1987)25.

(4) "PREPARATION OF ThN BY THERMAL DECOMPOSITION OF Th_3N_4"
M.Uno, M.Katsura and M.Miyake, Inorg.Chim.Acta, 140(1987)123.

(5) "THE DEGREE OF CRYSTALLINITY OF ThO_2"
M.Uno, M.Katsura and M.Miyake, to be submitted to the J. Less-Common Met.

(6) "RADIAL DISTRIBUTION ANALYSIS OF ThO_2"
M.Uno, M.Katsura and M.Miyake, to be submitted to the J. Less-Common Met.

(7) "PREPARATION AND PROPERTIES OF THORIUM NITRIDES"
M.Miyake, M.Katsura and M.Uno,
pp. 147-154, in Research on Thorium Fuel, Spey 21, Min.Educ.Cult., Tokyo(1987).

LIST OF LECTURES BY THE AUTHOR

A. INTERNATIONAL CONFERENCE

(1) "PREPARATION OF THORIUM NITRIDES AND THEIR OXIDATION BEHAVIOR"
M.Uno, M.Katsura and M.Miyake,
Actinides 85,
Aix en Provance, September 1985.

(2) "FORMATION OF $H_2Th(NO_3)_6 3H_2O$ FROM HNO_3 SOLUTION OF Th_3N_4 AND A NEW THORIUM NITRATE"
M.Uno, S.Nakamura, M.Katsura and M.Miyake,
The Second International Conference on the Basic and Applied Chemistry of f-Transition(Lanthanide and Actinide) and Related Elements,
Lisbon, April 1987.

(3) "PREPARATION OF ThN BY THERMAL DECOMPOSITION OF Th_3N_4"
M.Uno, M.Katsura and M.Miyake,
The Second International Conference on the Basic and Applied Chemistry of f-Transition(Lanthanide and Actinide) and Related Elements,
Lisbon, April 1987.

B. DOMESTIC MEETING

(1) "OXIDATION BEHAVIOR OF Th_3N_4"
M.Katsura, M.Uno, S.Yamanaka and M.Miyake,
Fall Meeting of the Atomic Energy Society of Japan,
Sapporo, September 1983.

(2) "STUDY ON THE CRYSTALLIZATION OF AMORPHOUS ThO_2 I"
M.Uno, M.Senga, M.Katsura and M.Miyake,
Annual Meeting of the Atomic Energy Society of Japan,
Osaka, March 1984.

(3) "STUDY ON THE CRYSTALLIZATION OF AMORPHOUS ThO_2 II"
M.Uno, M.Senga, M.Katsura and M.Miyake,
Fall Meeting of the Atomic Energy Society of Japan,
Tokai-mura, October 1984.

(4) "EFFECT OF OXYGEN ON THE FORMATION OF ThN and ThC_xN_{1-x}"
M.Uno, M.Katsura and M.Miyake,
Fall Meeting of the Atomic Energy Society of Japan,
Sendai, October 1985.

(5) "SOLUTION BEHAVIOR OF THORIUM NITRIDES IN HNO_3
-COMPOSITION AND CRYSTAL STRUCTURE OF THORIUM NITRATE HYDRATES-"
M.Uno, S.Nakamura, M.Katsura and M.Miyake,
Annual Meeting of the Atomic Energy Society of Japan,
Uji, March 1986.

(6) "EFFECT OF OXYGEN ON THE FORMATION OF ThN"
M.Uno, M.Katsura and M.Miyake,
Fall Meeting of the Atomic Energy Society of Japan,
Fukuoka, October 1986.

(7) "STUDY ON THE CRYSTALLIZATION OF ThO_2"
M.Uno, M.Katsura and M.Miyake,
Fall Meeting of the Atomic Energy Society of Japan,
Sapporo, October 1987.